Controlling the Electric-Field of Few-Cycle Laser Pulses on the Cycle-Scale

Von der Fakultät für Mathematik und Physik
der Gottfried Wilhelm Leibniz Universität Hannover
zur Erlangung des Grades

Doktor der Naturwissenschaften
- Dr. rer. nat. -

genehmigte Dissertation

von
M.Sc. (FH) Stefan Rausch
geboren am 07.05.1980 in Neuwied

2010

Referent: Prof. Dr. Uwe Morgner
Korreferent: Prof. Dr. Piet O. Schmidt
Tag der Promotion: 25.06.2010

Statement

I hereby certify, that the work presented in this dissertation is my own and work performed by others is cited appropriately.
In addition I certify, that this dissertation has never been used as diploma thesis or a similar work before.

Eidesstattliche Erklärungen zum Promotionsverfahren

Hiermit erkläre ich an Eides statt, dass ich meine Dissertation selbstständig verfasst habe und die benutzten Hilfsmittel vollständig angegeben sind.
Darüber hinaus erkläre ich an Eides statt, dass die von mir verfasste Dissertation nicht schon als Diplomarbeit oder ähnliche Prüfungsarbeit verwendet wurde.

.....
Stefan Rausch

Kurzfassung

Stefan Rausch

Manipulation des elektrischen Feldes von ultrakurzen Laserpulsen unterhalb der Schwingungsperiode

Die zeitliche Dauer von ultrakurzen Laserpulsen, wie sie von breitbandigen Titan:Saphir Oszillatoren erzeugt werden, nähert sich immer weiter der Periodendauer des zugrunde liegenden elektrischen Feldes an. Dadurch wächst neben der ultrakurzen Pulsdauer ebenfalls die Bedeutung des Feldes und der Wunsch nach einer direkten Einflussnahme darauf - für zahlreiche Experimente der aktuellen Ultrakurzpulsphysik ist dies bereits eine wichtige Voraussetzung geworden.

Diese Doktorarbeit beschäftigt sich mit der Erzeugung und Manipulation von ultrakurzen elektrischen Feld-Oszillationen im optischen Frequenzbereich. Dazu wird ein breitbandiger Feld-Synthesizer realisiert, der in der Lage ist durch spektrale und zeitliche Manipulation von oktavbreiten Eingangspulsen maßgeschneiderte Feld-Verläufe mit Dauern bis herab zu 3,6 Femtosekunden zu erzeugen. Der dafür realisierte Titan:Saphir Laser generiert die kürzesten Pulse, die jemals direkt aus einem Oszillator erzeugt worden sind und kann in seiner Träger-Einhüllenden-Phase stabilisiert werden.

Auch die Stabilisation dieser Träger-Einhüllenden-Phase von breitbandigen Titan:Saphir Oszillatoren wird im Rahmen dieser Arbeit vorangetrieben. So wird zum Beispiel ein oktavbreiter Laser auf konstante Träger-Einhüllenden-Phase stabilisiert und dadurch ein Pulszug erzeugt, der für jeden enthaltenen Puls die gleichen Feld-Eigenschaften besitzt. Mit diesem System war es zum ersten Mal möglich eine selbst-referenzierte spektrale Interferenz von mehr als 10^{11} Oszillatorpulsen zu demonstrieren.

Auch werden Ansätze bezüglich der Weiterentwicklung von breitbandigen Titan:Saphir Strahlquellen verfolgt. Zum Beispiel wird ein von einem Scheibenlaser synchron-gepumpter Titan:Saphir Laser realisiert, der neben einem selbst-startenden Verhalten zusätzlich eine Selbst-Synchronisation zu dem benutzten Pumplaser ermöglicht. Dadurch wird das kombinierte System neben der breitbandigen Laserstrahlung zusätzlich mit einem intensiven grünen Pumppuls ausgestattet, was z.B. für Pump-Abfrage Experimente relevant ist.

Schlagworte: Wenige-Zyklen-Pulse, Titan:Saphir-Laser-Oszillatoren, Träger-Einhüllenden-Phase, Oktavbreite Pulsformung, Wenige-Zyklen-Feld-Synthese

Abstract

Stefan Rausch

Controlling the Electric-Field of Few-Cycle Laser Pulses on the Cycle-Scale

The duration of femtosecond pulses generated by broadband Ti:sapphire laser systems is successively approaching the cycle period of the underlying electric field oscillation – 2.7 fs for a carrier oscillation of 375 THz (800 nm). Next to the few-cycle pulse duration thereby the full control of the electric field itself becomes more and more important and is meanwhile an indispensable prerequisite for numerous experiments in ultrafast science.

This thesis is concerned with the generation and control of electric-field oscillations approaching the single-cycle limit. A few-cycle field synthesizer is realized that allows for the temporal and spectral manipulation of octave-spanning input pulses to generate tailored field profiles with a duration as short as 3.6 fs. The realized octave-spanning seed oscillator delivers the shortest pulses ever generated directly from a laser oscillator and can be directly stabilized with respect to its carrier-envelope-offset phase to allow for an electric field control on attosecond time scales.

Also the carrier-envelope-offset phase stabilization of few-cycle laser oscillators has been under investigation within the scope of this thesis. In this regard an octave-spanning oscillator was realized that can be stabilized to deliver a pulse train with constant electric field properties for every pulse within the train. With this system a self-referencing spectral interference of more than 10^{11} oscillator pulses could be demonstrated.

Next to the seed oscillator, also different broadband Ti:sapphire laser sources have been target of interest. For example a synchronously-pumped Ti:sapphire oscillator, pumped by a frequency-doubled thin-disk oscillator, was realized featuring a self-starting ability, which is not present for continuously-pumped oscillators. This carrier-envelope-offset phase stabilized laser additionally showed a self-synchronization to the thin-disk pump source, adding another interesting aspect for seeding the field-synthesizer since an additional synchronized intense 'green' pulse would be available e.g. for pump-probe type experiments.

Key words: Few-cycle Ti:sapphire laser oscillators, carrier-envelope-offset phase stabilization, octave-spanning pulse shaping, few-cycle field synthesis.

Contents

1 Introduction

1.1 Motivation

Within the last fifty years hardly anything has influenced and improved our daily life like the laser. This manifold light source plays a key role in nowadays communications, industrial production, medicine, consumer electronics, navigation, and above all many branches of science. It still pushes the limits e.g. in terms of speed, precision and quality in manufacturing processes and enables the investigation of fundamental concepts of nature. Next to the well established laser systems used throughout the world for industrial and consumer applications, still scientists are searching for improved laser sources and novel concepts opening up new fields of research and novel characterization and measurement techniques. Although many of those scientific laser sources have not found their application within mass-market yet, they have an enormous impact for humankind, e.g. helping to understand the origin of our universe, or measuring physical constants with unsurpassed precision.

One of those scientific light sources is the Ti:sapphire laser, which is the key element of nearly all of todays ultrafast science. Within the last few years rapid developments in the field of ultrashort pulse generation by those lasers have led to pulses with durations as short as a few optical cycles with octave-spanning spectra generated directly from laser oscillators at high repetition rates [Kär05]. The duration of such few-cycle laser pulses in the order of a few femtoseconds ($1\,\mathrm{fs} \equiv 10^{-15}\,\mathrm{s}$) is hardly imaginable. One femtosecond is the millionth part of one billionth of a second. Although light travels a distance of about 300,000 km within one second, roughly a distance of 7.5-times around the globe - in one femtosecond it only propagates a distance of $0.3\,\mu\mathrm{m}$, one hundredth part of the thickness of a human hair.

These extreme short pulses can be considered as a slowly varying envelope with a fast oscillating carrier field underneath. Since the duration of the temporal envelope is already in the order of the underlying electric field oscillation and approaching the single-cycle – 2.7 fs for a central wavelength of 800 nm (375 THz) –, the electric field properties itself become a highly regarded parameter for many experiments in nowadays ultrafast science. The electric field characteristics of these few-cycle laser pulses are determined by their carrier-envelope-offset phase, that can be stabilized routinely [Müc05, Bar07, Cre08, Rau08b, Rau09], opening up for phase- and field-sensitive experiments [Apo04, Müc04, Nak06], frequency metrology and high-precision spectroscopy [Ude02b, Mar04, For06, Sto06], next to quantum interference control [Roo05, Rou07]. Amplified few-cycle pulses delivering

intensities in the order of 10^{14} W/cm^2 paved the way for investigating nonlinear light-matter interaction and attosecond science [Bal03, San06, Kre06], where a controlled electric field profile of the generating few-cycle pulse is an indispensable prerequisite. Because of their unique temporal and spectral properties, Ti:sapphire lasers are also ideal light-sources for high resolution optical coherence tomography (OCT) [Mor00], high-resolution CARS [Dud02, Vac06, Pos08] and femtosecond quantum control [Vog06]. To fully exploit these features pulse shaping techniques are used to manipulate the unique laser features to generate tailored pulse envelopes with durations of less than two optical cycles and flexible pulse sequences [Bin06].

1.2 Goal and outline of thesis

Goal of this thesis is the demonstration of a novel few-cycle field synthesizer to gain full control over electric field oscillations of femtosecond pulses approaching the single-cycle limit. Such a field synthesizer consists out of an octave-spanning Ti:sapphire seed oscillator that can be stabilized with respect to its carrier-envelope-offset phase and a broadband pulse shaper that is capable to independently manipulate the spectral phase and amplitude of the broadband seed pulses. This work comprises investigations in Ti:sapphire-based seed sources to generate the target field oscillations next to broadband pulse shaping techniques to control the waveform of these few-cycle pulses on the cycle scale.

The thesis is structured as follows: After this short motivation and introduction, the second chapter gives a brief access into the relevant theory for understanding. It mainly focuses on the electric field properties of few-cycle laser pulses and shows the route to their control, together with a discussion on important noise characteristics like timing jitter and phase noise. The third chapter deals with the generation of enhanced octave-spanning spectra directly from a laser oscillator and introduces a sub-4-fs Ti:sapphire laser oscillator that further pushes the limits in terms of few-cycle laser pulse generation. This laser system will be target for a carrier-envelope-offset phase and timing stabilization. Within the fourth chapter the feasibility of a synchronously-pumped octave-spanning Ti:sapphire laser will be under investigation in terms of self-starting behavior, carrier-envelope-offset phase stabilization and self-synchronization. Here first estimates of the performance and practicability of such a combined system for few-cycle laser physics will be made. The fifth chapter is concerned with an improved self-referencing scheme to lock the carrier-envelope-offset frequency of few-cycle laser pulses to zero, generating a pulse train with identical electric field profile for every pulse contained within the train. Using this novel system, field-sensitive experiments can be performed with nearly full oscillator power and pulse repetition rate. The last experimental chapter presents a few-cycle field synthesizer which is an unique combination of an octave-spanning, carrier-envelope-offset phase stabilized

Ti:sapphire oscillator with a double-LCD pulse shaper and a SPIDER pulse characterization apparatus. As will be shown in this chapter, this tool allows for manipulating the spectral phase and amplitude of the broadband input pulses to generate tailored pulse shapes and sequences in the time domain and control the underlying electric field oscillations on the cycle scale. Finally the work will be summarized followed by some future prospects into the field of few-cycle pulse generation and their applications.

2 General theory

This chapter deals with the fundamental theory and relevant basics for understanding the work presented in the following. Starting point will be a short introduction of few-cycle laser pulse generation using Kerr-lens mode-locking, followed by the analytical description of the electric field of few-cycle laser pulses in the time and frequency domain. In this content the carrier-evelope-offset phase, its origin, measurement and stabilization will be explained. Finally noise quantities associated with few-cycle femtosecond lasers and their characterization are discussed. Since an in-deep analysis and a fundamental theoretical treatment of few-cycle pulses, their generation and propagation is beyond the scope of this thesis, the interested reader is referred to the cited literature throughout the text, above all [Sve98, Ell03, Ye05, Kär05, Die06, Mor06, Mor07].

2.1 Few-cycle laser pulse generation

Femtosecond laser pulses with durations as short as a few optical cycles can be generated directly by Kerr-lens mode-locked (KLM) Ti:sapphire oscillators. This is because the optical Kerr-lens is a saturable absorber fast enough without bandwidth limitations that is capable of forcing the numerous modes that can be supported by a Ti:sapphire oscillator to oscillate with a fixed phase relation. In the time-domain this means that all individual standing waves will add constructively at one point, resulting in a very intense and short burst of light [Die06]. The unique combination of the Kerr-lens acting as fast 'artificial' saturable absorber with the broadband gain bandwidth of Ti:sapphire, featuring a full-width at half-maximum (FWHM) of about 95.3 THz [Sor05], is an indispensable prerequisite for the generation of few-cycle laser pulses since both, spectral bandwidth and pulse duration are directly coupled by the time-bandwidth product [Rul05].

The optical Kerr-effect is a $\chi^{(3)}$ nonlinearity that results in an increased refractive index for higher intensities: $n = n_0 + I \cdot n_2$ due to the nonlinear refractive index n_2. This Kerr-effect allows for the realization of a saturable absorber, since an intense burst of photons will experience an increased refractive index within a Kerr-medium and thus in case of a Gaussian intensity beam profile Kerr-lensing compared to low intensity continuous-wave (cw) light. By a suitable resonator design this effect can be used to favor pulsed operation over continuous wave operation. The simplest way in this regard is placing a hard aperture behind the Kerr-medium allowing the focused intense light to pass, whereas the low intensity

light is blocked. In this case the Kerr-lens introduces a loss modulation to the resonator, since the loss is lower for more intense light. The Ti:sapphire oscillators presented within the scope of this thesis use soft-aperture KLM to generate few-cycle laser pulses. Here the pulsed operation is favored over cw-operation via a gain modulation, since the resonator is designed such that only the Kerr-lens assisted, narrowing down intense beam experiences an optimal overlap with the pump beam in the Ti:sapphire crystal, shown in Fig. 2.1. Thus for soft-aperture KLM an intense pulsed operation will experience more gain within the crystal and will be energetically favored. This process of Kerr-lens mode-locking has to be externally initiated by perturbing the initial cw-operation. This perturbation leads to an initial small burst of light that will experience Kerr-lensing within the crystal and becomes amplified. For successive round-trips this effect increases and enhances itself resulting in more and more modes that will be locked to this process.

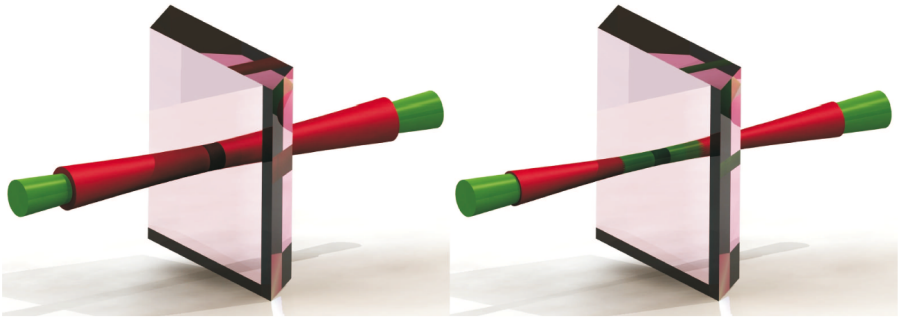

Figure 2.1: Illustration showing the principle of soft-aperture Kerr-lens mode-locking using a optimized pump spot overlap within the Ti:sapphire crystal, taken from [Sie09]. The left-hand-side shows the beam geometries at the crystal for continuous-wave operation whereas the red laser beam is considerably larger than the green pump beam. On the right-hand-side the case of mode-locked operation is shown, where the Kerr-lens assisted smaller mode size results in an optimal overlap of pump beam and resonator beam, leading to an enhanced gain and energetically favored operation.

Next to the missing self-starting ability, one main disadvantage of soft-aperture KLM is the need to operate the laser close to a stability limit of its resonator to enhance the Kerr-effect for stable pulse operation. As a consequence, much effort has to be done to design the resonator for long-term stability and hands-off operation.

2.2 The electric field of few-cycle laser pulses

The electric field $E(z,t)$ of a few-cycle laser pulse in the time domain, propagating along the z-axis can be denoted by:

$$E(z,t) = \frac{1}{2} \cdot A(z,t) \cdot e^{i(\omega_0 t - k(\omega_0)z + \phi_0)} + c.c. \tag{2.1}$$

with the slowly varying envelope $A(z,t)$ and a superimposed carrier oscillation with the angular carrier frequency ω_0. The additional phase term, the carrier-envelope-offset phase ϕ_0, gives the phase difference between the maximum of the envelope with respect to the next maximum of the carrier oscillation underneath, illustrated in Fig. 2.2. In this representation only plane waves are considered without a spacial dependency in x- and y-direction. Even though the measured quantities are real, it is in general more convenient to use the complex representation for these fundamental considerations [Die06]. In this regard the factor $1/2$ and the c.c. (complex conjugate) guarantee for a real electric field in the complex representation given in Eq. (2.1). For the subsequent considerations this is kept in mind but omitted for the following.

The temporal pulse intensity is proportional to the squared absolute value of the electric field: $I(t) \propto |E(t)|^2$ and gives the pulses appearance in the time domain. The pulse duration is typically defined by the full-width at half-maximum of $I(t)$.

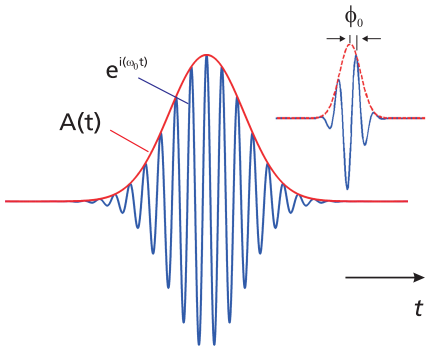

Figure 2.2: Few-cycle laser pulse and its electric field.

This pulse representation illustrated in Fig. 2.2 comprises many aspects of few-cycle laser pulse generation and propagation and will be used later on. In this regard a fundamental understanding of Eq. (2.1) is of importance and will be summarized in the following few paragraphs.

From the section before it is known that a few-cycle laser pulse is a phase-coherent superposition of numerous modes that can simultaneously oscillate within a femtosecond oscillator. For example the broadband gain spectrum of Ti:sapphire can support more than 10^6 modes within the resonator. The electric field of one single, linearly polarized wave with the angular frequency ω, propagating along the z-axis, can be written as:

$$E(z,t) = \tilde{E}_0 \cdot e^{i(\omega t - k(\omega) z + \phi_\omega)}, \tag{2.2}$$

with the propagation constant $k = 2\pi/\lambda = \omega/c \cdot n(\omega)$ and a random phase ϕ_ω of the specific mode. The pulse is established by a phase-locked superposition of all of these modes, now with a global phase ϕ_0:

$$E(z,t) = \int \tilde{E}_0(\omega) \cdot e^{i(\omega t - k(\omega) z + \phi_0)} d\omega. \tag{2.3}$$

Defining the angular carrier frequency ω_0 located within the optical frequency domain, the frequency of every mode can be written by the carrier frequency plus the particular frequency difference: $\omega = \omega_0 + \Delta\omega$. With this expression Eq. (2.3) writes to:

$$E(z,t) = \int \tilde{E}_0(\omega_0 + \Delta\omega) \cdot e^{i((\omega_0+\Delta\omega)t - k(\omega_0+\Delta\omega)z + \phi_0)} d\Delta\omega. \tag{2.4}$$

With $\Delta k = k(\omega_0 + \Delta\omega) - k(\omega_0)$ Eq. (2.4) can be decomposed into the slowly varying envelope $A(z,t)$ containing $\Delta\omega$, and the rapid carrier oscillation ω_0:

$$E(z,t) = \underbrace{\int \tilde{E}_0(\omega_0 + \Delta\omega) \cdot e^{i(\Delta\omega \cdot t - \Delta k \cdot z)} d\Delta\omega}_{\mathrm{A(z,t)}} \cdot e^{i(\omega_0 \cdot t - k(\omega_0)\cdot z)} \cdot e^{i\phi_0}. \tag{2.5}$$

Thus the electric field representation of a pulse propagating in time along the z-axis is given by Eq. (2.1):

$$E(z,t) = A(z,t) \cdot e^{i(\omega_0 \cdot t - k(\omega_0)\cdot z)} \cdot e^{i\phi_0}. \tag{2.6}$$

The time-domain and frequency-domain representations of a laser pulse are connected by the Fourier-transformation:

$$\tilde{E}(\omega) = \int E(t) \cdot e^{-i\omega t} dt; \qquad E(t) = \frac{1}{2\pi} \int \tilde{E}(\omega) \cdot e^{i\omega t} d\omega. \tag{2.7}$$

Thus, for the frequency domain the field is given by:

$$\tilde{E}(\omega) = A(\omega) \cdot e^{-i\varphi(\omega)} \tag{2.8}$$

with the spectral amplitude $A(\omega) = \left|\tilde{E}(\omega)\right|$ and spectral phase $\varphi(\omega)$. $A(\omega)$ gives the intensity contribution of each frequency involved, whereas the spectral phase $\varphi(\omega)$ denotes the corresponding phase. In the case of zero phase all frequencies will superpose constructively at $t = 0$ and form a Fourier-limited pulse. This direct connection between the frequency- and time-domain electric field of a laser pulse is important for the few-cycle field synthesizer presented in Chapter 6. There the temporal pulse envelope will be shaped by manipulation of the spectral amplitude and phase in the frequency domain.

2.2.1 Dispersion and pulse propagation

Summarizing the paragraphs above it is obvious that an ultrashort laser pulse comprises a broadband spectral characteristic and features in the ideal case – the Fourier-limited pulse – a constant spectral phase for all of the involved frequency components. But since the pulse

will experience dispersion while propagating, which is due to the wavelength dependency of the refractive index of the propagation media, pulse broadening will occur. Thus, especially for few-cycle pulses with their broad spectral bandwidths involved, dispersion is of major importance and the relevant terms will be named here. A comprehensive treatment of this topic can be found in cited text books and lecture scripts, e.g. [Mor06].

Most commonly used media feature a decreasing refractive index for longer wavelengths in the target wavelength region. This leads to a positive dispersion, since low-frequent light will travel with a higher phase velocity through the medium than high-frequent light that becomes delayed. For negative dispersion this relation is the other way round. To investigate the dispersion related effects on laser pulses like pulse broadening and chirping, it is common to expand the spectral phase in a Taylor series around ω_0 [Tre10]. This results in the group delay (GD) or first order dispersion, which is the first particular derivative of the spectral phase with respect to ω at ω_0, the group delay dispersion (GDD), or second order dispersion, which is the second particular derivative of the spectral phase with respect to ω at ω_0, and even higher order dispersion terms. The GD describes a pulse shift in time, whereas the GDD and higher orders are responsible for a temporal pulse broadening.

2.3 The carrier-envelope-offset phase

The carrier-envelope-offset phase (CEP) introduced by Eq. (2.1) denotes the phase difference between the maximum of the temporal pulse envelope and the maximum of the nearest electric field oscillation underneath. It can be used to drive field-sensitive experiments, whereas the sensitivity of a specific target is probed depending on the electric pulse field. Additionally, ϕ_0 has relevance for the generation of frequency combs by mode-locked lasers. The origin, measurement and stabilization of ϕ_0 will be discussed in more detail in the following section.

The carrier-envelope-phase of a pulse train can be divided into two components [Kär05], a 'static' offset phase and the pulse-to-pulse phase change $\Delta\phi_0$:

$$CEP = \phi_0 = \phi_{\text{stat}} + \Delta\phi_0. \tag{2.9}$$

$\Delta\phi_0$ has its origin in dispersion within the laser oscillator. This is because the carrier frequency ω_0 propagates with the phase velocity $v_{ph} = c/n(\omega_0)$ within the dispersive regime of the Ti:sapphire oscillator, whereas the pulse envelope experiences the group velocity $v_{gr} = \partial\omega/\partial k$. Since both velocities are in presence of dispersion not identical, ϕ_0 will evolve and slip underneath the envelope during propagation. This phase change depending on the length l of the specific dispersive medium can be calculated by:

$$\Delta\phi_0(l) = \omega \cdot l \cdot \left(\frac{1}{v_{gr}(\omega)} - \frac{1}{v_{ph}(\omega)} \right). \tag{2.10}$$

Every time the pulse hits the output-coupling mirror, a portion is coupled-out and the phase relation is fixed, which is defined by the phase condition at the output-coupling mirror. Since the cavity-pulse will continue to evolve with respect to its CEP during its next roundtrip, the successive pulses of the output pulse train, their delay defined by the roundtrip time $T = 1/f_{\mathrm{rep}}$, will feature a constant phase difference $\Delta\phi_0$ from pulse to pulse. The rate of change of $\Delta\phi_0$ within the pulse train is the carrier-envelope-offset frequency f_{CEO}, which is given by:

$$f_{\mathrm{CEO}} = \frac{\Delta\phi_0}{2\pi} \cdot f_{\mathrm{rep}} \Rightarrow \Delta\phi_0 = 2\pi \cdot \frac{f_{\mathrm{CEO}}}{f_{\mathrm{rep}}}. \tag{2.11}$$

For a free-running laser $\Delta\phi_0$ will have a non-specific value depending on the present resonator design and dispersion characteristics. For the later-on presented stabilization of the CEP there exist two prominent scenarios of the above written relation. In the first case f_{CEO} is an integer fraction n of the repetition frequency. In this case the electric field of every n^{th} pulse within the output-coupled pulse train will be identical. For example if f_{CEO} will be stabilized to a quarter of the repetition frequency, Eq. (2.11) results in a CEP change from pulse-to-pulse of about $\Delta\phi_0 = \pi/2$. As shown in Fig. 2.6 (A), every fourth pulse within the train will be identical. The second scenario occurs when the evolving phase exactly reproduces itself along one roundtrip, $\Delta\phi_0$ being an integer multiple of 2π. In this case the output-coupled pulses will feature a constant CEP without a pulse-to-pulse phase change and the electric field of each pulse will be identical and f_{CEO} zero, illustrated in Fig. 2.6 (B).

It can be shown that the periodic pulse train of a mode-locked laser produces a frequency spectrum that is a series of delta functions [Ude02a], when the number N of pulses approaches infinity:

$$I_N(\omega) \rightarrow I(\omega) \sum_n \delta(\omega T - \Delta\phi_0 - 2\pi n). \tag{2.12}$$

For an increasing number of pulses the initial continuous spectrum of a single pulse $I(\omega)$ evolves more and more to a discrete comb structure with a decreasing linewidth for an increasing N. From the positions $\omega T - \Delta\phi_0 - 2\pi n$ of the delta peaks given by Eq. (2.12), the frequency of each n^{th} (optical) comb mode is given by:

$$\omega_n = n \cdot \frac{2\pi}{T} + \frac{\Delta\phi_0}{T} \Rightarrow \nu_n = n \cdot f_{\mathrm{rep}} + f_{\mathrm{CEO}}, \tag{2.13}$$

and can be described by only two radio frequencies in the MHz range. The relation between the periodic output of a mode-locked laser and a discrete comb spectrum in the frequency domain is illustrated in Fig. 2.4. In this representation the carrier-envelope-offset frequency gives a constant offset from zero frequency for all comb modes that are spaced by f_{rep}.

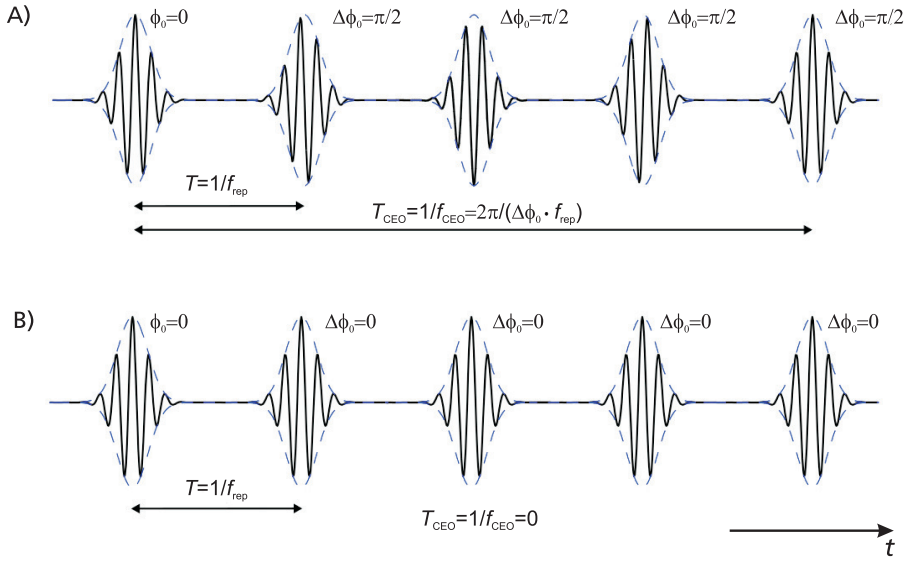

Figure 2.3: Pulse train emitted by a mode-locked laser; A) shown for a pulse-to-pulse change of $\Delta\phi_0 = \pi/2$ resulting in a reproduced field for every fourth pulse within the train; B) with $\Delta\phi_0 =$ constant, $f_{\mathrm{CEO}} = 0$ respectively. Every pulse is identical.

2.3.1 CEP measurement and stabilization

The techniques used to stabilize the pulse-to-pulse evolution of the carrier-envelope-offset phase are best understood in the frequency domain [Kär05], since from Eq. (2.11) we see immediately that a stabilization of $\Delta\phi_0$ is identical to a stabilization of f_{CEO}. The simplest way to measure f_{CEO} is to frequency-double the low frequency 'red' end of the spectrum and heterodyne it with the existing fundamental spectrum at the 'blue' end. Since for heterodyne detection it is essential that the two frequency components spectrally overlap, an octave-spanning spectrum containing both frequencies ν_n and ν_{2n} is required. This most prominent example of self-referencing, illustrated in Fig. 2.5, was first demonstrated by [Ude99, Tel99, Jon00] after non-linear broadening the spectrum to an octave-spanning bandwidth using a photonic crystal fiber.

Using the comb relation given by Eq. (2.13) it can be shown, that the heterodyne beat frequency f_b of the frequency-doubled 'red' component $(2 \cdot \nu_n)$ and the fundamental 'blue' component (ν_{2n}) is simply the carrier-envelope-offset frequency:

$$\begin{aligned} f_b &= 2 \cdot \nu_n - \nu_{2n} \\ &= 2 \cdot (n \cdot f_{\mathrm{rep}} + f_{\mathrm{CEO}}) - (2n \cdot f_{\mathrm{rep}} + f_{\mathrm{CEO}}) \\ &= 2n \cdot f_{\mathrm{rep}} + 2 \cdot f_{\mathrm{CEO}} - 2n \cdot f_{\mathrm{rep}} - f_{\mathrm{CEO}} \\ &= f_{\mathrm{CEO}}. \end{aligned} \tag{2.14}$$

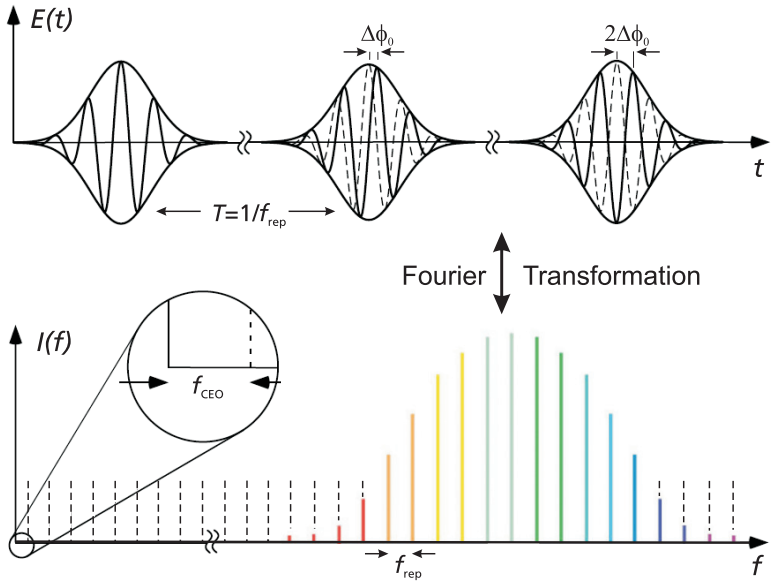

Figure 2.4: The periodic pulse train emitted by a mode-locked laser generates a frequency spectrum with discrete comb modes given by the Fourier-relation [Ude02a].

This beat signal can be generated in an *f*-to-*2f* interferometer, see e.g. Section 3.2.1, whereas the signal is detected with a highly sensitive photodiode. The phase term of the corresponding interference signal $I(t)$ features a linear dependency with respect to f_{CEO}:

$$\phi_{\mathrm{detect}} = 2\pi f_{\mathrm{CEO}} t + \phi_{\mathrm{stat}}. \tag{2.15}$$

The term ϕ_{stat} arise from the 'static' offset of the CEP (see Eq. (2.9)) and is constant for the interference signal. Since there is no dispersion in this ideal case, the intensity of all spectrally and temporally overlapping components will globally alternate in time with f_{CEO}. For a 'real world' *f*-to-*2f* interferometer the dispersion between the two interferometer arms, given by the different optical components and pathways, will introduce a spectral modulation to the interfering spectrum as given in Fig. 2.6. The frequency for zero delay can be altered by tuning one arm length of the interferometer, whereas the modulation strength is depending on the amount of dispersion between both interferometer arms. This spectral modulation has large impact for the detection scheme. All spectral components will still alternate in time with f_{CEO}, but due to the spectral modulation the successive spectral interference fringes will alternate converse with respect to each other. Since the detector integrates the intensity given by all detected frequency components, the measured intensity change resulting from f_{CEO} will wash out for the integration of several fringes. To overcome this problem a narrow spectral bandpass around the frequency component with zero delay

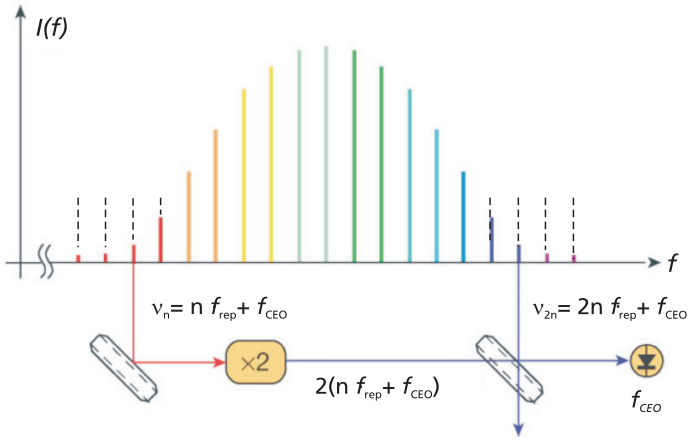

Figure 2.5: Principle of *2*-to-*2f* self-referencing. The low-frequent 'red' end of an octave-spanning spectrum is frequency doubled and spectrally overlapped with the existing 'blue' end for heterodyne detection [Goh06].

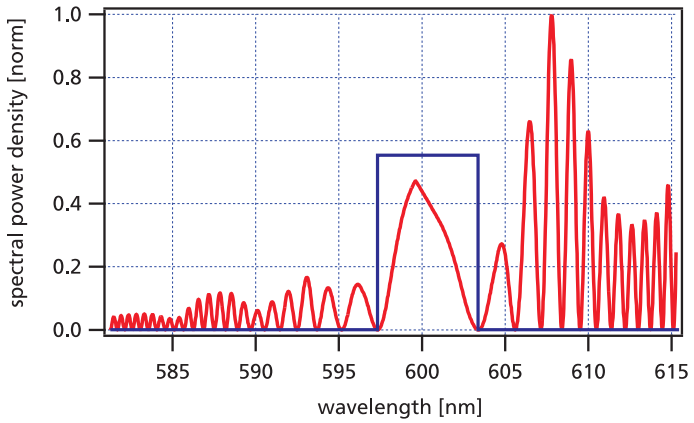

Figure 2.6: Modulated spectrum from the interference between the frequency-doubled 'red' end of the laser spectrum with the fundamental 'blue' end. The zero delay point is tuned-in for a wavelength of 600 nm. The blue plot indicates a spectral filter that has to be applied to detect f_{CEO} with sufficient contrast.

has to be filtered form the interfering spectrum, such that the detected intensity change given by f_{CEO} is large enough to deliver a sufficient signal-to-noise ratio for this signal. In the ideal case only one spectral interference fringe is filtered from the spectrum, indicated by the blue filter curve in Fig. 2.6. In case of $f_{\mathrm{CEO}} = 0$ the temporal modulation of the interference spectrum will be gone, opening up to detect a constant spectral interference pattern as shown in Fig. 2.6.

As already mentioned, for the *f*-to-*2f* self-referencing technique as presented above, an octave-spanning spectrum is a indispensable prerequisite. Fortunately meanwhile

Ti:sapphire laser oscillators are readily available, delivering such octave-spanning spectrum directly from the oscillator and allowing for f_{CEO} stabilization without additional external spectral broadening. This is preferable in terms of noise and requires much less spectral output power for the stabilization compared to e.g. spectral broadening within a nonlinear fiber, since for octave-spanning oscillators the necessary spectral components for self-referencing can be filtered from the laser's output spectrum and used directly for heterodyne beating.

Next to this 'standard' self-referencing technique using octave-spanning spectra, there exist different non-linear mixing processes that can be used to generate a heterodyne beat signal for f_{CEO} as well. For example also *2f*-to-*3f* mixing [Tel99] can utilized in this regard next to difference frequency generation within a periodically poled lithium niobate crystal (PPLN) [Fuj04]. In recent years this approach has become a serious alternative to spectral broadening using microstructured fibers. Here the beat signal is generated by a combination of self-phase modulation (SPM), leading to a broadening of the fundamental spectrum within the PPLN crystal, and difference frequency generation of the 'blue' end of the spectrum to the SPM-broadened 'red' end. Since both processes are realized simultaneously within the PPLN crystal, very compact detection setups can be realized.

For all interferometer-based techniques it is essential that the frequency components intended to interfere for heterodyne f_{CEO} detection have to overlap temporally and spatially. As above mentioned this can be accomplished using various types of interferometers. The most common setups in this regard are Mach-Zehnder-type and Michelson-type, the latter used in the scope of this thesis, see Section 3.2.1. But also so-called 'common path' interferometers [Gre09a] with an reduced noise contribution, or collinear setups whereas the temporal delay between the interfering pulses is optimized with several bounces on dispersion compensating mirrors [Müc05] are meanwhile utilized for f_{CEO} detection. All the named techniques also differ by the required power to generate a suitable f_{CEO} beat signal. Here the use of octave-spanning spectra directly from the oscillator is superior since only approximately 10 % (20 mW) of the available output power containing the spectral wings is required for the beat generation. Techniques relying on nonlinear broadening in fibers or crystals require up to 200 mW power for this conversion. This can only be tolerated since the utilized narrowband oscillators feature a higher average output power compared to octave-spanning systems. For octave-spanning laser oscillators an alternative approach for the separation of the *f-2f* components without impacting the spectral width and output power has been demonstrated using semitransparent mirrors at the *f* and *2f* wavelength [Cre08] and thus using a different output-port of the Ti:sapphire oscillator for stabilization.

After the carrier-envelope-offset frequency has been measured with sufficient signal-to-

noise ratio[1] (SNR) using the above presented techniques, its stabilization is straight forward. As it is known from Section 2.3 the CEP is determined by the dispersion conditions within the laser oscillator and will usually fluctuate e.g. due to acoustic noise for a free-running oscillator. Since all broadband laser systems contain elements for dispersion fine-tuning such as intra-cavity prisms or a wedge pair, see Section 3.2, it is possible to tune the CEP by changing the intra-cavity dispersion characteristics. On the other hand it was shown that a modulation of the applied pump power to a Ti:sapphire oscillator can be used to change the CEP [Pop01] as well, whereas at present time the physical mechanism is not clearly understood [Jon05]. Several possibilities may cause a sensitivity of ϕ_0 changing with the pump power, e.g. a nonlinear phase shift within the Ti:sapphire crystal [Apo00, Pop01]. Nevertheless with these knobs for controlling ϕ_0, f_{CEO} respectively, this frequency can be phase-locked to some reference.

Usually the reference frequency f_{Ref} used for stabilization is directly derived from the repetition frequency of the laser oscillator by dividing it down to an integer fraction, e.g. the fourth part. Using the intra-cavity dispersion fine-tuning element, f_{CEO} is tuned to frequency-match this reference. The stabilization is established by phase-locking f_{CEO} to f_{Ref} using a phase-looked loop (see App. B), controlling the applied pump power to the crystal via an acousto-optic modulator, or tilting a mirror within an intra-cavity prism-sequence.

2.4 Noise in femtosecond laser oscillators

Femtosecond laser oscillators are susceptible to different types of noise affecting their output characteristics and performance. For Ti:sapphire oscillators the origin of noise is dominated by mechanical vibrations, thermal effects and quantum fluctuations acting on the cavity and laser crystal [Pas06]. The following few paragraphs will focus on the relevant noise aspects important within the scope of this thesis, which are essentially phase noise contributions. A comprehensive treatment of noise related issues of mode-locked lasers in general can be found in [Lin86, Son92, Pas04a, Pas04b, Pas06, Pro09].

An important noise-related parameter of periodic events such as a pulse train emitted by mode-locked lasers is the timing jitter, which is the deviation Δt of the temporal pulse position at a specific time to that of a perfectly periodic pulse train with a periodicity $T = 1/f_{\mathrm{rep}}$. Phase noise describes the phase deviation $\Delta\varphi$ from the actual waveform e.g. at a zero-crossing from a perfectly homogeneous sinusoidal signal, illustrated in Fig. 2.7 (B). The timing- and phase fluctuations thereby are connected by:

1 A SNR of 25 dB - 30 dB measured within a 100 kHz resolution bandwidth was found to be at least necessary for a CEO stabilization.

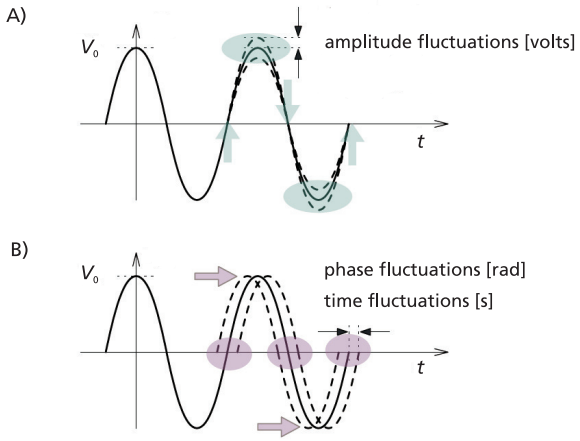

Figure 2.7: Noise related imperfection of a sinusoidal oscillator output [Rub06]. The output can be affected by amplitude noise A), and phase noise B), leading for mode-locked lasers to a temporal fluctuation of the pulse arrival time.

$$\Delta\varphi = 2\pi f_0 \Delta t \Rightarrow \Delta t = \frac{1}{2\pi f_0}\Delta\varphi. \tag{2.16}$$

The spectrum of an ideal, noiseless oscillator producing a pure sinusoidal output in time would be a single pair of delta functions at the oscillator's frequency. Since all real oscillators exhibit noise which spreads the power of a signal to adjacent frequencies, the delta spectrum will be accompanied by a symmetric sideband around the carrier frequency, referred to as two-sided power spectral density (PSD) $S(f')$. Here f' denotes the Fourier- or noise frequency relative to the carrier frequency.

The power spectrum of a mode-locked laser is the Fourier transform of the autocorrelation function of the emitted pulse train [Lin86, Son92]. Like for an ideal oscillator, this spectrum consists of distinct spikes at harmonics of the repetition frequency $f_{\mathrm{rep}} = 1/T$, but is surrounded by some pedestal accounting for the phase noise [Pop98]. Assuming a small timing jitter [Lin86] and no coupling between amplitude and phase noise, the power spectrum of the n^{th} harmonic of the repetition frequency the is given by:

$$P_n(f') \approx P_c \left[S_A(f') + (2\pi n f_{\mathrm{rep}})^2 S_\varphi(f') \right], \tag{2.17}$$

with $S_A(f')$ and $S_\varphi(f')$ being the power spectral densities of the amplitude and phase fluctuations respectively [Son92]. From Eq. (2.17) it can be seen that the phase fluctuation grows quadratically with the harmonic order n whereas the amplitude noise is constant with n, illustrated in Fig. 2.8.

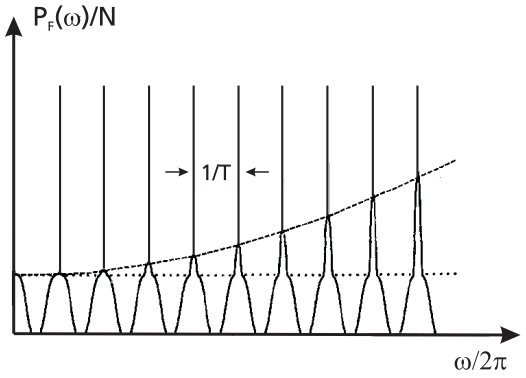

Figure 2.8: Power spectrum of a pulse train emitted by a mode-locked laser [Lin86]. The dotted line indicates the maxima of the noise bands representing amplitude noise, whereas the dashed line is proportional to n^2 marking the maxima for the phase noise contribution.

The noise power spectral density $L(f')$ of the n^{th} harmonic is given by:

$$L_n(f') = 10 \cdot \log \frac{P_n(f')}{\alpha B \cdot P_c}, \tag{2.18}$$

what is usually measured by radio frequency spectrum analyzers. $L_n(f')$ gives the relative noise power $P_n(f')$ in a narrow frequency band (B) at frequency offset (f') and is denoted in units dBc/Hz (dB below the carrier per Hz of bandwidth). The factor α accounts for the equivalent noise bandwidth of the used spectrum analyzer. According to *von der Linde* [Lin86] and *Son* [Son92] the relation given by Eq. (2.17) and (2.18) can be used to extract the phase noise power spectral density $L_\varphi(f')$ by measuring the noise PSD of the fundamental repetition frequency $L_1(f')$ and that of a higher harmonic n, $L_n(f')$, and dispose the amplitude noise by subtracting $L_1(f')$ from $L_n(f')$:

$$L_\varphi(f') = 10 \cdot \log \left\{ \left[10^{\frac{L_n(f')}{10}} - 10^{\frac{L_1(f')}{10}} \right] / (n^2 - 1) \right\}. \tag{2.19}$$

This method can only be applied if there is no coupling between amplitude and phase noise as for Eq. (2.17). For the phase noise analysis performed within this thesis, this correction with respect to amplitude noise is not performed, since the measurements were all performed at a harmonic order large enough that the influence of amplitude noise can be disregarded, what was experimentally approved. Thus the phase noise power spectral density is given by:

$$L_\varphi(f') = 10 \cdot \log \left\{ \left[10^{\frac{L_n(f')}{10}} \right] / n^2 \right\}. \tag{2.20}$$

$L_\varphi(f')$ can be directly used to calculate the accumulated root-mean-square (rms) timing jitter $\sigma_{\Delta t}$ via the rms phase error $\sigma_{\Delta\varphi}$ by integrating over the noise frequency within a specific frequency range defined by f_L and f_H:

$$\sigma_{\Delta t} = \frac{1}{2\pi f_0} \cdot \sigma_{\Delta\varphi} = \frac{1}{2\pi f_0} \cdot \left[2 \int_{f_L}^{f_H} L_\varphi(f') df' \right]^{1/2} . \tag{2.21}$$

3 Octave-spanning Ti:sapphire laser system

The first experimental chapter of this thesis deals with the octave-spanning Ti:sapphire laser system that has been realized to generate femtosecond pulses with electric field oscillations as short as 1.5 optical cycles. At the beginning of this chapter a few important aspects concerning the generation of octave-spanning spectra directly from Ti:sapphire oscillators will be discussed, followed by the presentation of the octave-spanning prism-less laser system featuring a Fourier-limited pulse duration as short as 3.7 fs. Secondly, the carrier-envelope-offset phase stabilization and timing control of this system will be explained followed by considerations in order to generate a frequency comb.

3.1 Generation of broadband spectra from Ti:sapphire oscillators

From Chapter 2 it is known, that an ultrashort laser pulse necessarily requires a broadband spectral characteristic. For few-cycle laser pulses as generated within the scope of this thesis the underlying output spectra feature a width spanning a whole optical octave[1]. Next to a broadband gain medium and an ultrafast mode-locking mechanism, the generation of such broadband output spectra directly from a laser oscillator requires a mechanism that compensates for the positive dispersion within the cavity to re-compress the pulses within the Ti:sapphire crystal at every round-trip. This broadband dispersion compensation is usually done by a set of dispersion compensating mirrors or in combination of those with a prism sequence. The design of such chirped multilayer coatings is a quite challenging task, since it is not possible by using standard chirped mirror techniques to generate a high reflectivity for a broadband wavelength range together with a smooth dispersion characteristic covering the whole supported spectral range [Kär05]. Next to bandwidth limitations the crucial aspects here are dispersion oscillations, that result from interference between the slight reflection in the front section and strong reflections from the back within the layer structure of the chirped mirror stack, next to the impedance mismatch between the ambient medium and the

1 Few-cycle laser pulses with declared octave-spanning output spectra do not feature this bandwidth at the FWHM of the spectral power density. For those laser systems results a beat note with a signal-to-noise ratio greater than approximately 25 dB, when frequency doubling the 'red' end of the spectrum and heterodyning it with the available spectrum at the 'blue' end.

back mirror [Kär05]. In this regard the development of the double-chirped mirror[1] (DCM) in 1997 [Kär97] was the foundation for the generation of few-cycle laser pulses directly from Ti:sapphire oscillators. Using this mirror concept together with a low-dispersion glass material for an intra-cavity prism sequence, it was possible to generate pulses as short as 5.4 fs (FL: 4.9 fs) [Mor99] directly from an oscillator.

Within the last decade many approaches have been made to generate even broader output spectra supporting bandwidths exceeding one optical octave. Key to these investigations was the theoretical work on dispersion-managed mode-locking [Che99], predicting a bandwidth limitation mainly arising from the used dispersion compensating mirrors and not from the gain medium. This was followed by a successive development of the double-chirped mirror pairs (DCMPs) [Kär01], featuring a reflectivity greater than 99.8 % for an octave-spanning bandwidth, second and third order dispersion compensation over the whole spectral range and residual weak dispersion oscillations. One of the pair-mirrors features an additional quarter-wave layer between the antireflection coating and the back mirror, a schematic given in Fig. 3.1. This new mirror concept tolerates larger dispersion oscillations for the single pair-mirror, since due to the additional quarter-wave layer these oscillations will cancel out for successive reflections on both mirrors.

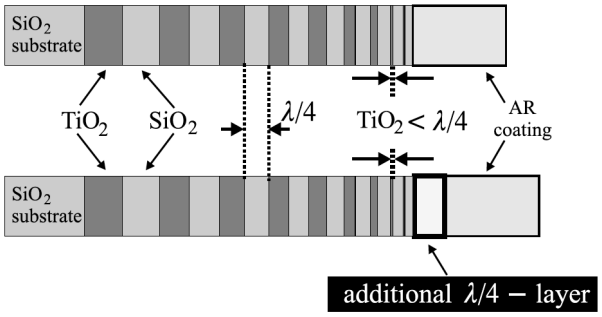

Figure 3.1: Schematic layer structure of the mirrors contained in a double-chirped mirror pair, taken from [Ell03]. Both pair mirrors differ from each other by one additional quarter-wave layer resulting in a π-shifted phase with respect to each other. Used in combination, the dispersion oscillations of both mirrors will cancel out.

Like for other chirped mirrors the desired dispersion curve is obtained by varying the Bragg resonance with the penetration depth into the mirror. The resonance for low frequency components is situated deeper in the stack than for higher frequency components, resulting

1 Next to a broadband reflectivity and negative dispersion characteristic, these DCMs feature an antireflex (AR) coating for impedance matching the mirror to the ambient air and a gradually increasing thickness of the high index material layer within the mirror Bragg-stack, called double-chirp. A comprehensive introduction and overview of the challenges associated with broadband dielectric multilayer mirrors can be found in [Kär05].

in a negative dispersion characteristic, delaying longer wavelength with respect to shorter ones.

The availability of octave-spanning mirror pairs alone is not sufficient to generate output spectra from Ti:sapphire oscillators spanning the whole supported mirror bandwidth. A mechanism has to be found to generate additional spectral components beyond the native Ti:sapphire gain spectrum. In this regard self-phase modulation was found suitable to generate additional spectral components within Ti:sapphire oscillators. Ell et. all used a combination of broadband DCMPs together with a second intra-cavity focus where nonlinear effects in a BK7 substrate generate additional SPM to broaden the spectrum and enhance KLM. The obtained output spectrum of this system supports a Fourier-limited pulse duration as short as 4.3 fs and a re-compressed pulse duration of 5.0 fs [Ell03]. Binhammer et al. extended this concept and replaced the BK7 substrate by a BBO crystal, further broadening the intra-cavity spectrum and leading to a Fourier-limited pulse duration as short as 4.1 fs and re-compressed pulses as short as 4.6 fs [Bin06]. Both oscillators featured a CaF_2 prism sequence as part of the intra-cavity dispersion compensation, since the higher order dispersion of the used mirrors was designed in this respect.

Meanwhile the mirror design and manufacturing of DCMPs was successively improved, now supporting a high reflectivity and tailored negative dispersion characteristic over more than one optical octave. These mirrors allow for robust, prism-less resonator designs by employing only DCMPs and an output-coupling mirror [Sch03], avoiding the need for a second intra-cavity focus and an additional prism sequence within the laser. Here the emission spectrum of Ti:sapphire is enhanced by SPM within the crystal itself. For these type of oscillators, which are similar to the one presented in this thesis, Fourier-limited spectra below 4 fs could be demonstrated [Sch03, Müc05].

The spectral characteristic of the DCMPs used here is given in Fig. 3.2. As it can be seen these mirrors show a high-reflectivity spanning from 600 nm up to 1200 nm and a second order dispersion of -60 fs^2 for 800 nm with minor remaining oscillations for the pair. Like for other dispersion compensating mirrors the material used for manufacturing these multilayer mirror coatings is TiO_2 (n=2.4) and SiO_2 (n=1.48). The mirror design features altogether 82 layers for the back mirror and the anti-reflex coating. One of the mirrors called 'green' features a spectral transmission window with low reflection for 515 nm - 532 nm, for pumping the Ti:sapphire crystal. The remaining dispersion oscillations within the mirror characteristics, measured with a white-light interferometer, arise from slightly shifted dispersion characteristics of the two mirrors with respect to each other, see Fig. 3.2 (B). This is because the sophisticated layer structure of the mirror design makes great demands for the fabrication process, since the different layers have to be realized with sub-nm precision for a single layer. The dispersion characteristics are extremely sensitive to variations in the layer thickness. Up to now this high-precision fabrication process can exclusively be done by ion beam sputtering (IBS) [Sch94]. The dispersion characteristic of these mirrors is designed to compensate for Ti:sapphire and Barium Fluoride (BaF_2). Here BaF_2 is included,

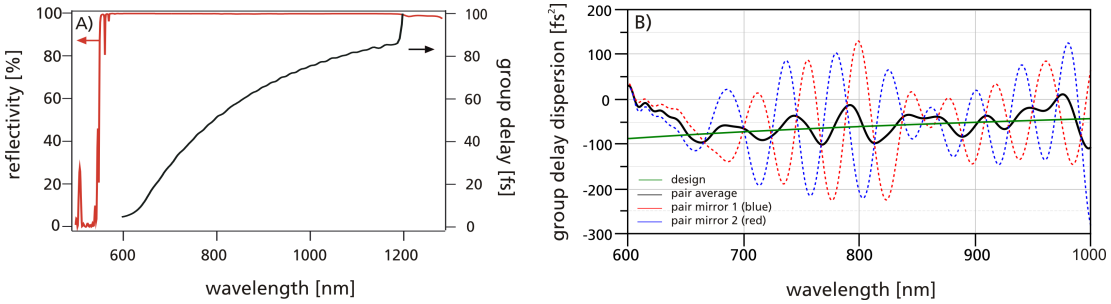

Figure 3.2: Characteristics of the double-chirped mirror pairs used within the scope of this thesis; A) Octave-spanning reflectivity and nearly smooth group delay; B) Dispersion oscillations given for the single pair mirrors and the average of both. The remaining oscillations result from slight variations of the layer structure given by the design and the manufacturing process.

because this glass material features a similar ratio of second and third order dispersion to that of air and thus can be used for dispersion fine-tuning within the resonator.

3.2 Ti:sapphire oscillator with 3.7 fs Fourier-limited pulse duration

The octave-spanning Ti:sapphire oscillator built-up during this thesis uses the above presented double-chirped mirror pairs and features a prism-less design without the need for a second intra-cavity focus. The unique feature of this laser oscillator compared to others [Sch03, Müc05] is the combination of DCMPs with a specially designed broadband dispersive output coupling mirror (OC), which is utilized instead of the standardly used ZnSe-MgF_2 OC. Especially for broadband femtosecond oscillators the output-coupler characteristic is important for the overall laser performance since it is responsible for the intra-cavity pulse energy, pulse dynamics, the spectral shape and thus duration of the pulses coupled out. The novel broadband output-coupling mirror used here consists of overall 36 alternating layers of TiO_2 and SiO_2, its output characteristics are shown in Fig. 3.3 (blue) in comparison to a broadband ZnSe-MgF_2 quarter-wave stack output-coupling mirror (red) which is used for the generation of octave-spanning spectra as well. It can be seen that the output-coupling bandwidth of the used OC is more broadband compared to the standard quarter-wave stack and allows for an increased intra-cavity bandwidth. The supported spectral bandwidth at FWHM is approximately 200 nm more broadband allowing for a superior laser performance as depicted in the sections below. At 800 nm the output-coupling ratio is about 2 % @ 800 nm and about 1 % higher than that of the standard OC. Next to the larger spectral bandwidth this novel output-coupling mirror features a dispersion characteristic that allows in combination with the cavity mirrors for an improved laser performance since it completes the former odd number of DCMP mirrors.

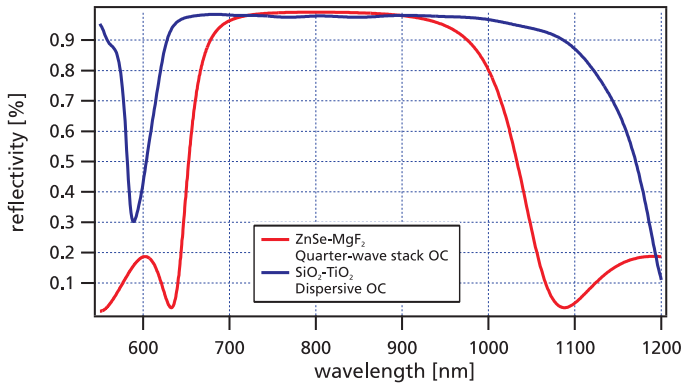

Figure 3.3: Characteristic of two different broadband output coupling mirrors used to obtain octave-spanning spectra directly form a Ti:sapphire oscillator.

The schematic setup of the laser system is given in Fig. 3.4. This design holds for all Ti:sapphire oscillators presented within the scope of this thesis, with slight changes in terms of used mirror sets including the output-coupling mirror and different resonator lengths. This type of resonator is designed for soft-aperture Kerr-lens mode-locking, see Section 2.1. Optical pumping of this laser is done by focusing approximately 5.0 W of 532 nm

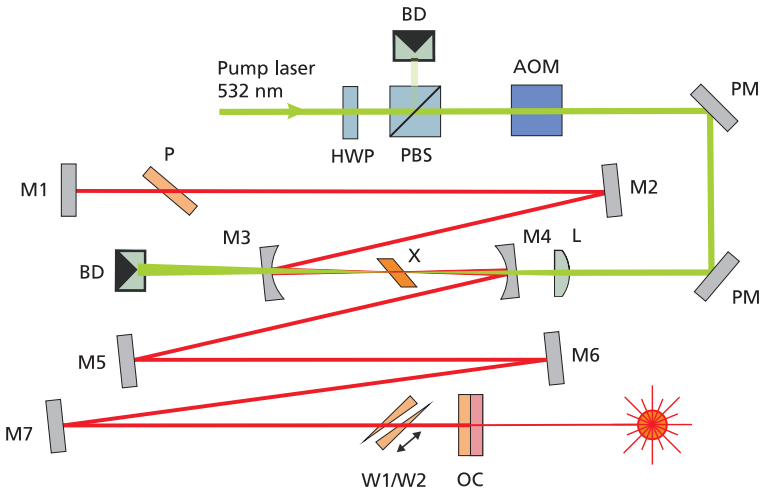

Figure 3.4: Schematic setup of the octave-spanning Ti:sapphire oscillator; AOM: acousto-optic modulator, BD: beam dump, HWP: half-wave plate, L: focusing lens, M1-M7: dispersion compensating mirrors (DCMPs), OC: output-coupling mirror, P: BaF_2 plate, PBS: polarizing beamsplitter cube, PM: pump aligning mirror, W1/W2: BaF_2 wedge pair, X: Ti:sapphire crystal.

light emitted by a frequency-doubled Nd:YVO_4 laser (Coherent Verdi V18) through cavity mirror M4 – one of the 'green' resonator mirrors – into the Ti:sapphire crystal. The applied pump power can be either fine-tuned by a combination of half-wave plate and polarizing

beamsplitter cube or an acousto-optic modulator placed in the pump beam, used later on for carrier-envelope-offset frequency control, see Section 3.2.1. Together with a radius of curvature of the two central resonator mirrors (M3 & M4) of -100 mm, a focused spot size of approx. 20 μm results within the laser crystal. The Ti:sapphire rod is placed under Brewsters angle into the central position of this laser and features a path length of 2 mm.

For mode-locked operation this resonator features two stability regions depending on the distance between the central resonator mirrors and the crystal position. For this laser best mode-locked performance is achieved for the 'outer' region with both mirrors approximately 104 mm separated from each other and the crystal placed some millimeters closer to the short arm of the oscillator, featuring an arm-length ratio of 1:2, see Fig. 3.4. Around this central part an astigmatism-compensated z-folded cavity is built-up by overall seven broadband DCMP mirrors. With respect to the astigmatism-compensation the incident angles are chosen to be 6° resulting in a folding angle of 12° for this laser. The mirror design already accounted for this mode of operation, since a differing incident angle on the mirror layer structure would lead to a different effective layer thickness and thus varying spectral mirror characteristics. Dispersion balancing and fine-tuning is achieved by a BaF_2 wedge pair with a central thickness of 1.7 mm and 1.9 mm respectively, placed in the longer arm, and an additional BaF_2 plate with a thickness of 2.0 mm placed in the shorter arm of the laser. The overall amount of additional glass material is distributed in both arms to balance in combination with the DCMP mirrors the dispersion. This balancing is important for the overall laser performance since it influences the stability by enhancing KLM [Che99]. All the glass material is uncoated and put under Brewsters angle of 55° into the beam to minimize reflection losses. By altering the insertion of one BaF_2 wedge, the net intracavity dispersion can be tuned for optimum laser performance and broadest output spectrum. The output-coupling mirror placed at the end of the longer resonator arm leads to a collimated output beam with a beam radius of approximately 500 μm.

The ultra-broadband output spectrum of this laser oscillator is shown in Fig. 3.5 on a linear (left) and logarithmic scale (right). It covers more than one optical octave, which is already reached at approx. -17 dBc, supporting Fourier-limited pulses as short as 3.7 fs. At -30 dBc the spectral width exceeds 700 nm and even on a linear scale spectral parts beyond 1200 nm are clearly visible. The characteristic peak around 630 nm results from the characteristic roll-off of the output coupling mirror starting at this wavelength to be high-reflective, see Fig. 3.3. In comparison to different octave-spanning output spectra generated from Ti:sapphire oscillators, the spectral characteristic of this unique laser system is much more broadband reaching far into the infrared wavelength region and features much more intensity in the central part of the spectrum. For comparison reasons Fig. 3.6 shows this spectrum next to a different octave-spanning one exemplarily from [Bin06], that

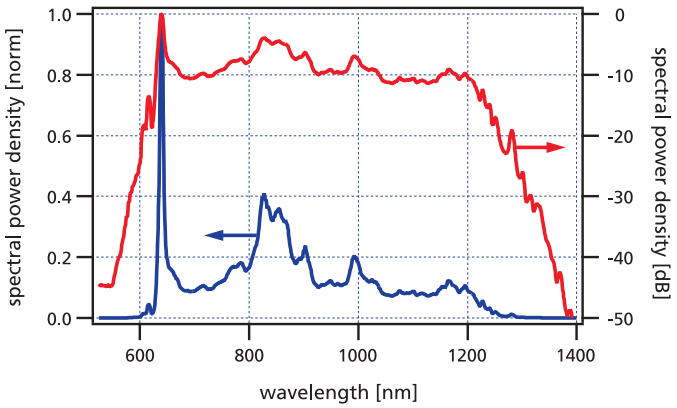

Figure 3.5: Octave-spanning output spectrum supporting Fourier-limited pulses as short as 3.7 fs, shown on a linear (left axis) and logarithmic scale (right axis).

features due to the more M-shaped profile[1] a Fourier-limited pulse duration as short as 4.1 fs. Although the improvement in the resulting pulse duration is in the order of some tenth of a femtosecond, the difference of the emitted spectral characteristics is striking. This enhancement in the spectral output characteristic allows first of all for providing an experimentally more favorable spectrum, e.g. as used for the few-cycle field synthesizer presented in Chapter 6. On the other hand a CEP stabilization of this laser system without additional spectral broadening is straight forward, as presented in Section 3.2.1.

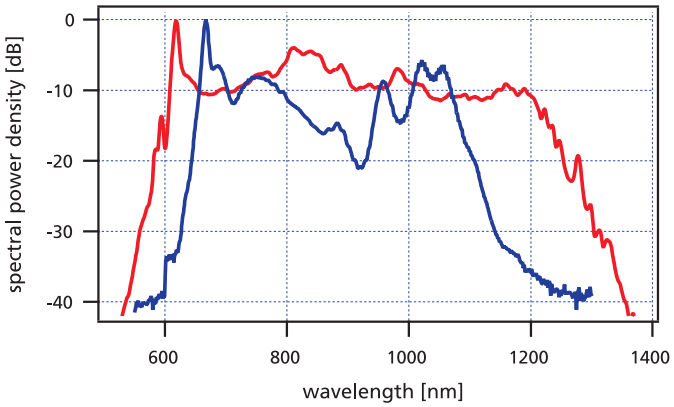

Figure 3.6: Comparison of the octave-spanning output spectra by the 3.7 fs-laser (red) and a different octave-spanning Ti:sapphire oscillator with 4.1 fs Fourier-limited pulse duration (blue) [Bin06].

The emitted few-cycle femtosecond pulses were characterized by a home-built SPIDER system, see App. A for the principle of SPIDER. To compensate for the extra-cavity dispersion

1 It is known, that due to the Fourier-relation an M-shaped spectrum leads to a shorter Fourier-limited pulse duration compared to a e.g. rectangular spectrum featuring the same spectral width.

a pulse re-compression was realized with overall six reflections on DCMP mirrors and some BaF_2 bulk material for dispersion fine-tuning. The used components are analog to those used within the laser cavity. The reconstructed temporal pulse intensity profile is plotted in Fig. 3.7 next to the measured temporal phase.

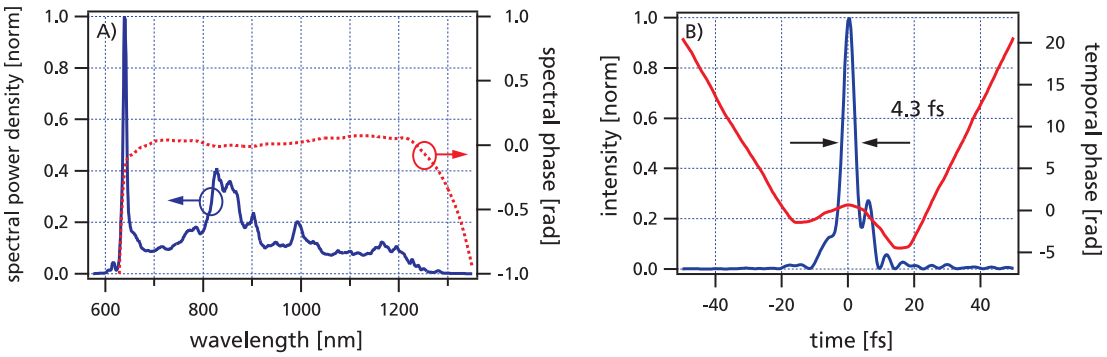

Figure 3.7: Pulse characterization with SPIDER; A) Spectrum and measured spectral phase; B) Intensity profile and reconstructed temporal phase, revealing a pulse duration as short as 4.3 fs.

The pulse duration is measured to be as short as 4.3 fs (FWHM), so far to the best of our knowledge the shortest pulses ever generated directly from a Ti:sapphire oscillator [Rau08b]. The central part of the pulse shown in Fig. 3.7 (B) carries 80 % of the emitted energy. The pre-pulse with approx. 20 % relative intensity that can be found close to the few-cycle pulse can be explained by the laser characteristic and pulse re-compression scheme. First of all the structured spectrum of the laser leads to pre-pulsing by Fourier-transforming this signal with assumed flat spectral phase into the time domain. Secondly, the pulse compression with several bounces on DCMP mirrors leads to a modulated spectral phase enhancing pre-pulsing as well. This influence arises from the target design curve and minimal deviations in the manufacturing process of both mirrors included in the pair. Due to this imperfection the dispersion ripples do not cancel out perfectly, resulting in a net dispersion modulation, given in Fig. 3.2 (B). Within the laser this is cleaned by the KLM process.

A radio-frequency analysis of the emitted pulse train is shown in Fig. 3.8, verifying a stable and clean mode-locked operation for this laser without double-pulsing and q-switching.

Beside pulse duration and spectral bandwidth, the other specifications of this laser oscillator are given in Tab. 3.1. This system features an average output power of about 100 mW at a pulse repetition frequency of 80 MHz resulting in pulse energies of 1.25 nJ. The pulse peak power was estimated by calculating the amount of energy in the central part of the pulse and relating this to the pulse duration of 4.3 fs.

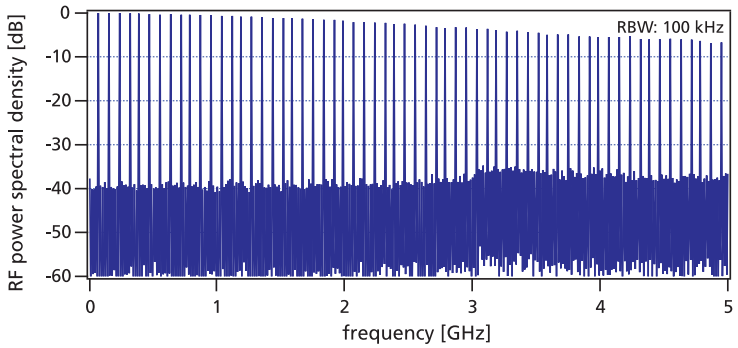

Figure 3.8: Radio frequency analysis of the 3.7 -fs oscillator measured with a fast photodiode detector. The distinct spikes are separated by f_{rep}.

Table 3.1: Specifications of the Ti:sapphire laser oscillator

Parameter	Value
Spectral bandwidth	600 nm @ -17 dBc
Pulse duration	3.7 fs (Fourier-limited), 4.3 fs (SPIDER characterized)
Average output power	100 mW
Pulse repetition frequency	80 MHz
Pulse energy	1.25 nJ
Pulse peak power	224 kW

The octave-spanning spectrum of this laser system allows for a direct stabilization of the system's carrier-envelope-offset frequency without any additional spectral broadening using *f*-to-*2f* self-referencing as presented in the section below.

3.2.1 Carrier-envelope-offset phase stabilization

Due to the octave-spanning output spectrum of this laser, the carrier-envelope-offset phase can be stabilized directly, without any additional spectral broadening, using the *f*-to-*2f* self-referencing technique, see Section 2.3. The two required spectral components chosen here, centered at 570 nm and 1140 nm, can be extracted from the output spectrum by using a two-color multichroic transmission filter (MCF, an extra-cavity used broadband output-coupling mirror). Due to the spectral characteristics of this optical element the central part of the spectrum becomes reflected with approx. 98 -99 % and can be used with unchanged beam quality for subsequent experiments. Although the filtering process slightly reduces the spectral width of the reflected beam – mainly in the NIR region, as shown in Fig. 3.11 (A) – it still supports a Fourier-limited pulse duration as short as 3.9 fs.

The overall average output power decreases down to 90 % of the initial value. The applied output-coupling mirror features an increased transmission at the spectral edges, since it was originally intended for delivering an higher output-coupling ratio of these wavelength regions. Thus it is ideally suited for filtering the spectral wings for CEP stabilization from this spectrum. Figure 3.9 shows a schematic setup of the *f*-to-*2f* interferometer used for CEP stabilization of this laser oscillator.

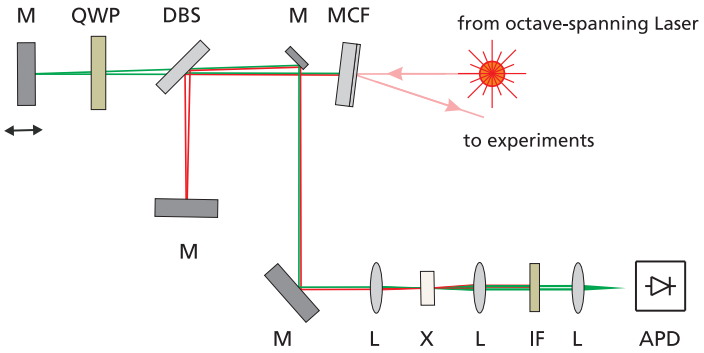

Figure 3.9: *f*-to-*2f* interferometer setup; APD: avalanche photodiode, DBS: dichroic beamsplitter, IF: interference filter (570 nm), L: focusing lens, M: silver mirror, MCF: multichroic transmission filter; QWP: quarter-wave plate, X: LBO crystal (1 mm, SHG 1140 nm).

Within the interferometer the transmitted spectral components located at 570 nm (called 'blue') and 1140 nm (called 'red') are separated using a dichroic beamsplitter (DBS), allowing for tuning the temporal delay and polarization of both with respect to each other. The DBS is a so-called 'extended hot mirror' (CVI, EHR1.0), reflecting the 1140 nm light and being transparent for the 570 nm radiation. Usually this type of mirror is used to reduce the IR-load by reflecting this unwanted radiation out of the experiment. Polarization and delay tuning is done in the 'blue' interferometer arm, where a quarter-wave plate (QWP) allows for a polarization rotation about 90° with respect to the output beam, passing the QWP twice. The relative delay between the arms can be tuned by varying the arm length using a manual translation stage. As it can be seen from Fig. 3.9, this interferometer-part of the overall setup is built-up with a minimal tilt to allow for a beam separation of input and output beam to picking-up the latter for the subsequent frequency-doubling of the infrared radiation and the intended interference detection.

The re-combined beam coming from the interferometer part of the setup is focused into a 1 mm long LBO crystal cut for type-I phase matching to generate the second harmonic radiation of 1140 nm at 570 nm. The fundamental radiation at 570 nm is not affected by this process and becomes simply transmitted. The polarization of the type-I generated SHG radiation, which is perpendicular to the input polarization, is accounted for by tuning the quarter-wave plate in the 'blue' interferometer arm that both frequency components, now located at 570 nm, feature an identical polarization and can interfere with sufficient contrast after filtering with a narrowband interference filter (IF) with a bandwidth of 10 nm.

The heterodyne beat signal is detected by a highly sensitive avalanche photodiode (Menlo Systems APD210).

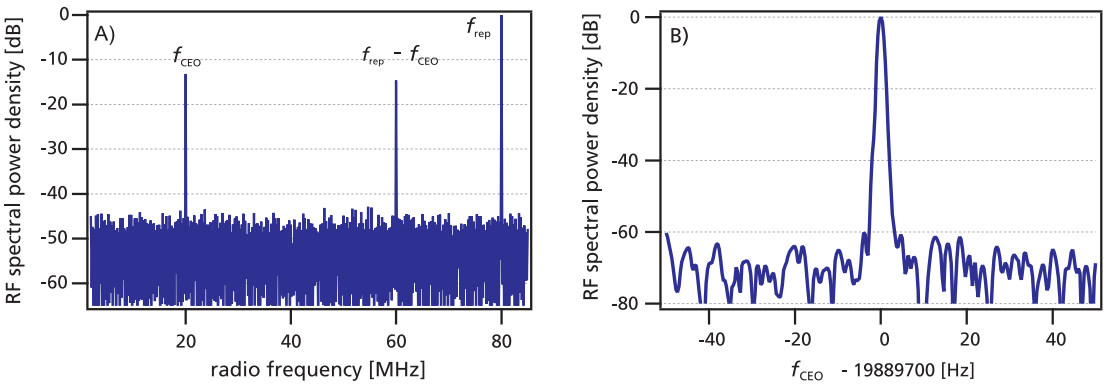

Figure 3.10: Radio-frequency analysis of the carrier-envelope-offset frequency; A) Frequency span showing the laser repetition rate f_{rep} and the f_{CEO} beat signal, which exhibit a signal-to-noise ratio (SNR) of approx. 30 dB in a 100 kHz resolution bandwidth. B) Zoomed-in stabilized CEO frequency beat note with a SNR of 60 dB and narrow linewidth recorded with a device limited resolution bandwidth of 1 Hz.

Figure 3.10 (A) shows the measured CEO-frequency beat signal f_{CEO} located at one fourth of the laser repetition frequency f_{rep} at approx. 80 MHz next to a signal at f_{rep} - f_{CEO}. Within 100 kHz resolution bandwidth (RBW) the f_{CEO}-beat features a signal-to-noise ratio (SNR) of 30 dB and is sufficient for an active CEP stabilization of the oscillator. This stabilization is realized by regulating the applied pump power to the oscillator via an acousto-optic modulator (AOM, IntraAction AFM-405) within the pump beam. This device is controlled by a phase locking-electronics (Menlo Systems XPS800) which generates a phase-lock between the quarter of the laser repetition frequency at 20 MHz and the measured CEO frequency at 20 MHz. Due to the fractional connection between f_{rep} and f_{CEO} of one fourth, the CEP will exhibit a constant phase change from pulse to pulse of $\pi/2$, resulting in a reproduced electric field for each 4^{th} pulse within the train, see Eq. (2.11). For establishing this phase-lock both signals, the repetition frequency measured with a fast photodiode and the CEO frequency measured by the APD, have to be fed to the locking-electronics with sufficient power levels. Here a power level of -30 dBm for the f_{rep} signal and -40 dBm for f_{CEO} were found sufficient, since both become amplified and filtered by the electronics itself in the next step. The phase-locked loop (PLL) locking-electronics compares both input frequencies with a digital phase detector and generates an intermediate or error frequency[1]. This signal is quenched through a loop filter and feed back to the laser in terms of driving the AOM, modulating the applied pump power. The error signal between the quartered repetition frequency and f_{CEO} can be monitored via an oscilloscope. For free-running operation this signal exhibits

1 More information concerning phase-locked loops can be found in App. B

a modulation with a period given by the difference frequency of both input frequencies. By changing the insertion of the intra-cavity BaF_2 wedge, f_{CEO} is tuned in that way that the beat signal crosses zero, both frequencies match respectively. For the locked case, the monitor signal at the oscilloscope becomes flat with a voltage level of 5 mV peak to peak. The stabilized CEO-frequency can now be analyzed in more detail using an RF-analyzer with high resolution. Figure 3.10 (B) gives a zoomed-in, stabilized beat note in a 100 Hz span measured with device-limited resolution bandwidth of 1 Hz. A clean and stable peak with an excellent signal-to-noise ratio of about 60 dB can be observed, indicating a good CEP lock[1].

Also the CEP-stabilized pulses of this laser system were characterized with SPIDER, employing the same compression setup with DCMP mirrors and BaF_2 glass material as described above. A pulse duration as short as 4.4 fs was measured with approx. 90 mW average output power. The corresponding SPIDER measurement results for this pulse are given in Fig. 3.11.

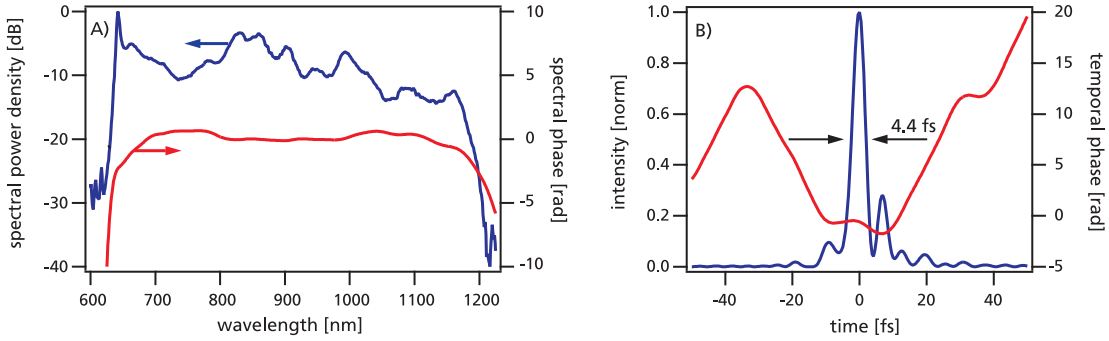

Figure 3.11: A) Reflected residual spectrum remaining for experiments after extracting the spectral parts for *f*-to-*2f* self-referencing. This spectrum supports a Fourier-limited pulse duration as short as 3.9 fs, plotted together with the measured spectral phase. B) Pulse intensity profile and temporal phase (measured with SPIDER) for the phase stabilized pulses revealing a pulse duration as short as 4.4 fs.

This present state of the laser system is used in Chapter 6 for seeding a few-cycle field synthesizer allowing for the manipulation of the electric field of this oscillator below the cycle-scale.

1 At this time of the thesis unfortunately the phase noise tool of the used RF spectrum analyzer was not available for a phase noise analysis of this beat note. But by comparing this signal to the one presented in section 5.2.1 the resulting corresponding CE timing jitter of this signal can be assumed to be even better.

3.2.2 Repetition rate stabilization

One concern of femtosecond laser oscillators is their drift in the repetition frequency, which has to be controlled especially for frequency comb and synchronization applications. Even for very rigid and temperature stabilized laser oscillators this drift cannot be disregarded and has to be counteracted. In this respect a laser-cavity as presented above can be equipped with piezo-mounted mirrors allowing for a fine-tuning of the resonator length and thus control of its repetition frequency, that enables to lock it to some microwave standard.

The importance of a stabilization with respect to f_{rep} can be clearly seen in Fig. 3.12. Here the free-running repetition frequency of the Ti:sapphire oscillator is tracked over a time of 24 hours (blue curve). The laboratory temperature was recorded simultaneously and is plotted in red. From this plot is obvious that the repetition frequency of the laser changes due to thermal variations in the laboratory and follows the temperature curve. At 17:45 p.m. the maximum temperature is reached, coinciding with the minimal tracked repetition frequency. From this point on the laboratory begins to cool down again and reaches its minimal temperature in the early morning, where the maximum repetition frequency is recorded shortly after. At 9:15 a.m., when most of the laser systems and equipment are switched-on for daily operation, the temperature starts increasing again.

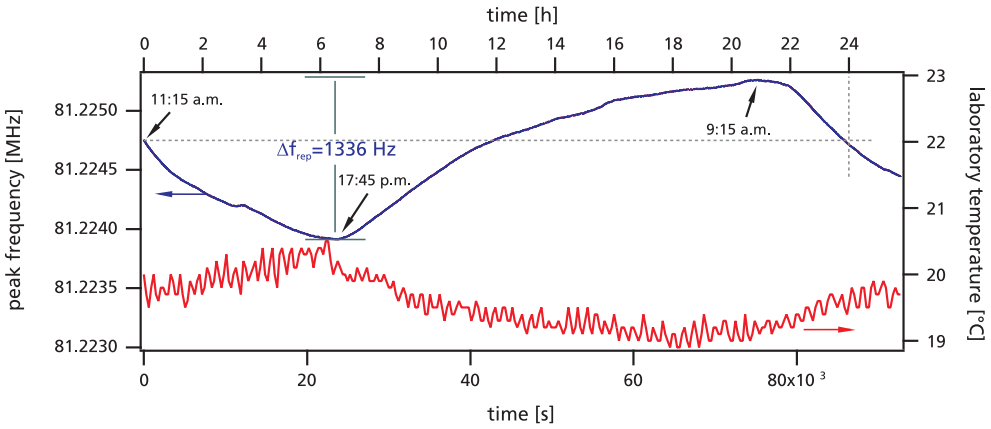

Figure 3.12: Repetition frequency drift of a free-running Ti:sapphire oscillator traced over a time of 24 hours (blue), together with the laboratory temperature (red).

This definite correlation between the laboratory temperature and repetition frequency change results from the thermal expansion of the materials used for building the laser, mainly the large aluminum breadboard. Since aluminum features a thermal expansion coefficient of approx. $23\,\mu\mathrm{m\,m^{-1}K^{-1}}$, thermal variations within the laboratory will affect the laser in terms of resonator length changes in the order of some µm. During night the laboratory temperature decreases and the breadboard thermally relaxes. This results in a shrinking resonator length and a rising repetition frequency. For increasing temperatures this behavior is the other way around. The resulting maximal frequency drift measured for

this laser for one day under normal thermal conditions within the laboratory was in the order of 1350 Hz what is equivalent to a resonator length change of approximately 61 µm at 81.25 MHz. This is in the order of the material expansion given by the overall temperature hub for this period of 1.5° C. This behavior results in a frequency drift of 113 Hz per hour, a resonator length change of approx. 5 µm in that time respectively.

Not only the thermal variations within the laboratory contribute to the repetition frequency drift, also the temperature stability of the chiller used for cooling the laser crystal and breadboard has a direct influence on the f_{rep}-stability as well. For a low-priced chiller used earlier in this project an additional modulation within f_{rep} was observed following the cooling cycle of the chiller with a periodicity of approximately 8 min.

In order to account for the above presented thermal drift of the repetition frequency together with fast fluctuations given by acoustic noise, the laser oscillator presented in this chapter was equipped with a timing control. In this regard first of all a different broadband ZnSe-MgF_2 output-coupling mirror is being used instead of the dispersive one. This OC allows for the generation of a less broadband but still octave-spanning output spectrum with an increased, nearly doubled average output power. Secondly the resonator was equipped with two tiny quarter-inch sized mirrors, one of them attached on a 'fast' piezo-transducer to control the rapid fluctuations of the repetition frequency, the second quarter-inch sized mirror is used to complete this mirror pair. Another half-inch sized mirror is mounted on a second piezo to account for slow drifts in the resonator-length. Again all used mirrors are DCMP mirrors.

The quarter-inch sized mirror at M7 is glued onto a small piezo-chip with a resonance frequency greater than 500 kHz (Piezomechanik, PSt150/7x7/2). Although this mirror is very light-weight with a thickness of only 2 mm the overall mass-load and mounting reduces the resonance frequency to approx. 300 kHz, still sufficient bandwidth that the locking performance is not affected. This piezo provides a maximum resonator length change of 4 µm but is usually driven only to a small fraction of that. Mirror M2 was replaced for this laser as well. This is because during the mirror manufacturing process there can be differences in the dispersion characteristics depending on their position and height within the coating chamber. Using a second 1/4-inch mirror completing this DCMP pair guarantees for a better laser performance, since the remaining dispersion oscillations of this pair now cancel out. Mirror M1 is glued onto a 'slow' piezo-stack (Piezomechanik, PSt150/5/80) to counteract drifts e.g. due to thermal fluctuations. This piezo is driven up to a frequency of 100 Hz and features an overall hub of 80 µm, changing the resonator length twice as much for one round-trip.

The adapted laser setup is shown in Fig. 3.13. For this version the overall resonator length was changed to support a repetition frequency of 81.25 MHz enabling to lock the 16^{th} harmonic to a 1.3 GHz microwave standard. A higher harmonic of the repetition frequency is chosen for locking the repetition frequency, since this increases the resolution for the used phase detector and thus leads to a more accurate phase-lock, see App. B.1. Here

a frequency of 1.3 GHz gives a good trade-off between harmonic order and manageable working frequency.

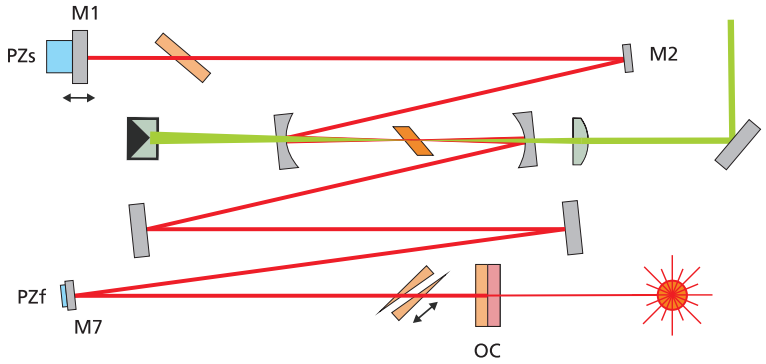

Figure 3.13: Schematic setup of the Ti:sapphire oscillator equipped with two piezo-mounted mirrors for repetition frequency control; M1,M2 & M7: DCMP mirrors, OC: output-coupling mirror, PZf, PZs: fast & slow piezo-transducer.

The PLL stabilization electronics used for locking is a TEM Messtechnik 'LaseLock 3.0', which was extended within the scope of this thesis by a phase detector and an additional high-voltage piezo driver. Figure 3.14 shows a schematic diagram of the final locking circuit. The repetition frequency is detected with a fast photodiode with a bandwidth greater than 2.8 GHz (Melles Griot 13 DAH 001). This photodiode is capable of detecting the f_{rep}-harmonic at 1.3 GHz with a good signal-to-noise ratio and sufficient power. Here a spurious reflection given by some optics within the laser or by a glass substrate placed directly in the output beam can be used. This signal is filtered with a narrowband RF-filter with respect to 1.3 GHz and fed to one input port of the phase detector at the locking-electronics. In case of a power level below -40 dBm after filtering, this signal has to be amplified with a low-noise RF-amplifier.

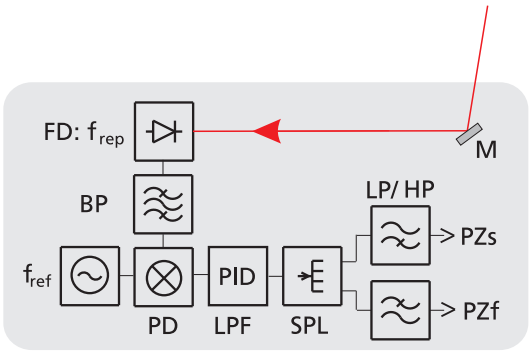

Figure 3.14: Schematic diagram of the f_{rep} locking circuit; BP: bandpass filter, HP: highpass filter, LP: lowpass filter, LPF: loop filter (PID regulator), M: mirror, FD: photodiode, PD: phase detector, PZf: piezo (fast), PZs: piezo (slow), SPL: RF-splitter.

The stable reference frequency used for locking is provided by an radio frequency signal source (IFR Marconi 2024) and fed to the second port of the phase detector. This signal has to feature a much higher power level of about -10 dBm and should be as good as possible in terms of phase noise and long-term stability, since the locking-electronics transfers this crucial characteristic directly to the laser repetition frequency. For a long-term stabilization and global comparison a 10 MHz GPS reference signal can be used to give an external timebase to the RF-synthesizer. Similar to the CEP stabilization presented earlier in this chapter, the phase detector of the locking electronics generates a beat signal between the applied frequencies, their difference frequency respectively. This signal is quenched through a PID loop filter and feed back to the laser by controlling the cavity length using the piezo mounted mirrors.

Timing-stabilized laser performance

In contrast to Fig. 3.12, Fig. 3.15 shows the same laser but locked with respect to its repetition frequency, characterized at the 287^{th} harmonic at 23.32 GHz. Even at this high radio frequency no drift can be seen within the frequency tracking (blue curve) even with highest possible resolution bandwidth of the measurement device of one Hz, except for one period, where the lock is switched off intentionally to show the difference. The plotted red curve gives the power level of the detected frequency beat. For this measurement it is important to synchronize the used equipment with respect to their time bases to exclude relative frequency drifts of the internal oscillators falsifying the measurement result.

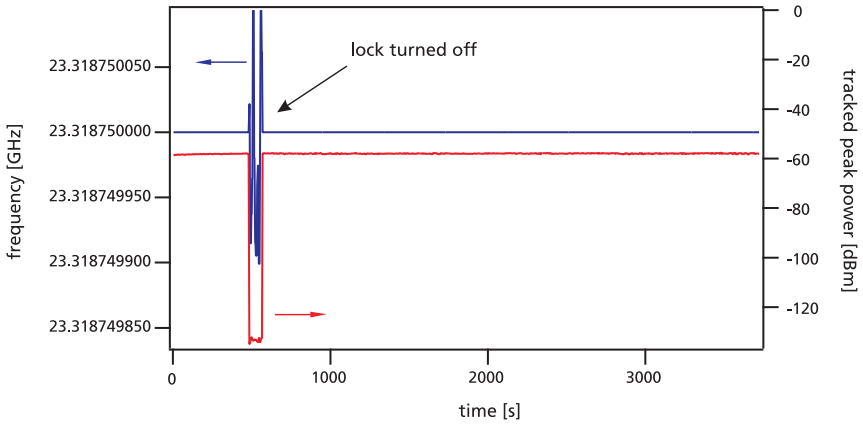

Figure 3.15: Laser system running with locked repetition frequency. f_{rep} is tracked at the 287^{th} harmonic (blue) with 1 Hz resolution bandwidth together with the corresponding power level in the tracked frequency (red). To visualize the influence of the lock, it is once turned-off intentionally.

Calculating the drift down for the fundamental frequency at 81.25 MHz by assuming a fluctuation of less than 1 Hz for the 287^{th} harmonic, this fundamental fluctuation can be expected to be smaller than 3.48 mHz = 1 Hz/287, giving a relative stability better than

10^{-11}. From this measurement the stabilization can be expected to be even better since the fluctuation cannot be recorded with higher resolution nor at higher frequency due to limited measurement devices. The measurements presented here are long-term characterizations since the recording intervals for peak tracking are in the order of one second. Statements concerning short term issues can be derived via phase noise analysis, shown in Fig. 3.16. From the presented noise power spectral densities is can be seen, that the acoustic noise can

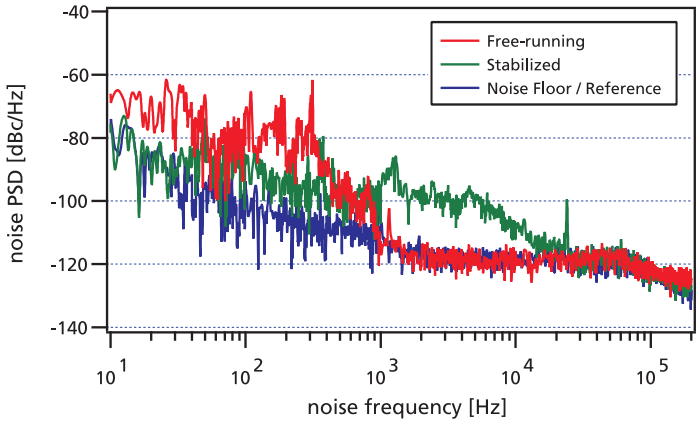

Figure 3.16: Noise PSD of the repetition frequency of the Ti:sapphire oscillator measured at 1.3 GHz shown for the free-running system (red) and timing stabilized operation (green) next to the measurement noise floor (blue). The acoustic noise of the free-running laser can be suppressed by the timing stabilization below 1 kHz.

be effectively suppressed for frequencies below 1 kHz by the timing stabilization. On the other hand it can be seen as well, that for times scales shorter than 1 ms the intrinsic noise performance of the Ti:sapphire oscillator is much better for the free-running operation and cannot be measured since the noise level is in the order of the measurement noise floor.

3.2.3 Frequency comb generation

One important feature mode-locked lasers provide for nowadays science is their potential to generate optical frequency combs, which have revolutionized the field of precision metrology in recent years. Using this unique tool of light it is possible to build optical clocks and link optical frequencies to RF frequencies. A detailed treatment of optical frequency combs can be found elsewhere, e.g. [Ude02b, Ye05, Goh06].

As it is known from Section 2.3, each optical mode ν_n of a frequency comb is defined by only two microwave frequencies f_{rep} and f_{CEO}:

$$\nu_n = n \cdot f_{\mathrm{rep}} + f_{\mathrm{CEO}}. \tag{3.1}$$

Thus by a combined implementation of the above presented techniques to stabilize the 3.7 fs-laser oscillator in terms of its carrier-envelope-offset phase and repetition frequency, the generation of a Ti:sapphire-based frequency comb is straight forward. Since the modifications done in order to stabilize the laser's repetition frequency do not affect the ability to lock it's CEO phase, both stabilizations can be performed simultaneously without further changes.
Because the stabilization of the repetition frequency is performed with a microwave reference and scales with a factor n of the harmonic order of 10^5 - 10^6 to the optical, the quality of the optical comb modes can be dramatically affected by the stabilization process itself. Therefore some important considerations and estimates have to be made for the generation of a suitable frequency comb, given in the following paragraphs.

Equation (2.17) implies that fluctuations within the fundamental repetition rate scale linear with the harmonic order to the optical. For the present configuration this scaling factor is $n = 328.2\,\mathrm{THz}/81.25\,\mathrm{MHz} \approx 4 \cdot 10^6$. Thus a multiplication of the drift of less than 3.48 mHz for the fundamental stabilized repetition frequency at 81.25 MHz, see Section 3.2.2, by n corresponds a drift of ν_n in the optical within a range below 15 kHz. For the free-running oscillator the drift for the fundamental repetition frequency is approximately 1.9 Hz/min, see Section 3.2.2, and would result in a drift of ν_n of 7.6 MHz/min. Secondly, Eq. (2.17) implies as well that the phase noise is transferred quadratically with the harmonic order to the optical frequency domain. Although the stabilization is performed at the 16^{th} harmonic of the repetition frequency, reducing the scaling by a factor of 16 to $\approx 2.5 \cdot 10^5$, the transferred spectral density of the phase noise is still multiplied with a factor of $n^2 = 6.25 \cdot 10^9$. This results in a global increase of phase noise of about 108 dB. Thus by stabilizing f_{rep} to a microwave reference frequency as presented above, would directly result in a so-called carrier collapse [Wal75, Ude02b], whereat in the optical frequency domain the carrier oscillation is lost in the phase noise. For these considerations the influence of the carrier-envelope-offset frequency is neglected, since the characterization for f_{CEO} given in Fig. 3.10 can be directly transferred to the optical frequency regime in terms of drift and linewidth. Here the linewidth of the stabilized beat note is recorded device-limited with a resolution bandwidth of 1 Hz and thus much lower than the influence given by repetition frequency in the order of some megahertz assumed here. The same holds for the f_{CEO} drift.

There exist some basic 'tricks' to overcome this scaling problem to generate a usable Ti:sapphire-based frequency comb in the optical frequency domain. The first parameter that can be influenced is the scaling factor n itself. By minimizing n, e.g. by locking the repetition frequency at an even higher harmonic, the level of the transferred phase noise can be reduced. Of course a direct minimization of the contributing phase noise should be realized above all. Here one approach is to use a control bandwidth smaller than one kHz for the phase lock loop stabilization, since the noise of a typical Ti:sapphire laser falls below that of high quality microwave sources on time scales less than 1 ms [Did05], what can be seen in Fig. 3.16 as well. This is because due to the Kerr-lens mode-locking the laser acts like an inert flywheel making the oscillator less susceptible for fast frequency fluctuations of the optical

modes [Ude02b]. Thus for noise frequencies higher than 1 kHz the phase-lock transfers the noise of the used reference frequency to the Ti:sapphire oscillator and dramatically worsen its performance. For all regards a signal source with a very good spectral purity should be used for the generation of the reference frequency. Another possibility to overcome the scaling problem in general is to totally omit the stabilization in the microwave frequency range and simultaneously comparing two optical beats of the comb with two different reference lasers. Thereby the fluctuations resulting by the free-running comb will affect both beat notes and fall out.

In the near future the Ti:sapphire frequency comb comprising the above mentioned aspects will be referenced to a magnesium lattice clock, based on the $^1S_0$ - $^3P_0$ transition of ^{24}Mg in a thermal atomic beam at 457 nm, provided by a neighboring group at the Institute of Quantum Optics [Fri08]. Thereby a very powerful tool will be established allowing for various spectroscopic applications next to an experimentally connection using a optical fiber link to the Physikalische Technische Bundesanstalt (PTB) in Braunschweig e.g. for comb and optical clock comparison between Hannover and the PTB.

4 Quasi-synchronously pumped octave-spanning Ti:sapphire laser

From the introduction and the last chapter it becomes clear that few-cycle Ti:sapphire femtosecond lasers are unique light sources with outstanding characteristics that are important for many fields of research. Although most of their properties are unsurpassed, in some points they are disadvantaged compared to other laser systems. For example, such Kerr-lens mode-locked laser systems lack of a self-starting ability and have to be externally started. Secondly, they are usually pumped by frequency-doubled continuous-wave solid-state lasers, which are most likely twice as expensive as the Ti:sapphire laser being pumped. These arguments mainly prevent the generation of robust, cost-efficient turn-key few-cycle Ti:sapphire systems, which would be also usable for industrial applications and medicine.

To overcome the first problem it was already shown for more narrowband Ti:sapphire systems that a semiconductor saturable absorber mirror (SESAM) can be used for assisting the Kerr-lens mode-locking [Sut99] for pulses with durations down to 5.8 fs. For even shorter pulses those devices suffer from spectral bandwidth. Another promising approach is the technique of quasi-synchronous pumping, whereas the Ti:sapphire crystal is not being pumped by continuous-wave light, but with radiation from a pulsed laser source. Such a pulsed pumping is very interesting for Ti:sapphire, since it accounts for both aspects, cost-efficiency and self-starting ability. Ell et al. already demonstrated self-starting for a few-cycle Ti:sapphire laser oscillator using a commercial green picosecond pump laser [Ell05]. In recent years the development of such pulsed pump sources was very successful now delivering e.g. up to 100 W of infrared light generated by thin-disk oscillators [Mar08, Bae10]. For those pulsed sources frequency doubling can be done externally and with high efficiencies of more than 50 %. In contrast decent continuous-wave laser systems are limited up to date to 20 W frequency-doubled output commercially available, since frequency doubling has to be done intra-cavity with lower conversion efficiencies.

In this chapter the concept of quasi-synchronous pumping will be expanded to an octave-spanning laser system pumped by femtosecond pulses from an Yb:KLuW thin-disk oscillator. Next to the self-starting behavior, also the ability of a CEP control will be investigated together with the potential for self-synchronization of both, pump source and few-cycle oscillator [Sei02]. These findings can be used to develop a novel combined light source with locked timing characteristics which would be interesting for spectroscopic applications

like pump-probe type experiments. For example this source would be highly beneficial for two-photon photoelectron spectroscopy (see Section 5.5.1), since pump pulses at 1030 nm and 515 nm would be available next to a temporally locked broadband few-cycle pulses for probing.

4.1 (Quasi-)synchronous pumping

A special pumping scheme that can be applied for pulsed laser systems is synchronous pumping, whereas the pump light is not delivered continuously, but by short light pulses to the target laser system. In this thesis a Ti:sapphire laser that is usually pumped by continuous-wave radiation, is pumped by a frequency-doubled thin-disk oscillator. Given by the specific target laser system, the upper-state life-time of the active medium and the nonlinear coupling within the crystal, different modes of operation can occur, depending on the difference in repetition frequency of both laser systems and the involved intensities. For Ti:sapphire oscillators three different regimes can be distinguished in this regards:

1. Quasi-cw-pumped operation occurs when the repetition frequency of the pump laser and the Ti:sapphire laser are different, and their pulsing is completely independent from each other. For this case, the Ti:sapphire oscillator behaves like a cw-pumped system where mode-locking has to be initially started by an external perturbation resulting in an independent operation of both systems.

2. Quasi-synchronous operation occurs when both laser systems have nearly the same repetition frequency and the cumulative gain perturbation induced by the pulsed pump source leads to a self-starting of the Kerr-lens mode-locked operation of the Ti:sapphire oscillator. This behavior is similar to the last case, but here the gain modulation is too weak to trigger synchronized operation.

3. Synchronous operation occurs when both laser systems exhibit the same or an integer multiple repetition frequency and the gain modulation induced by the pump laser is that high, that it can influence the Ti:sapphire operation in terms of a serious gain modulation. This can lead to a restoring force to the Ti:sapphire pulses, resulting in a compensation of round-trip time mismatch within a certain locking range. In this regime both laser systems establish a phase-locked, synchronous operation. Since the upper-state life-time of Ti:sapphire of 3 µs is quite long, this restoring force can be expected to be weak. Another aspect leading to a synchronous operation of both laser systems can be a nonlinear coupling between the pump pulses and the intra-cavity Ti:sapphire pulses within the laser crystal, both pulses featuring comparably high intensities at this point.

Figure 4.1 gives an illustration of the three different modes of operation that can occur for a pulsed-pumped Ti:sapphire oscillator depending on the repetition frequency difference of both systems. In the very most cases quasi-cw operation occurs, whereas self-starting or quasi-synchronous operation is limited to a range of below 250 Hz in repetition rate difference. The range for synchronous operation can be expected within a small part of the self-starting regime.

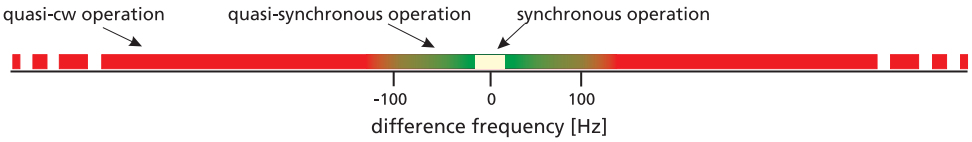

Figure 4.1: Illustration showing the modes of operation that can be expected for a pulsed pumped Ti:sapphire oscillator depending on the difference in repetition frequency of both laser systems.

4.2 Optical setup

The optical setup of the overall laser system is shown in Fig. 4.2. For the desired investigations the target Ti:sapphire oscillator – similar to the one presented earlier in this thesis – is pumped by a frequency-doubled passively mode-locked Yb:KLuW thin-disk oscillator [Pal08]. This solitary mode-locked laser, shown on the left hand side, delivers pulses with a duration of sub-500 fs and a pulse energy of 0.6 µJ. It is diode-pumped by 140 W of 980 nm radiation and utilizes a Yb:KLuW thin-disk with a thickness of 116 µm and a diameter of 7 mm which is passed four times for one resonator roundtrip. The detailed output specifications of this laser are given in Tab. 4.1.

Table 4.1: Specifications of the Yb:KLuW thin-disk oscillator [Pal08]

Parameter	Value
Pulse duration	440 fs
Pulse energy	0.61 µJ
Central wavelength	1032 nm
Spectral bandwidth (FWHM)	2.54 nm
Average output power	21.3 W
Pulse repetition frequency	34.7 MHz
M^2	1.09
Frequency-doubled average output power	> 9 W

The infrared output of the disk laser is frequency doubled in a 1 mm long BBO crystal cut for type-I phase matching with a conversion efficiency of more than 50 %. The applied power for frequency-doubling can be tuned using a half-wave plate (HWP) and a polarizing

beamsplitter cube (PBC) placed in front of the SHG crystal. A dichroic beamsplitter (DBS) is used for spectral filtering the output beam after frequency doubling with respect to the remaining fundamental radiation. The generated 515-nm-light with up to 9 W average output power can now be used for pumping the Ti:sapphire crystal.

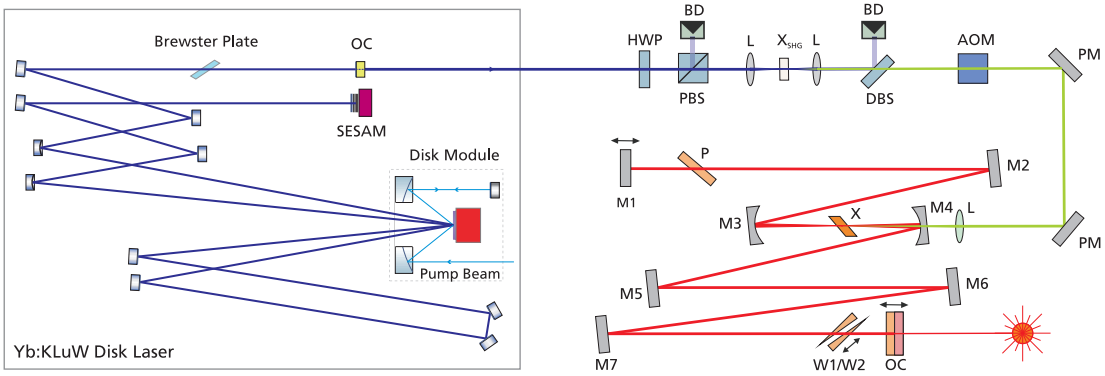

Figure 4.2: Overall setup of the thin-disk-pumped Ti:sapphire laser; Left: thin-disk oscillator [Pal08], OC: output-coupling mirror; Right: Ti:sapphire laser as given in Fig. 3.4 with additional DBS: dichroic beamsplitter and X_{SHG}: BBO crystal for second harmonic generation.

With respect to quasi-synchronous pumping, the cavity length of the Ti:sapphire oscillator is adapted to match the doubled repetition frequency of the thin-disk oscillator of $2 \cdot 34.7\,\text{MHz} = 69.4\,\text{MHz}$, thus pumping is done at a sub-harmonic of the original repetition frequency. Resonator length fine-tuning can either be done by a manual translation stage placed at the output-coupling mirror or a piezo-driven translation stage (Newport Agilis AG-LS25) at M1 to exactly match the frequencies. This pumping scheme implies two important aspects. First of all approximately every 30 ns a pump pulse is applied to the crystal, having an upper-state life time of about 3 µs. On the other hand the Ti:sapphire pulses pass the crystal three times without a pump pulse present. Both processes together lead to a complex gain modulation within the crystal.

If sufficient pump power at 515 nm is present, this Ti:sapphire oscillator shows a similar behavior like continuous-wave-pumped systems. For comparable output specifications approximately 1 W more of pump power has to be applied, what can be attributed to the elliptic pump beam resulting from the SHG generation and a smaller pump beam size, both leading to a sub-optimal pump mode geometry within the Ti:sapphire crystal. Also the gain dynamics associated with the pulsed pump source could play a role in this consideration. Although the overall laser system is not stabilized in terms of the involved repetition frequencies nor amplitude noise of the applied pump intensity, it operates stabely over several hours, the details are given in the following sections.

4.3 Quasi-synchronously pumped laser characteristics

As mentioned earlier, the output characteristics and system-specific behavior of the synchronously-pumped Ti:sapphire oscillator can be compared to similar cw-pumped systems as presented in the chapter before. As for those systems mode-locked operation has to be externally initiated for a repetition frequency far-off resonance. By tuning f_{rep} according to the doubled pump frequency, self-starting can be observed as already reported for standard Ti:sapphire oscillators in [Ell05].

The octave-spanning output spectrum of this laser is shown in Fig. 4.3 (A), next to a spectrum recorded while chopping the intra-cavity beam by periodically blocking laser operation with a chopper wheel (B). Due to self-starting the laser starts immediately mode-locking again after the cavity has been blocked[1]. The laser output characteristics in terms of octave-spanning spectrum and average output power of around 180 mW are similar to the other discussed systems, especially the one presented in Chapter 5, since the used broadband dispersion compensating mirrors and the output-coupling mirror are identical. The spectral bandwidth shown in Fig. 4.3 (A) supports a Fourier-limited pulse duration as short as 4.0 fs. An achievable compressed pulse duration can be estimated to be in the order of sub-4.5 fs for this system.

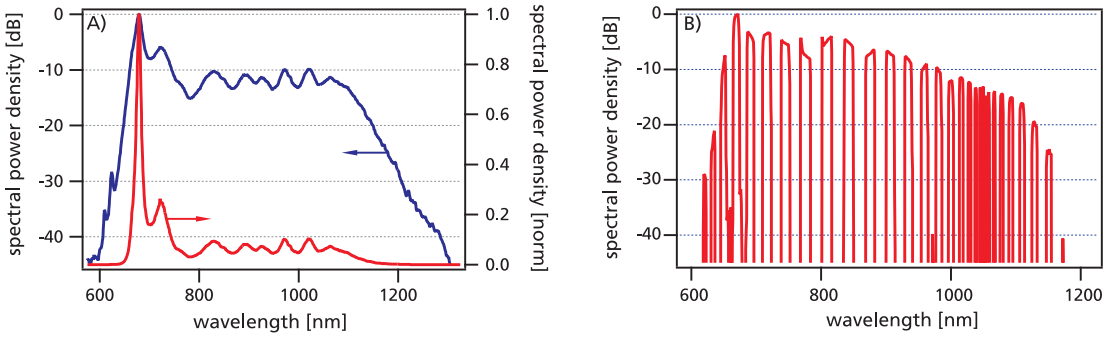

Figure 4.3: Spectral characteristics and self-starting ability of the quasi-synchronously pumped Ti:sapphire oscillator; A) Octave-spanning output spectrum shown on a logarithmic and linear scale supporting a Fourier-limited pulse duration as short as 4.0 fs; B) Output Spectrum measured while chopping the intra-cavity beam, proving the self-starting behavior of this system.

To investigate the self-starting behavior in more detail, especially the supported detuning range, the piezo-controllable translation stage at the end-mirror M1 is used to scan the resonator length with step-sizes in the order of 50 nm – changing f_{rep} about 1.6 Hz @ 69.4 MHz. As both lasers are not stabilized in terms of cavity length, some substantial drift in the order of several tens of Hz can be observed for each single repetition frequency, what

1 In Fig. 4.3 the spectrum appears chopped since the sweep time of the optical spectrum analyzer used is much slower than the chopping frequency and thus this device scans over the alternating laser operation.

can be explained by the variations of the room temperature and the chiller performance. To minimize the influence of these drifts on the desired measurement data, a simultaneous measurement of both repetition frequencies is performed with a fast photodiode and an automated read-out of the actual difference frequency, measured by a radio-frequency analyzer with high resolution. A chopper-wheel placed intra-cavity of the Ti:sapphire oscillator now repetitively blocks and releases the cavity with a low chopping-frequency of 100 Hz. A measure for self-starting is the probability the laser starts mode-locking again after the cavity has been blocked by the chopper wheel. This probability can be measured by detecting the oscillator's output power behind a 1000 nm long-pass filter, giving a definite indication whether the laser operates in pulsed operation after the resonator was released by the chopper wheel. Here the power levels for 'always starting' and 'no starting' determine the 100 % and 0 % levels respectively. Using this method, statistical data and a self-starting probability in dependence of the repetition rate detuning can be obtained, the resulting self-starting regime is shown in Fig. 4.4.

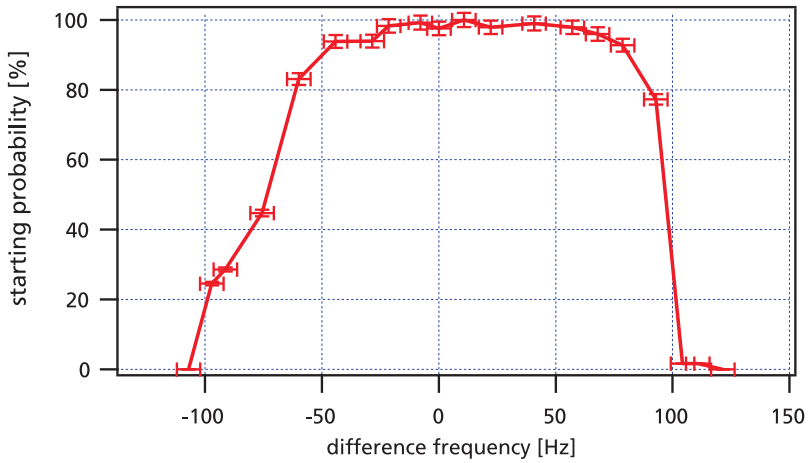

Figure 4.4: Self-starting probability measured depending on the difference frequency of both laser systems. Within a range of 150 Hz the system shows an 80 % probability for self-starting.

This measurement results in a self-starting probability with more than 80 % in a range of 150 Hz. This corresponds to a relative resonator length difference of 10.9 µm for the center frequency of 69.4 MHz or a time delay per round-trip of 36.3 fs. For difference frequencies larger than ± 100 Hz no self-starting can be observed anymore and mode-locking has to be externally initiated again. Although the gain medium has a lifetime of 3 µs, the slight temporal modulation of the gain is sufficient to perturb the laser from cw operation and initiate mode-locking. The high sensitivity to cavity length changes compared to the pulse duration of the pump pulse of approximately 500 fs indicates that a cumulative perturbation of the initially induced fluctuation is required to trigger the self-starting operation.

For a different laser system external gain and loss modulation has been demonstrated to

be a suitable method for a synchronization of two laser systems [Sei02]. In this scheme, a slight detuning in cavity lengths of both oscillators with respect to each other can be compensated by the temporal structure of the provided gain gradient. A pulse will experience an increased amplification for its wing located closer to the maximum of this gradient, acting like a restoring force and able to provide a certain compensation of round-trip time mismatch within a limited locking range. For the presented synchronously pumped Ti:sapphire oscillator the restoring force can be expected to be very weak due to the long lifetime of the gain medium. Nevertheless, by analyzing the pulse trains in time-domain with a fast photodiode, a change in behavior can be observed if the repetition rate detuning becomes very small and a synchronized operation can be observed for this system as shown in the corresponding oscilloscope trace given in Fig. 4.5 (A).

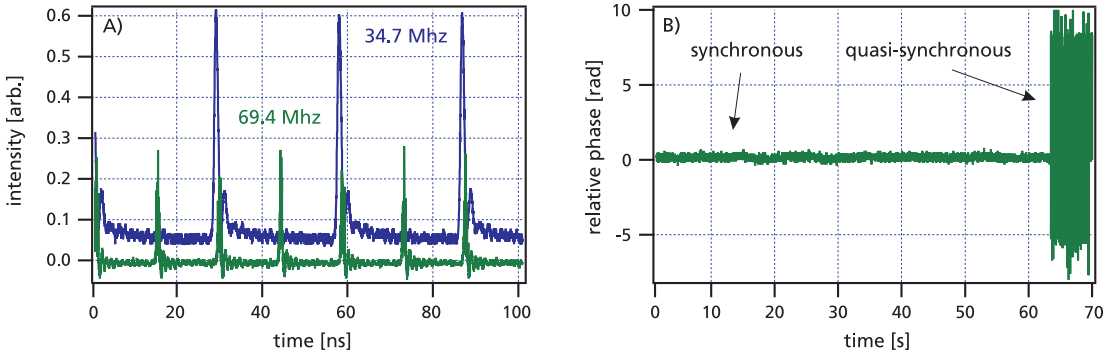

Figure 4.5: Synchronous operation between the pulsed pump laser and the Ti:sapphire oscillator; A) Oscilloscope trace showing both repetition frequencies in locked operation; B) Locked phase between both frequencies measured with lock-in detection.

The left-hand-side gives an oscilloscope signal of both independently measured repetition frequencies, while triggering is done only with respect to the 34.7 MHz repetition rate of the pump laser. For a detuning of more than 50 Hz, the measured pulse sequence at the second channel is not trackable anymore, as both signals are not synchronized. If the piezo-stage is moved towards equal cavity lengths, a static sampling of the second pulse train can be observed as well, indicating self-synchronization of both lasers. This behavior can only be found in a very small region within the self-starting range and vanishes for a larger detuning from this region. In order to further prove this statement Fig. 4.5 (B) shows a measurement of the phase relation between both laser systems for synchronous and quasi-synchronous operation. For this measurement the relative phase of both repetition frequencies is measured with the phase detector of a high-frequency lock-in amplifier (Stanford Research 844), the second harmonic of the pump laser used as reference and the fundamental repetition rate of the Ti:sapphire oscillator as signal input. For an observation time of about 60 s a clean phase-lock can be observed. After this time the synchronous mode of operation is lost. Since the effect of pump-laser induced gain modulation can be assumed

to be very weak and limited to a very small range of repetition frequency difference, this can be mainly attributed to the drift of both resonator lengths with respect to each other. The frequency drifts of both free-running laser systems are shown in Fig. 4.6.

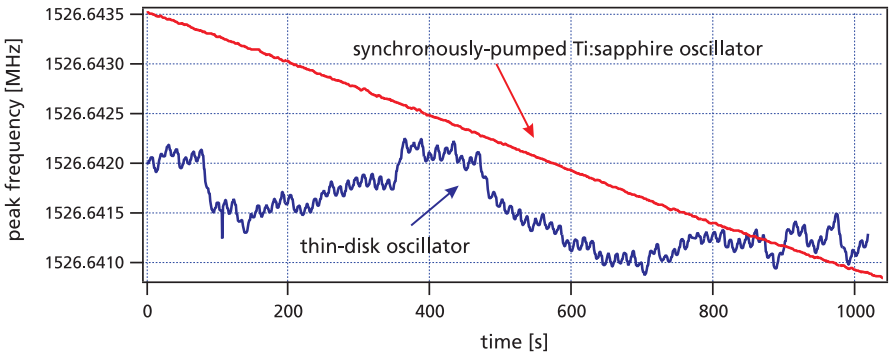

Figure 4.6: Comparison of the repetition frequency drifts by the thin-disk oscillator (blue) and the Ti:sapphire oscillator (red) recorded at a higher harmonic (22^{th}) for increased measurement resolution.

Figure 4.6 shows a frequency tracking of the thin-disk repetition frequency over time, next to the drift of the Ti:sapphire oscillator for comparison. It can be seen that the timing of the thin-disk oscillator is very unstable following a random nature, whereas the Ti:sapphire oscillator exhibits a slow, but larger temperature drift that can be attributed to a laboratory temperature change, see Section 3.2.2. For the thin-disk oscillator a fast modulation can be recognized on top of the general drift that can be related to the cooling of the thin-disk which is directly water-cooled from the back and therefore very susceptible to chiller-induced thermal variations.

Another important aspect for synchronous operation can be the phase noise of the pump laser, since for this mode an exact timing of both lasers is crucial. Figure 4.7 (A) shows the noise power spectral density of the thin-disk pumped Ti:sapphire oscillator (red) next to the noise PSD of the thin-disk oscillator itself (blue) and a Verdi-pumped Ti:sapphire oscillator (green) for comparison. The noise PSDs are each measured at a higher harmonic of the laser's repetition frequencies[1] with a fast, low-noise photodiode. The signals are amplified with respect to sufficient power levels and analyzed with a built-in phase noise measurement tool of the used radio frequency spectrum analyzer (Agilent E4440A). For comparable measurement data the measured noise PSDs at the higher harmonics of f_{rep} are corrected with respect to their native repetition frequency according to Eq. (2.21). From the noise PSDs first of all it can be noted, that the noise of the thin-disk laser is seriously higher than the Ti:sapphire noise in general, especially between 1 kHz and 100 kHz. Here,

1 The noise PSD of the thin-disk oscillator is measured at 832 MHz, its 24^{th} harmonic respectively. The noise of the quasi-synchronously pumped Ti:sapphire oscillator is measured at the same frequency, what is its 12^{th} harmonic.

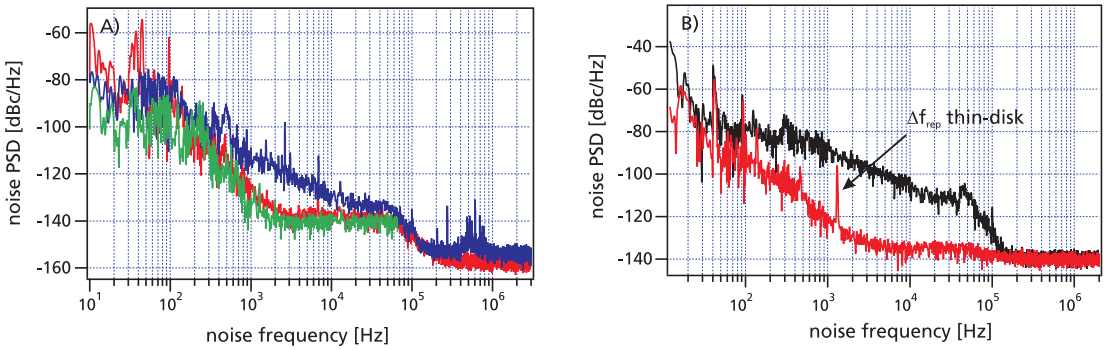

Figure 4.7: A) Noise PSD of the repetition frequency shown for the quasi-synchronous pumped Ti:sapphire oscillator (red) next to the noise PSD of the thin-disk oscillator (blue) and a cw-pumped Ti:sapphire laser (green); B) Noise PSD shown for the Ti:sapphire repetition frequency pumped by the thin-disk oscillator. The red curve shows the noise for a repetition frequency mismatch of about 1.4 kHz, whereas the black plot shows the disturbance for identical frequencies.

for frequencies above 1 kHz the noise of the Ti:sapphire laser is still limited by the noise floor of the measurement device. On the other hand it can be seen as well, that since both frequencies are not identical, the phase noise of the thin-disk laser seems not to influence the noise of the Ti:sapphire oscillator. Figure 4.7 (B) shows the noise PSD of the Ti:sapphire again while tuning the cavity to match the exact doubled pump frequency. For a difference frequency of some kHz there seems to be no coupling from the pump laser to the Ti:sapphire laser (red), whereas within the self-starting regime (black) a dramatic rise of the phase noise can be observed. This is an indication, that for similar repetition rates a strong coupling occurs and the increase in noise can be obviously assigned to the cumulative perturbation of the Ti:sapphire laser by the pulsed pump. For synchronous operation, where both repetition rates are locked, this is expected to be reduced again.

Unfortunately, a synchronous operation could not be reproduced after a realignment of the pump laser, thus preventing an in-deep analysis of the crucial parameters for that special mode of operation. Next to noise aspects, also an interplay of nonlinearities within the Ti:sapphire crystal induced by both lasers are key to a successful lock of both. Next to the restoring force provided by the pump pulse induced gain gradient, the observed synchronous operation can be explained in terms of nonlinear coupling between the pump pulse and the intracavity Ti:sapphire pulse within the gain medium, which feature comparably high intensities at this point. In this regard a longitudinal cavity locking scheme based on cross-phase modulation was reported in [Wei01, Bet04]. Furthermore, as the Kerr effect acts transversally as fast saturable absorber, a temporal overlap of both pulses will strongly influence the absorber modulation depth and thus might provide an additional contribution to the stabilization mechanism for the synchronized operation mode. In this case not only the exact timing, but also accurate lateral alignment of the focal spots of both lasers within the Ti:sapphire crystal are of importance.

4.4 Carrier-envelope-offset phase stabilization

The octave-spanning output spectrum of this laser system allows for a direct CEP stabilization, which can be performed directly by measuring f_{CEO} with an f-to-$2f$ interferometer as presented in Section 3.2.1, and locking the measured beat signal to the fourth part of the laser's repetition frequency. Figure 4.8 (A) shows a 75 MHz frequency span recorded with a 100 kHz resolution bandwidth giving the measured CEO frequency beat note with sufficient SNR for locking of approximately 30 dB next to the repetition frequency at 69.4 MHz.

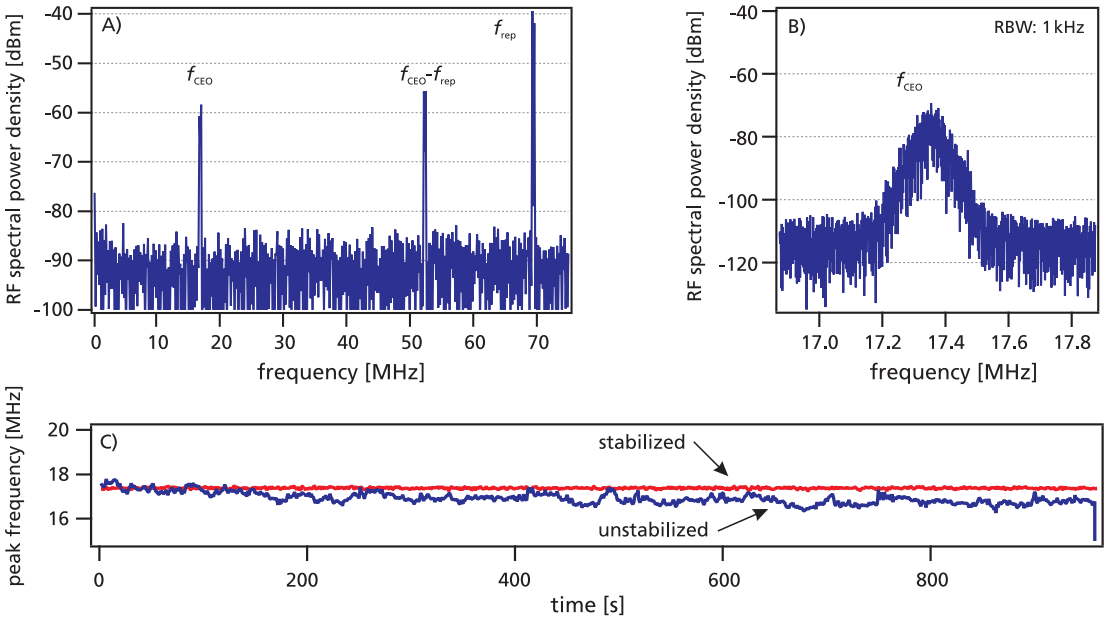

Figure 4.8: Carrier-envelope-offset phase control of the quasi-synchronously pumped Ti:sapphire oscillator; A) Frequency span recorded with a RBW of 100 kHz showing f_{CEO} next to f_{rep} at 69.4 MHz with 30 dB SNR; B) Stabilized beat note recorded with a RBW of 1 kHz; C) Tracking of a locked (red) and free-running CEO beat note (blue).

Using a PLL locking electronics to control the pump-power-feedback by a AOM, this synchronously pumped octave-spanning Ti:sapphire oscillator can be successfully stabilized with respect to its carrier-envelope-offset frequency, what is to the best of our knowledge the first CEP stabilization of a synchronously-pumped laser system [Bin10]. Successful phase-locking can be verified by the error signal of the phase-locking electronics and the f_{CEO} peak tracking shown in Fig. 4.8 (C), comparing the locked beat note evolution to the free-running case. However, the locking performance of this system, a zoomed-in stabilized beat note shown in Fig. 4.8 (B), lacks from the typical narrow linewidth of Ti:sapphire

oscillators pumped by low-noise continuous-wave pump sources. The shown beat note is recorded with a resolution bandwidth of 1 kHz and features a line width of about 1 MHz and low signal-to-noise ratio. For comparison, Fig. 3.10 shows a beat note recorded with 1-Hz device limited resolution and 60 dB SNR of a cw-pumped oscillator.

A similar locking result was found in [Wit04] where the poor locking performance could be attributed to the frequency noise of the pump laser. Since the thin-disk pump source in this work is not stabilized with respect to timing and output power, the here presented locking behavior is not surprising at all. Nevertheless to claim a definitive reason for this behavior other aspects which could influence the locking performance have to be excluded before. In this regard first of all the CEP locking procedure itself was target of interest. Here above all the input frequency range by the frequency divider and the APD amplifier have been checked for correct operation at 69.4 MHz and 17.35 MHz respectively. Although especially the latter is at the edge of the input range no negative influence of these parameters could be found to limit the performance.

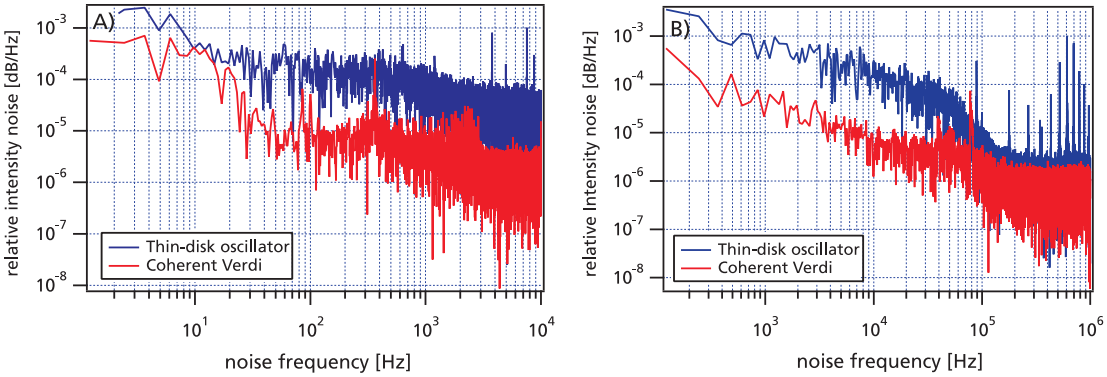

Figure 4.9: Comparison of the intensity noise by the frequency-doubled Yb:KLuW thin-disk oscillator (blue) and a continuous-wave Nd:YVO laser (Coherent Verdi, red) measured with a low-noise photodiode and shown A) from 1 Hz up to 10 kHz, and B) from 10 Hz up to 1 MHz. For the thin-disk laser a rms value of 0.2 % was retrieved, whereas the noise of the Verdi laser is considerably lower with an rms value of 0.001 %.

Since the used *f*-to-*2f* interferometer, PLL locking electronics, feedback optics (AOM) and Ti:sapphire setup are identical for this system to those delivering an optimal locking performance, the frequency noise of the thin-disk pump source seems to be the limiting factor. Figure 4.9 shows a comparison of the intensity noise of a Coherent Verdi (red) and the thin-disk oscillator (blue). The noise is measured with a low-noise photodiode set-up to measure only the intensity noise contributions and being 'blind' for the pulses given by the thin-disk oscillator. It can be seen that the noise of the thin-disk laser is well above the noise of the continuous-wave laser. An analysis of the noise traces with respect to their corresponding root-mean-square values revealed for the Coherent Verdi a result of 0.001 % – integrated from 1 kHz up to 1 MHz – whereas the thin-disk laser was

found to be considerably noisier with an rms value of 0.2 % in this frequency range. The CEP-stabilization is based on modulating the applied pump power to the Ti:sapphire laser using an AOM within the pump beam, thus the influence of intensity noise of the used pump laser has always been the crucial criterion for successful CEP locking [Wit04] as it directly transfers into fluctuations in f_{CEO}. This is still the reason for exclusively qualifying a few suitable pump sources (e.g. Coherent Verdi Uno series) for pumping a CEP-stabilized Ti:sapphire laser system.

4.5 Discussion

The (quasi-)synchronously pumped Ti:sapphire oscillator presented in this chapter reveals very interesting results in terms of self-starting, CEO phase stabilization ability and the feasibility of synchronous operation of such a combined system. The presented performance is already very promising and shows much potential for further improvements of this system.

The experimental results of this project show that noise-related aspects are the main challenges of the overall system and so far limiting the performance in terms of synchronized operation and CEP-stability. Since both lasers are completely free-running and not stabilized with respect to any crucial parameter, this behavior is not surprising at all. In this regard a timing and output-power stabilization could be easily established by using standard techniques and methods. Here the optimization of the thin-disk pump laser with respect to its timing and intensity noise can be assumed to have the highest impact on the performance of the overall system. The synchronous and quasi-synchronous operation of the Ti:sapphire oscillator are among others directly linked to the relative repetition frequency drift and timing jitter of the pump source, whereas the CEP performance is limited by the intensity noise of this laser. A timing stabilization can be realized straight forward by phase-locking the repetition frequency of the thin-disk laser to a stable reference frequency generated by a suitable signal source, as presented in Section 3.2.2 for a Ti:sapphire oscillator. In this respect the cavity can be equipped with two piezo-mounted resonator mirrors as well, to account for the fast and slow fluctuations of the repetition frequency. For this system this step is already planned for the near future. Secondly, the repetition frequency of the Ti:sapphire oscillator can be locked to the disk-laser following the same approach. The amplitude noise of the frequency-doubled output by the thin-disk laser could be also stabilized by standard power-stabilization techniques, e.g. by gating the output by an AOM, before it is applied to pump the Ti:sapphire oscillator.

For considerations in terms of designing a completely reviewed overall laser system, many basic design-features affecting the noise of such a laser system could be accounted for as well. Since both oscillators were primarily not intended to be used for such a combined system, most of these aspects are still open. First of all the whole system should be integrated onto one common temperature stabilized breadboard to lower thermal variations between both

oscillators and minimize the distances. Because the present cooling mechanism of the thin-disk seems to be responsible for the faster variations of the pump laser's repetition frequency – the thin-disk is directly sprayed with water from the back – this cooling technique should be reviewed as well and could lead to a reduced noise. Another aspect that might be contributing to the noise of the thin-disk oscillator can be the noise of the applied pump diodes for pumping the disk, which have to be characterized in this regard.

Next to the benefits for experimental issues of such a novel combined and stabilized synchronously pumped laser system, this light source will be interesting from the laser physical point of view as well. Because the basic noise contributions should not be limiting the performance of the novel system anymore, much more precise characterization measurements could be performed to analyze the complex dynamics in more detail and to fully understand the mechanisms responsible for the different modes of operation.

Taking the above mentioned points into account, it should be possible to establish a self-starting, CEO-phase stabilized and self-synchronized unique light source for spectroscopic applications delivering both, an intense infrared or frequency-doubled pump pulse and a synchronized octave-spanning, CEP-stabilized probe pulse. Additionally this system avoids the uses of expensive cw-pump sources. It could be directly applied for applications such as two-photon photoemission spectroscopy as presented in Section 5.5.1, since these experiments suffer at present time from sufficient pulse energy to pump the electrons to the image-potential states below the ionization energy. Here the green pump pulse could deliver both, an much increased pulse energy together with an improved pumping wavelength of 515 nm (2.5 eV) for driving the transition. For applications relying on the field oscillations this system can be used for seeding the few-cycle field synthezier presented in the next chapter as well.

5 Oscillator pulse train with constant carrier-envelope-offset phase

As presented in Section 2.3, the carrier-envelope-offset phase of few-cycle laser pulses can be routinely stabilized to a fraction n of the pulse repetition rate using f-to-$2f$ self-referencing. This results in a pulse train with reproduced field characteristics for every n^{th} pulse within the emitted pulse train. Some applications especially sensitive to the electric field profile of few-cycle laser pulses would essentially benefit from a pulse train with identical field properties, constant CEP respectively. For a pulse train generated by the standard f-to-$2f$ locking technique, the desired investigations have to be performed as a series of single shot measurements whereas longer integration times can only be used if appropriate pulse picking at an integer multiple of the n^{th} fraction is done to select the identical pulses. For amplified laser systems this can be implemented simply by picking a multiple of n from the pulse train at kHz-rates and applying a second slow feedback loop [Bal03]. Especially for few-cycle laser pulses in the sub-5-femtosecond regime and pulse repetition rates of around 80 MHz to 100 MHz, it is still sophisticated to find an appropriate pulse picking mechanism fast enough and experimentally feasible together with negligible pulse distortion in terms of dispersion. This 'picking problem' can be directly overcome by stabilizing the carrier-envelope-offset frequency of the original pulse train to zero, generating an identical pulse field for every pulse contained within the train. Using this concept, pulse picking can be completely avoided and a light source with full oscillator repetition rate, output power and beam quality can be established for the desired experiments.

This chapter deals with the implementation of a powerful technique to stabilize the carrier-envelope-offset frequency of an oscillator pulse train to zero. After a brief overview of the actual methods available for the generation of such a pulse train, the stabilization scheme used in the scope of this thesis is explained in more detail, followed by the presentation of the achieved experimental results and characterization measurements. The locking performance of this system is compared with competing stabilization techniques next to a quick outlook on intended experiments using the overall stabilized laser system.

5.1 Routes to stabilize the carrier-envelope-offset frequency to zero

Although CEP stabilization of few-cycle laser pulses is a commonly used technique, the stabilization with respect to carrier-envelope-offset frequency zero is still a discussed problem. Here the standardly used phase-coherent locking technique fails since it is based on measuring f_{CEO} with a good signal-to-noise ratio and lock it to a stable reference frequency. It is obvious that this implementation cannot hold for f_{CEO}-to-zero locking since it would compromise measuring and phase-coherent locking f_{CEO} in the DC-noise contributions. Within the last few years only three methods proved their capability to overcome this problem. The first technique, introduced by Lee et al. in 2005 and called the 'direct locking method', utilizes a time-domain signal to generate a pulse train with constant carrier-envelope-offset phase [Lee05]. Secondly, in 2009 Grebing et al. presented a novel method working in the frequency domain, shifting f_{CEO} to zero using an acousto-optic frequency shifter (AOFS) within the laser output beam [Gre09b]. The latest method was practically realized in the scope of this thesis and utilizes an extended f-to-$2f$ self-referencing scheme, suggested ten years ago by Jones et al. [Jon00], to generate a pulse train with constant field profile for each subsequent pulse.

5.1.1 Direct-locking method

The 'direct-locking method' [Lee05] was the first technique used to generate a pulse train with constant CEP. Unlike the conventional self-referencing technique, the direct-locking method uses the time-based interference signal between the frequency-doubled 'red' end of the spectrum with the fundamental 'blue' end, the experimental setup shown in Fig. 5.1. The filtered interference signal can be regarded as sinusoidal modulation and represents the CEP evolution of the laser pulses [Lee05]. The variation from peak to valley thereby corresponds to a phase change of π. The direct-locking method minimizes the amplitude of the interference modulation to a constant DC level. For the practical realization the initial interference modulation is used as an error signal and quenched to a specific DC level using a locking servo, controlling the applied pump power to the laser oscillator. Thereby a pulse train with constant CEP value can be generated whereas the absolute phase value has to be experimentally determined and is dependent on the chosen reference DC level. The locked pulse train can be established without using any frequency-related equipment such as an radio frequency spectrum analyzer, establishing a very economical solution for CEP stabilization of femtosecond lasers [Lee08].

A schematic setup showing the relevant aspects of this method is depicted in Fig. 5.1. In the first step a fractional amount of the original output power of the target Ti:Sapphire laser system is split and spectrally broadened using a photonic crystal fiber (PCF) to establish the octave-spanning spectrum needed for generating the f-to-$2f$ interference signal. For the generation of this signal a Mach-Zehnder-type f-to-$2f$ interferometer is used, featuring

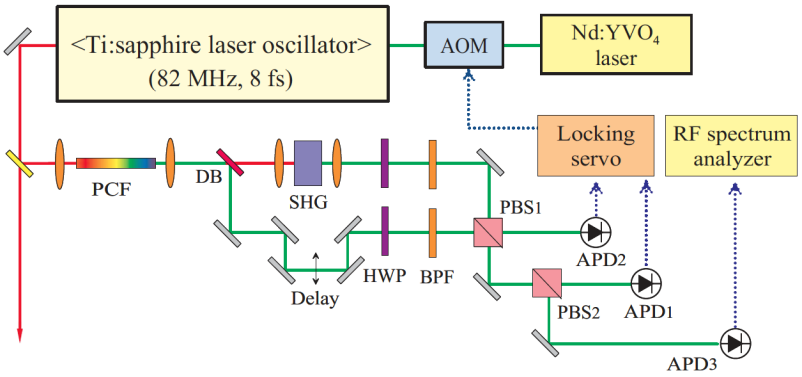

Figure 5.1: Schematic setup used for the direct-locking method [Lee05]; AOM: acousto-optic modulator, APD: avalanche photodiode, BPF: bandpass filter, DB: dichroic beamsplitter, HWP: half-wave plate, PBS: polarizing beamsplitter, PCF: photonic crystal fiber, SHG: second-harmonic-generation crystal.

two completely separated arms for both frequency components. Splitting is done using a dichroic beamsplitter (DB) whereas recombination is realized later-on with a polarizing beamsplitter cube (PBS1). Within the interferometer the second harmonic signal of the 'ν'-component is generated using a KTP crystal. The temporal delay between both arms can be balanced via a small delay-line within the fundamental arm. Both arms are each spectrally bandpass filtered and pass a half-wave plate (HWP) for tuning the intensity for detection, before they are recombined again. The interference signal is detected using an avalanche photodiode (APD1) and writes to:

$$I_{APD1} = A \cdot I_{\nu_{2n}} + B \cdot I_{2\nu_n} + C \cdot \sqrt{I_{\nu_{2n}} I_{2\nu_n}} \cdot \sin(2\pi f_{\mathrm{CEO}} t + \phi_{\mathrm{const}}), \tag{5.1}$$

with A and B being coefficients representing the DC levels arising from both arms and ϕ_{const} a constant phase. To get rid of the DC influences and to isolate the desired interference term, APD2 is set-up that way that it separately detects only the sum of both DC-contributions. This way it can be used to extract the beat signal from the initially detected interference term simply by subtraction. In this respect both DC levels are balanced using the half wave plates within the interferometer arms. The remaining net beat signal can be used in the next step as error signal to suppress the CEP fluctuations. The signal coupled out in the beam before APD1 by the second polarizing beamsplitter cube (PBS2) is used for monitoring issues, e.g. to tune the modulation period close to zero so that it is small enough to be suppressed by an electronic feedback loop, whose operational bandwidth is around 100 kHz [Lee05]. This is done by tuning one intra-cavity prism of the laser oscillator, whereas the modulation signal can be monitored on a simple oscilloscope. In the second step the DC-levels in both interferometer arms are balanced as mentioned above followed by switching on the locking servo suppressing the modulation signal and lock the laser to constant CEP.

Meanwhile this technique was further improved utilizing balanced heterodyne detection

for detecting the desired modulation signal with an increased signal-to-noise ratio and proved its long-term performance [Lee08]. Nevertheless, very less information can be found in the underlying publications giving information on the overall locking performance of this technique. Noise characterizations are only presented up to the low kHz-range and no specifications of the input requirements, e.g. how much laser intensity is necessary for establishing a good stabilization. From the practical point of view working with DC levels of photodiode as reference level for stabilization can be assumed to be very challenging, since even small level changes e.g. given by the laboratory illumination, will lead to a disturbance of the locking scheme. Also the operational bandwidth around 100 kHz of the servo electronics is demanding for the experimental realization, since it requires an initial un-stabilized CEP fluctuation within this range.

5.1.2 Shifting the CEO frequency to zero within the output beam

Another method for generating a self-referenced optical frequency comb with constant CEP was introduced by Grebing et al. in 2009 [Gre09b]. This method combines elements of the traditional *f*-to-*2f* phase coherent locking technique with a self-referencing scheme proposed by Baltuška et al. for parametric amplified pulses, automatically generating a pulse train with vanishing carrier-envelope slipping [Bal02]. This combined method is transferred here to oscillator pulses, the setup shown in Fig. 5.2.

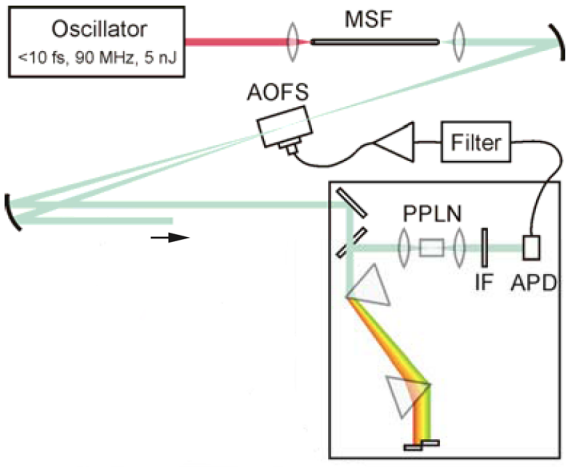

Figure 5.2: Stabilization setup using an AOFS within the output beam to generate a self-referenced optical frequency comb [Gre09b]; AOFS: acousto-optic frequency shifter, APD: avalanche photodiode, IF: interference filter, MSF: microstructured fiber, PPLN: periodically poled lithium niobate crystal (SHG generation).

This technique uses the first order of an acousto-optic frequency shifter (AOFS) within the output beam of a femtosecond laser to shift the CEO frequency to zero. For the experimental implementation the output of a femtosecond Ti:Sapphire laser (< 10 fs, 90 MHz, 5 nJ) is

broadened within a microstructured fiber (MSF) to generate an octave-spanning spectrum for f_{CEO} detection. In the second step this broadened radiation is focused into an acousto-optic frequency shifter (AOFS) splitting the input beam into two output beams: the zero-order beam passes the AOFS without experiencing any frequency shift and the diffracted first-order beam, frequency-shifted relative to the zero-order beam according to the frequency applied to the AOFS. After collimation, the zero-order beam is guided into a common path interferometer [Gre09a] to detect the f_{CEO} beat signal by an avalanche photodiode. Frequency doubling of the 'red' component is done with a periodically poled lithium niobate (PPLN) crystal. After bandpass filtering and amplification, the measured beat signal is fed back to the AOFS shifting the first order beam according to the measured CEO frequency and generating a signal with zero CEO frequency.

This technique is advantageous compared to the traditional phase-coherent locking approach since it does not rely on sophisticated (and expensive) locking electronics and leaves the initial laser oscillator untouched. In this case no direct feedback to the oscillator like pump-power modulation or mirror translation is required to influence f_{CEO}, what would also influence the output power and the stability of the oscillator - all is done 'behind' the laser source. This fact is especially important in terms of long-term performance. The only prerequisite for using this technique is a measurable f_{CEO} signal [Gre09b] with sufficient signal-to-noise ratio. Nevertheless the disadvantages of this method are also obvious. The main drawback is the use of the first diffraction order of an AOFS as applicable laser output. This device will first of all affect the output beam in terms of dispersion, especially for the stabilized few-cycle laser pulses. The additional amount of glass material within the beam will complicate the pulse re-compression with respect to the intended experiments. This is because usually such acousto-optic devices with modulation capabilities up to several tenth of MHz rely on Dense Flint (SF) or Tellurium Dioxide (TeO_2) glass material with length of 12.7 mm up to 25.4 mm, a detailed consideration and dispersion comparison can be found in Section 5.2.1. Next to the temporal dispersion, the output beam will also be affected by angular dispersion due to the broadband diffracted spectra, that has to be compensated for as well. Also the diffraction efficiency of the AOFS is of importance. Assuming a typical single-pass efficiency of about 50 %, the usable stabilized output power will decrease below 50 %.

5.1.3 Extended *f*-to-*2f* self-referencing

As mentioned earlier, the technique adapted within the scope of this thesis follows a more traditional way to generate a pulse train with constant CEP, using an *f*-to-*2f* interferometer for generating the heterodyne beat signal. But because the generation of a pulse train with constant CEP is equivalent to a carrier-envelope-offset frequency zero, given in Eq. (2.11), this intention is not realizable using the basic locking scheme straight forward, since this

necessarily requires to measure f_{CEO} separated from zero frequency. To overcome this dilemma, a suggestion made by Jones et al. in 2000 [Jon00] was resumed here and an acousto-optic frequency shifter integrated in one arm of the *f*-to-*2f* interferometer. In the present implementation this device constantly shifts the frequency components contained within this arm resulting in a measured and shifted CEO frequency f_{CEm} at the photodiode according to:

$$f_{\mathrm{CEm}} = f_{\mathrm{CEO}} \pm f_{\mathrm{AOFS}}. \tag{5.2}$$

This quite simple connection can be derived by including the AOFS driving frequency into the considerations from Eq. (2.14):

$$\begin{aligned} f_{\mathrm{CEm}} &= 2 \cdot (\nu_n) - (\nu_{2n} \pm f_{\mathrm{AOFS}}) \\ &= 2 \cdot (n \cdot f_{\mathrm{rep}} + f_{\mathrm{CEO}}) - (2n \cdot f_{\mathrm{rep}} + f_{\mathrm{CEO}} \pm f_{\mathrm{AOFS}}) \\ &= 2n \cdot f_{\mathrm{rep}} + 2 \cdot f_{\mathrm{CEO}} - 2n \cdot f_{\mathrm{rep}} - f_{\mathrm{CEO}} \pm f_{\mathrm{AOFS}} \\ &= f_{\mathrm{CEO}} \pm f_{\mathrm{AOFS}}. \end{aligned} \tag{5.3}$$

Integrating the AOFS within the nonlinear interferometer and shifting f_{CEO} apart, now opens up for the generation of a pulse train with desired zero CEO frequency, since for $f_{\mathrm{CEO}} = 0$ one detects $f_{\mathrm{CEO}} = f_{\mathrm{AOFS}}$. This frequency is in the order of tenths of MHz and sufficiently separated from zero frequency allowing for stabilization of this signal to a suitable reference as presented below. With this technique it is now possible to achieve the locking performance of the traditional self-referencing locking scheme and generate a phase-locked pulse train with identical field profile for every pulse. Although this approach is more sophisticated in terms of equipment than the alternatives presented before, it is straight forward and the resulting locking-performance unsurpassed, since it can rely on well established phase-coherent locking circuits that proved its capability to generate a carrier-envelope-offset timing jitter as low as 10 attoseconds [Hel03]. The details and results of the experimental implementation of this method are depicted comprehensively in the following sections.

5.2 Laser system stabilized to carrier-envelope-offset frequency zero

The octave-spanning laser oscillator stabilized with respect to carrier-envelope-offset frequency zero is based on a similar system as presented in Chapter 3, with minor changes. For this laser, output coupling is not done with a dispersive output-coupling mirror, but with a standard broadband ZnSe-MgF_2 quarter-wave stack mirror. Additionally, the pulse repetition

rate is changed to 100 MHz. Pumping of the 2 mm thick Ti:Sapphire crystal is done by 532 nm cw-radiation of a frequency doubled Nd:YVO_4 laser (Coherent Verdi V10). Due to the fact that the overall phase-stabilized laser system aims to scientific cooperations, it is mounted together with the pump laser on a common portable breadboard measuring 700 x 900 mm. The aimed at experiments are meanwhile located at the university of Marburg, see Section 5.5.1.

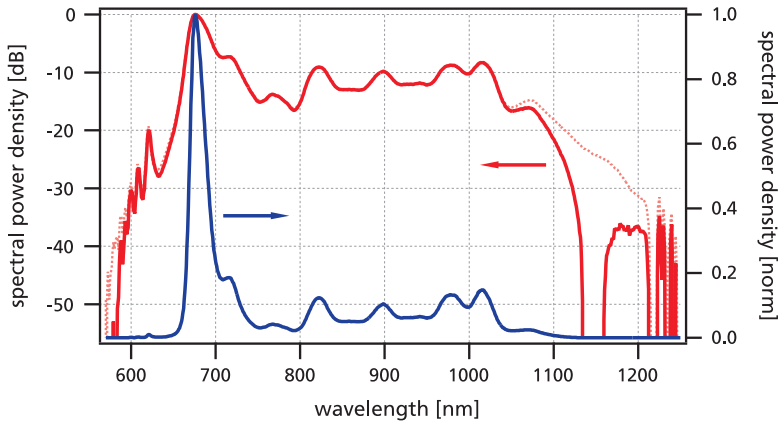

Figure 5.3: Octave-spanning output spectrum shown on a logarithmic (left) and linear scale (right). The dotted logarithmic spectrum illustrates the full oscillator spectrum (Fourier-limit: 4.1 fs), whereas the solid one gives the spectrum remaining for experiments after CEP stabilization (FL: 4.3 fs).

The octave-spanning output spectrum of this laser system is shown in Fig. 5.3. It supports a Fourier-limited pulse duration as short as 4.1 fs (dotted red line) and is sufficient for CEP stabilization without any additional spectral broadening. In this respect, again only the spectral wings centered at 570 nm and 1140 nm are filtered from the spectrum using a multichroic filter to generate the heterodyne beat signal within an *f*-to-*2f* interferometer. The filtered spectrum remaining for subsequent experiments, shown by the solid red line in Fig. 5.3 still supports a Fourier-limited pulse duration as short as 4.3 fs. Without the intensity filtered for f_{CEO} detection – only approximately 20 mW are launched into the interferometer – more than 90 % of the original output power of about 220 mW are available for subsequent experiments. With a pulse repetition rate of 100 MHz this results in a CEP-stabilized pulse energy of approximately 2.2 nJ. The phase-stabilized few-cycle laser pulses emitted by this laser system were characterized with a home-built SPIDER. After extra cavity compression with four bounces on dispersion compensating mirrors and BaF_2 glass material for dispersion fine-tuning, the phase-stabilized pulses were measured to be as short as 4.5 fs, the temporal pulse profile is given in Fig. 5.4.

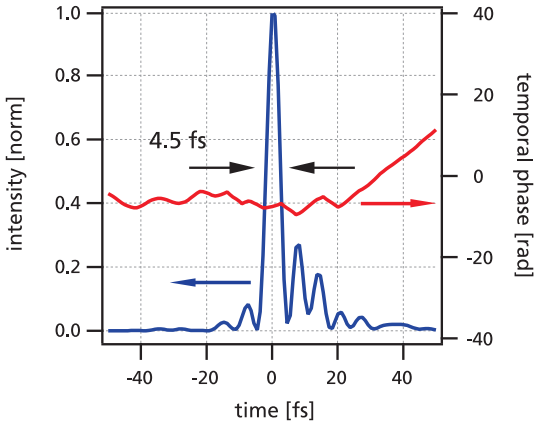

Figure 5.4: Few-cycle CEP-stabilized pulse measured with SPIDER to be as short as 4.5 fs. The pulse was re-compressed using four bounces on DCMP mirrors and some BaF_2 glass material for dispersion fine-tuning.

5.2.1 Carrier-envelope-offset phase stabilization

Extended *f*-to-*2f* interferometer

A schematic setup of the extended *f*-to-*2f* interferometer is given in Fig. 5.5. Within the interferometer the spectral wings centered around 570 nm and 1140 nm, transmitted by the multichroic transmission filter (MCF) are separated by a dielectric dichroic beamsplitter (DBS, CVI Melles Griot). This beamsplitter is made out of BK7 glass material, featuring an higher reflectivity and optical quality compared to the typically used 'extended hot mirrors'. In the present interferometer configuration the 'blue' components at 570 nm become reflected by the DBS whereas the 'red' components at 1140 nm are transmitted. The 'red' arm contains an adjustable quarter-wave plate and can be length-changed, thus the light traveling this arm can be tuned in terms of polarization and delay to allow later on for interference of both frequency components on the highly sensitive avalanche photodiode (Menlo Systems APD210).

The 'blue' arm contains the acousto-optic frequency shifter (AOFS, IntraAction AOM-801), the essential device of this setup. The beam send through this element is collimated and features a radius of approximately 1 mm. The diffracted first order becomes shifted by the AOFS's driving frequency f_{AOFS} and is back-reflected in a way that the beam follows the zero order of the AOFS for the return path. In this implementation the AOFS is driven by a constant frequency of $f_{\mathrm{AOFS}} = 80\,\mathrm{MHz}$, provided by a corresponding RF-amplifier module (IntraAction ME-801). This leads to a 80 MHz-shift of the frequencies contained in this arm as well. Together with the oscillator's repetition frequency of 100 MHz, the chosen 80 MHz allow for the generation of a mixed-down signal of 20 MHz, see below. In the next step

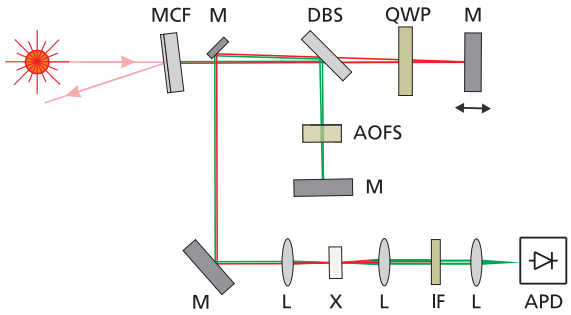

Figure 5.5: Schematic setup of the extended *f*-to-*2f* interferometer - AOFS: acousto-optic frequency shifter; APD: avalanche photodiode; DBS: dichroic beamsplitter, IF: interference filter, L: focusing lens, M: mirror, MCF: multichroic filter, QWP: quarter-wave plate, X: SHG crystal.

both arms are recombined at the DBS and leave this interferometer part of the setup slightly displaced from the input beam to allow for a beam pick-up. The subsequent part is built-up common-path - both frequency components travel collinearly through the components. The infrared light is frequency-doubled in a nonlinear crystal (1 mm LBO) cut for type-I phase matching. Focusing into the crystal is done with an uncoated lens featuring a focal length of $f = 30$ mm. The polarization within the 'blue' arm is tuned by the quarter-wave plate to match the orthogonal polarization of the generated second-harmonic radiation, that the frequency components - now both located around 570 nm - feature the same polarization. After collimation and spectral filtering with a narrowband interference filter (IF) at 570 nm, the radiation is focused onto the highly sensitive avalanche photodiode for heterodyne detection. This measured signal is referred to as f_{CEm}.

Although the AOFS leads to a reduced intensity for the interfering frequency components, still a signal-to-noise ratio greater than 30 dB in a 100 kHz resolution bandwidth results for the detected beat signal, shown in Fig. 5.6. The measurement signal gives the f_{CEm} beat note for switched-on AOFS. Please note that this signal is shifted relative to the laser repetition rate f_{rep}[1] by $f_{\mathrm{AOFS}} = 80$ MHz, resulting in the presented beat signal of $f_{\mathrm{CEm}} = 20$ MHz for $f_{\mathrm{CEO}} = 0$. This offset from zero now allows for a stabilization of the oscillator using a standard phase-locked loop locking-electronics (Menlo Systems XPS800), controlling the applied pump power via an acousto-optic modulator in the pump beam.

Acousto-optic frequency shifter

The used acousto-optic frequency shifter is made out of Dense Flint Glass (Schott SF-4). With an overall length of 12.7 mm and a GDD of 295 fs^2/mm @ 570 nm, it introduces an overall amount of $\approx 7500\,\mathrm{fs}^2$ second order dispersion for the double-pass into this

1 For all these considerations the laser repetition frequency f_{rep} serves as reference point.

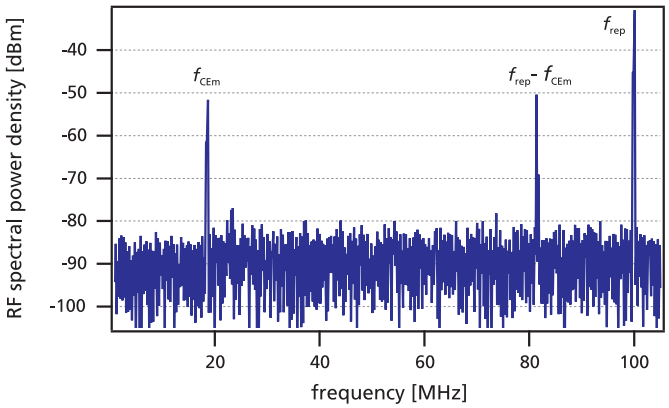

Figure 5.6: 100 MHz frequency span recorded with a 100 kHz resolution bandwidth showing the f_{CEm} beats next to the repetition frequency of 100 MHz with a SNR of about 30 dB.

interferometer arm, which still allows for detection of the interference after a narrowband spectral filtering using a single interference filter. For comparison, an earlier used AOFS with similar frequency specifications but made from 21.8 mm Tellurium Dioxide (TeO_2) glass material introduced an overall amount of $\approx 40500\,\mathrm{fs}^2$ second order dispersion to the setup. With this TeO_2 AOFS no interference signal could be detected. This would comprise a spectral filtering below 1 nm for an observable interference, since the GDD given by this device would lead to a much faster spectral modulation as given in Fig. 2.6. The intensity diffracted into the first order of the AOFS, carrying the desired frequency shifted signal, is in the order of 50 % for the single pass. Thus for the double-pass operation chosen here results an overall shifted intensity of about 25 %. Here the diffracted beam is back-reflected through the zero order of the AOFS for the return path. This intensity is still sufficient to achieve a beat signal with reasonable signal-to-noise ratio as shown in Fig. 5.8. Nevertheless the loss introduced by the AOFS can only be tolerated within the fundamental arm of the interferometer, whereas sufficient initial signal intensity is available at 570 nm.

The locking reference

For the generation of a pulse train with constant CEP and a minor CEO timing jitter, the locking reference f_{Ref} is another essential parameter. For the standard self-referencing scheme this locking-reference is derived from the pulse repetition frequency, and a fluctuation of f_{rep} will be directly translated to f_{CEO}, guaranteeing for a reproduced field for every n^{th} pulse within the train. For the present case also variations of the AOFS driving frequency can contribute to a fluctuation of the carrier-envelope-offset phase, what has to be accounted for as well to establish a pulse train with constant CEP for every pulse. In this regard f_{Ref} is generated by mixing f_{AOFS} at 80 MHz with the laser's repetition frequency of approximately 100 MHz down to a signal located at 20 MHz, schematically shown in Fig. 5.7. For this

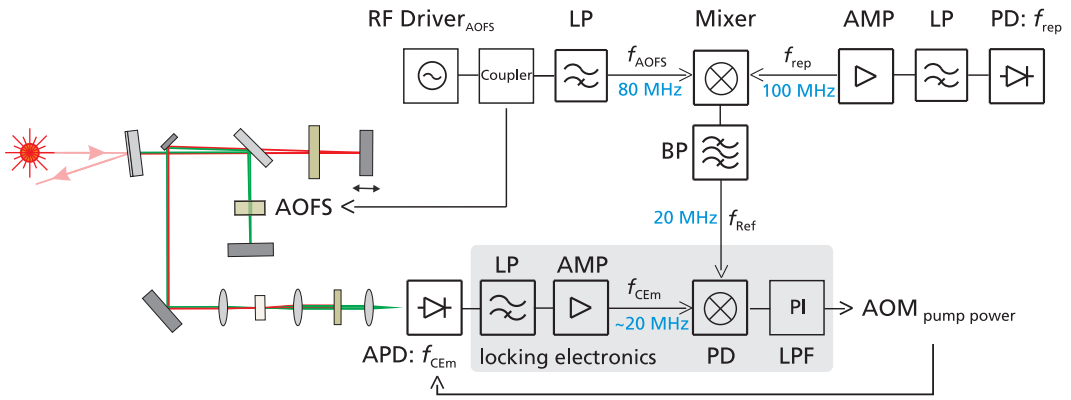

Figure 5.7: Generation of the locking reference; f_{Ref} is generated by mixing the AOFS driving frequency $f_{\mathrm{AOFS}} = 80\,\mathrm{MHz}$ with the repetition frequency $f_{\mathrm{rep}} = 100\,\mathrm{MHz}$ down to 20 MHz. f_{CEO}-locking is accomplished by a PLL controlling the applied pump power; AMP: amplifier, BP: bandpass filter, LP: lowpass filter, LPF: loop filter, PD: phase detector.

mixing process a fraction of the initial RF-power is coupled from the AOFS driver unit. Since this contains additional harmonics, it is lowpass filtered with respect to 80 MHz. On the other hand, the repetition frequency of the laser is detected with a fast photodiode (Thorlabs, DET10A) and lowpass filtered with respect to higher harmonics as well. Due to the fact that the device used for mixing f_{rep} with f_{AOFS} needs sufficient signal levels for proper operation, the filtered photodiode signal is amplified using a low-noise RF-amplifier (MiniCircuits, ZX60-33LN+). Next to the desired signal located at approx. 20 MHz, the mixer output contains several intermediate frequencies and thus has to be bandpass filtered around 20 MHz. The resulting signal can be used directly as reference signal to phase-lock the measured carrier-envelope-offset frequency and fed into one input of the phase detector of the locking electronics. Here the frequency divider, usually used to divide the laser repetition frequency down to a signal around 20 MHz, can be avoided. By including f_{AOFS} and f_{rep} within this reference signal, their fluctuations - also affecting f_{CEm} - are present for both input frequencies of the phase detector and will fall out. With a sufficient SNR of 30 dB measured in a 100 kHz resolution bandwidth, the locking performance of this extended f-to-$2f$ interferometer can be compared to conventional phase-coherent locking, see Section 5.3.1. Figure 5.8 shows a stabilized f_{CEm}-needle recorded in a 100 Hz span with a device limited resolution bandwidth of 1 Hz. With 60 dB above the noise floor this is a very good and clean locking result characterized in more detail in the following paragraphs.

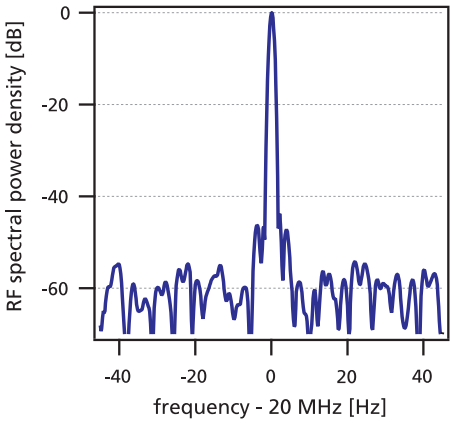

Figure 5.8: In-loop characterized CEP-stabilized f_{CEm} beat note at 20 MHz shown in a 100 Hz span and recorded with 1 Hz resolution bandwidth featuring a SNR greater than 60 dB.

5.3 Characterization of the locking performance

In the following paragraphs the stabilized laser system is characterized in more detail. This characterization is performed in-loop, analyzing the present signals used for stabilization itself, and out-of-loop, utilizing a second *f*-to-*2f* interferometer built-up in the traditional way without an acousto-optic frequency shifter.

5.3.1 In-loop characterization

The in-loop characterizations are based on measuring the frequencies and signals directly involved in the stabilization process. This technique is the only way to characterize the stabilized f_{CEO} beat note, where substitutional the shifted f_{CEm} signal can be characterized. For the out-of-loop case the f_{CEO} beat note is not accessible. A stabilized and in-loop measured f_{CEm} needle was already shown in Fig. 5.8. Figure 5.9 gives the corresponding noise power spectral density of this beat note (red), next to the measurement noise floor (blue) and the noise locking reference f_{Ref} (green). First of all it can be noted that the locking-reference, its noise performance respectively, is nearly as good as the measurement noise floor and does not limit the locking-performance at all. Next, according to the method presented in Section 2.4, the accumulated root-mean-square CEO phase error $\sigma_{\Delta\varphi}$ of the noise PSD can be obtained from this measured data by integrating over the frequency leading to the corresponding timing jitter $\sigma_{\Delta t}$, see Eq. (2.21). For the rms phase noise of the locked beat note a value of $\sigma_{\Delta\varphi}$=164 mrad integrated from 3 Hz to 3 MHz results, giving an rms CEO timing jitter of 64.5 as by relating this value to the carrier frequency f_0 at 375 THz. Similar values have been achieved for the standard locking schemes with $f_{\mathrm{CEO}} = f_{\mathrm{rep}}/4$, ranging between 10 as and 50 as [Müc05, Hel03, Cre08] for a similar frequency range.

Unfortunately, a comparison between this and other techniques used to stabilize f_{CEO}

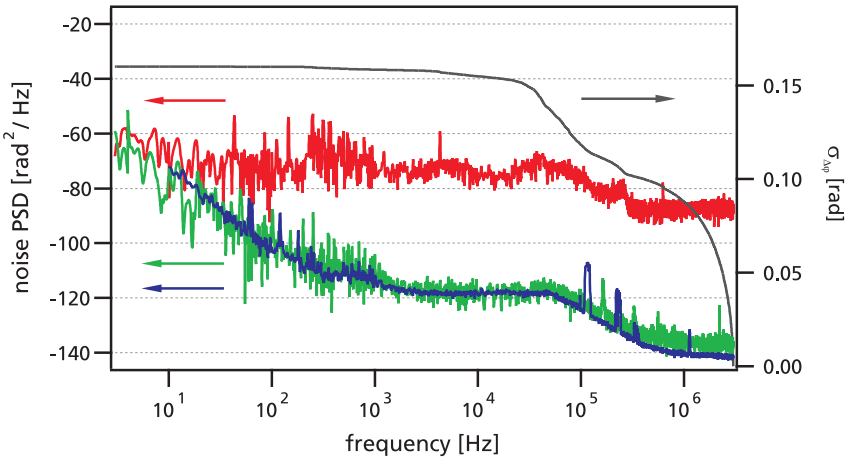

Figure 5.9: In-loop characterized noise PSD of the CEP fluctuations (red), the locking reference (green), and measurement noise floor (blue, 5 averages) next to the integrated rms phase error for the CEP fluctuations (grey, right).

to zero suffers from comparable characterization schemes and measurement data. Lee et al. measured an in-loop accumulated phase error of 50 mrad (100 mrad out-of-loop) integrated from 0.3 Hz only up to 1.5 kHz [Lee05]. Grebing et al. can only rely on characterization measures using an out-of-loop interferometer. For their RF-analysis they obtained an accumulated phase error of about 500 mrad (0.5 Hz - 400 kHz). The analyzed signal results from a homodyne detection of f_{CEO} at zero using two output ports of the out-of-loop interferometer [Gre09b].

5.3.2 Out-of-loop characterization

To verify and characterize the identity of subsequent field profiles out-of-loop, the laser output is split by a broadband 50:50 beamsplitter (Nanolayers GmbH) and guided into a second *f*-to-*2f*-interferometer, the experimental arrangement is given in Fig. 5.10. This out-of-loop interferometer is built-up as the one presented in Section 3.2.1 and does not carry an AOFS for frequency shifting and reveals the unshifted, actual carrier-envelope-offset frequency and phase change for the laser oscillator. Although the laser output is split in front of the out-of-loop interferometer, a f_{CEO} signal with a SNR well above 20 dB in a 100 kHz RBW could be measured here. For the in-loop interferometer a signal with more than 25 dB SNR remains, still sufficient for locking the oscillator even for the reduced intensity levels. The interference signal is fiber-coupled and can be either given to an APD detector (Menlo Systems APD210) for RF-analysis or launched into a highly sensitive fiber-coupled CCD-spectrometer (ANDOR SR300i & Newton^{EM} 970) for spectral characterization.

Since for f_{CEO} locked-to-zero no beat signal would be visible at the out-of-loop interfer-

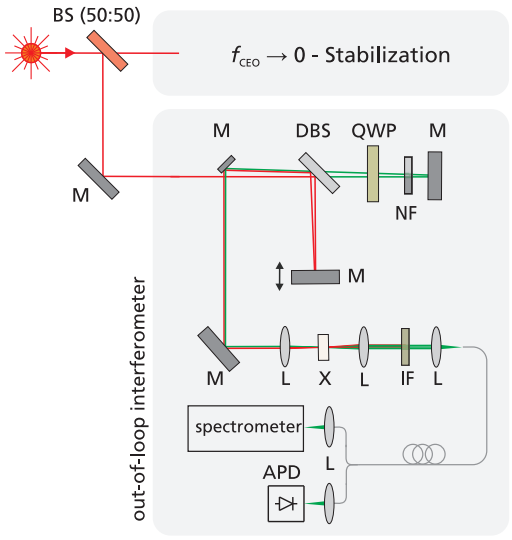

Figure 5.10: Out-of-loop characterization - experimental setup. The laser output is split and launched into the main f-to-$2f$ interferometer from Fig. 5.5 for zero locking and a second f-to-$2f$-interferometer for out-of-loop characterization; APD: avalanche photodiode, BS: beamsplitter, DBS: dichroic beamsplitter, IF: interference filter, L: focusing lens, M: mirror, NF: neutral density filter, QWP: quarter-wave plate, X: SHG crystal.

ometer at all, the RF-characterizations shown below are performed for an un-stabilized, or intentionally bad-locked operation, to visualize the presents of f_{CEO}. For example Fig 5.11 illustrates the relation of the measured CEO frequency between both, in-loop and out-of-loop interferometer. For an in-loop measured f_{CEm}-signal at ≈ 20 MHz the out-of-loop interferometer detects a 80 MHz-shifted signal close to the repetition frequency, $f_{\mathrm{CEO}} \approx 0$ respectively. After locking the laser to zero the out-of-loop f_{CEO} needle vanishes within zero frequency and is not detectable anymore, even with highest possible resolution. For an intentionally bad-locked CEP a comparison of both, zoomed-in stabilized f_{CEm} signal at ≈ 20 MHz and out-of-loop measured repetition frequency, yields some symmetric features around both signals arising from the stabilization process, shown in Fig. 5.12. For switched-off phase lock they vanish at the repetition frequency. Because these features are located around f_{rep} for switched-on lock, this is also a good indication for a locked-to-zero carrier-envelope-offset frequency. Please note that these features are not present for usual operation.

An analog influence of the locked-to-zero CEO frequency can be found in the noise PSD of the f_{rep} signal. Here a clear difference can be found between a loose-locked CEP with a loop gain of '4' and a optimal locked phase with a gain of '7'. In the second case the phase noise is not distinguishable from the f_{rep}-noise without any f_{CEO}-influence anymore, whereas for the loose-locked-case the noise becomes much worse, shown in Fig. 5.13.

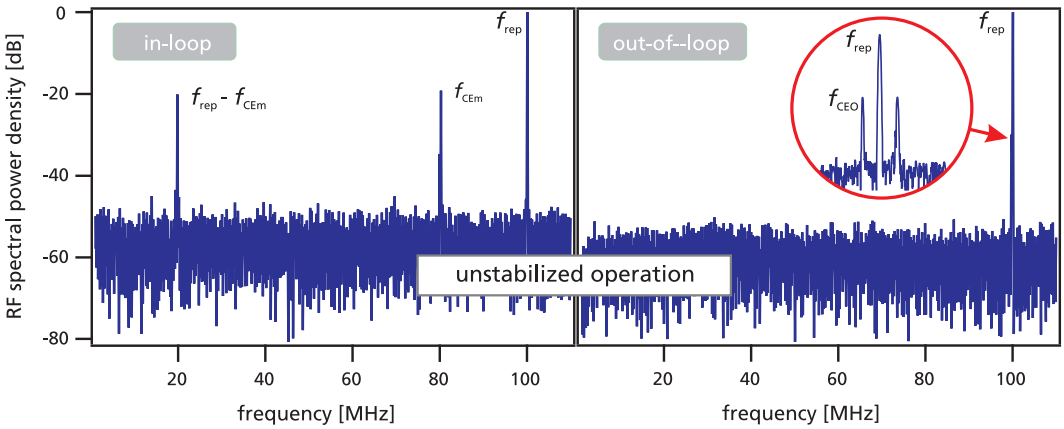

Figure 5.11: Frequency relation between in-loop and out-of-loop interferometer illustrating the 80 MHz shift between the measured CEO frequencies resulting from using a AOFS within the in-loop interferometer. This measurement is recorded for a free-running CEP of the laser.

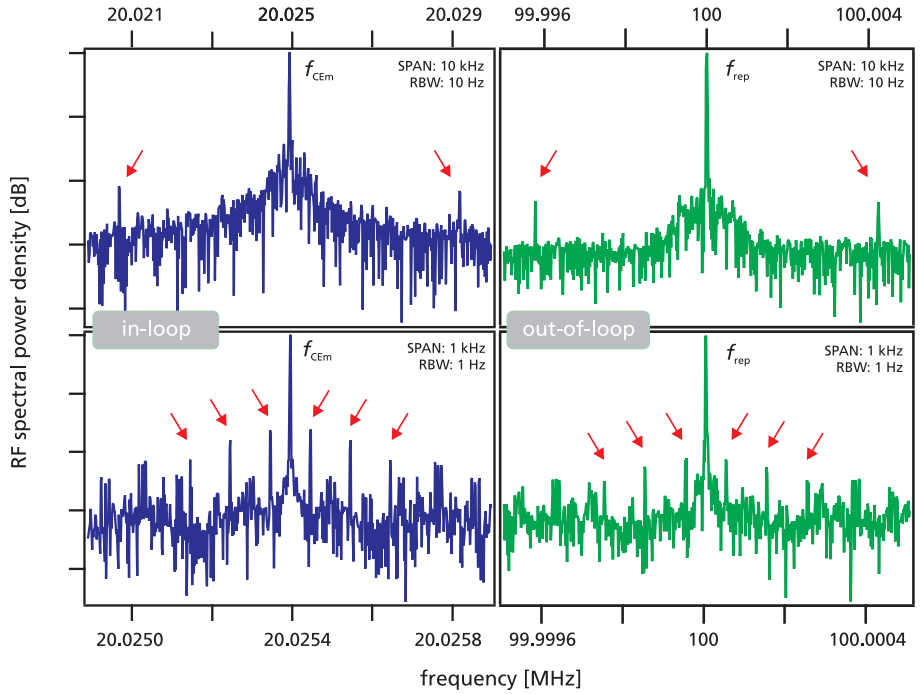

Figure 5.12: Electronic features arising from an intentionally made-bad CEP stabilization process are located symmetrically around f_{CEm} and f_{rep}, shown for two different frequency spans and resolution bandwidths (RBW). For switched-off stabilization these features vanish.

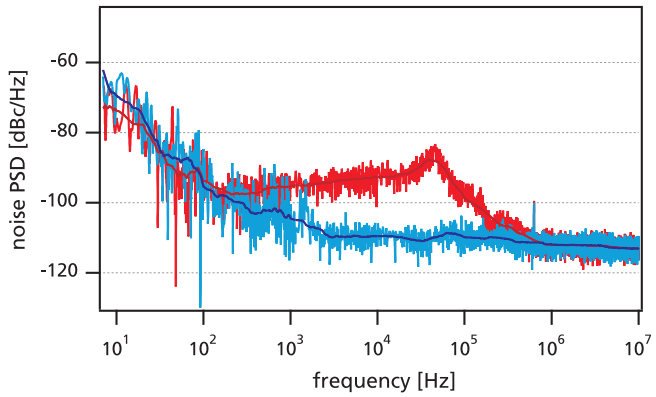

Figure 5.13: Noise PSD shown of the repetition frequency recorded for locked-to-zero operation. The blue plot shows a good CEP lock, whereas in comparison the red curve shows the noise PSD for a loose lock. For both plots an averaged value is plotted as well. In the first case no noise contribution given by the CEP can be noticed, what is different for the loose lock.

The final verification of a locked field profile is a visualization of the spectral interference between the frequency doubled 1140 nm radiation and the fundamental 570 nm light as it is done similarly for low repetition rate amplified pulses [Man06, Ada08]. The crucial aspect for oscillator pulses is that for a typical spectrometer integration time of several milliseconds and a pulse repetition rate of 100 MHz, millions of pulses have to interfere with visible interference contrast, what was never demonstrated before. For capturing such an interference pattern, the output of the out-of-loop interferometer is coupled into the highly sensitive CCD-spectrometer. For contrast reasons the power levels in both interferometer arms are balanced using a neutral density filter attenuating the fundamental arm. Prerequisite for a noticeable interference modulation is a slight delay detuning of the two signals from zero delay of about 50 µm resulting in the interference pattern given in Fig. 5.14 (A), what is to the best of our knowledge the first time that such an measurement result is shown for oscillator pulses, whereas the modulation period can be tuned by altering the delay between both arms. The obtainable contrast of the recorded interference is highly sensitive to the locking strength and immediately vanishes for switched-off lock. The measured spectral data can be corrected with respect to a background given by the single spectral components without interference. Such a corrected interference pattern is shown in Fig. 5.14 (B).

Figure 5.15 shows an interference pattern as given in Fig. 5.14 (B) traced for a time sequence of 2500 s. This impressive interference progression shows the very good locking performance of this system, since it directly visualizes the phase-coherence and stability of millions of interfering pulses. For each single underlying interferogram 10^7 oscillator pulses interfere with negligible phase distortion, for the recorded time of 2500 s all together more than 10^{11}. Figure 5.15 reveals a very slow wavelength drift of the interference pattern

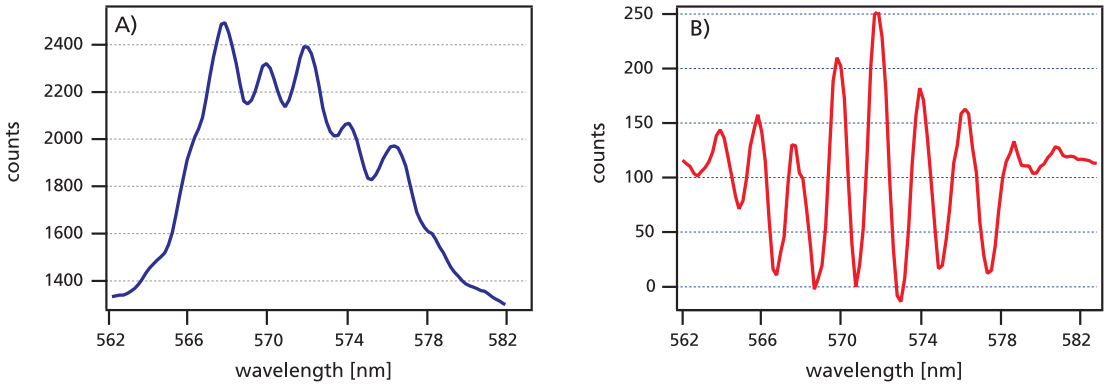

Figure 5.14: Interference pattern of the frequency-doubled 'ν' and fundamental '2ν '-component at 570 nm; A) Smoothed interference modulation recorded with an integration time of 0.1 seconds; B) Signal for a different interference modulation corrected with respect to the measurement background given for switched-off CEP lock.

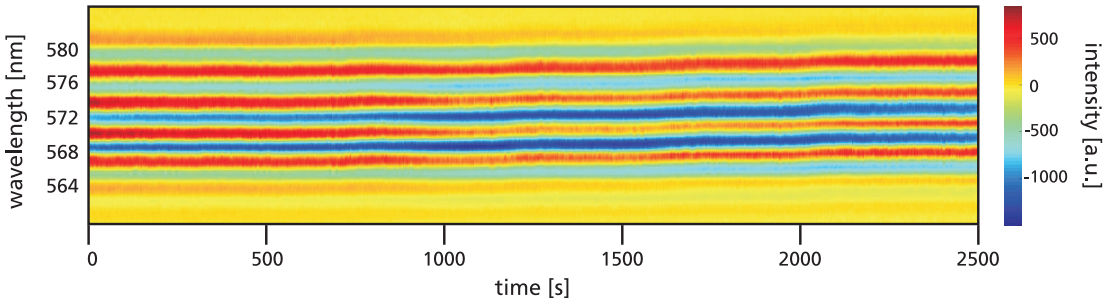

Figure 5.15: Out-of-loop interference of the ν and 2ν components of the stabilized pulse train. The interference is recorded over 2500 seconds with a spectrometer integration time of 0.5 seconds.

over time, whereas the interference contrast in general is not affected. This residual phase drift can be analyzed by Fourier-transforming the interference signal, thereby extracting the phase and tracking this value over the observation time. For the presented measurement a slow phase drift of about 2 rad accumulated over 2500 s results, shown in Fig. 5.16. For shorter time scales this drift can be disregarded since it does not play a role for typical measurement and integration times up to a few seconds. The origin to this drift can be related to thermal variations of the laboratory conditions since the breadboard for the laser and the interferometers is not actively temperature stabilized. This small temperature drift can affect the relative phase between the interfering frequency components resulting e.g. from minimal beam misalignments within the out-of-loop interferometer. Without any slow feedback loop as used in amplified field stable systems this behavior is not surprising at all.

Figure 5.17 shows a comparable interference pattern to Fig. 5.15 while tuning the absolute phase by moving a BaF_2 wedge through the applicable output beam of the laser system. For the experimental realization a wedge pair is placed in Brewsters angle into the laser beam

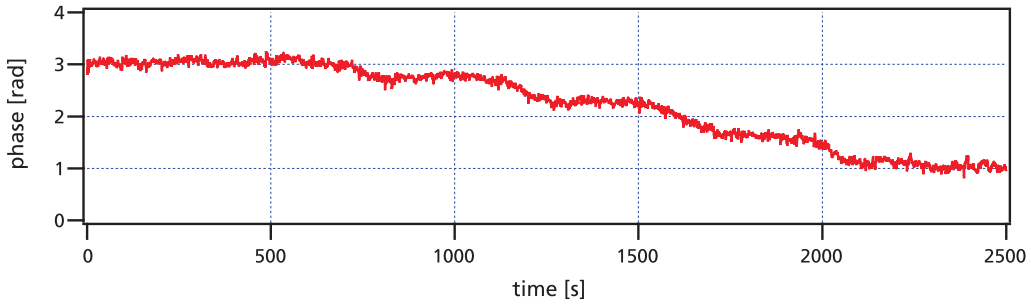

Figure 5.16: Extracted phase of the interference progression given in Fig. 5.15. The overall phase drift within 2500 s is about 2 rad and can be neglected for typical measurement timescales of a few seconds.

in front of the out-of-loop interferometer whereat one wedge is mounted on a electronically controllable translation stage (Newport Agilis series) and can be positioned with 50 nm resolution. After approximately 47 s of recording time, the movable wedge is constantly translated to introduce additional BaF_2 material into the beam what results in a constant shift of the interference maxima within the interference progression. From the analytically extracted phase in the middle of Fig. 5.17 becomes obvious, that after $\approx 65s$ the phase has slipped about a value of 2π. According to Eq. (2.10) the carrier-envelope-offset phase can be shifted about 2π by introducing additional BaF_2 material with a thickness of about 75 µm into the beam. For the interferometric measured phase slip about 2π shown in Fig. 5.17, a measured thickness-change of approximately 81 µm was obtained, what is in good agreement with the theoretical value taking the measurement tolerances into account.

The electric field profiles of the underlying ultrashort pulses are shown in the lower section of Fig. 5.17 for three different phase conditions and the relevant center part of the pulse: at the time t_1 for $\phi_0 = 0$, at t_2 for $\phi_0 = \pi/2$ and at t_3 for $\phi_0 = \pi$. At the time t_4 the CEP lock is switched off and the interference pattern vanishes immediately. The absolute phase is initially chosen to be zero, since it can only be determined experimentally and will evolve on the way to the experiment. Because the presented system is capable to generate a pulse train with constant CEO phase and features the ability to tune this phase about a value of 2π, any experimentally required phase condition or phase dependency can be realized.

Please note that the presented results give only a lower estimate of the system performance because the SNR of the in-loop measured beat note is reduced by about 50 % due to splitting the laser output power for both, stabilization and out-of-loop characterization. Thus for usual operation at full available power the performance can be assumed to be even better.

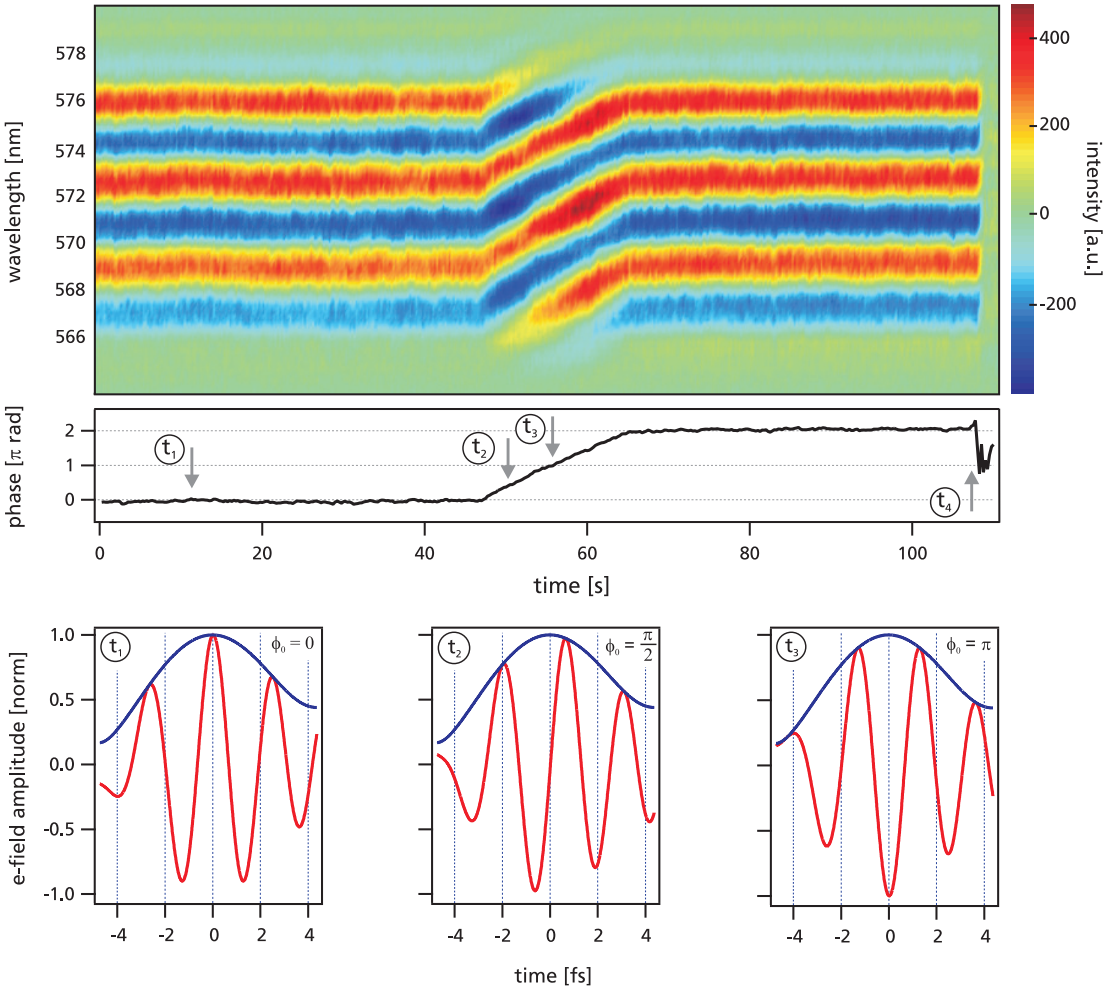

Figure 5.17: CEP interference pattern while shifting the absolute phase with a BaF_2 glass wedge; Top: Out-of-loop spectral interference pattern - starting at approximately 47 s the absolute phase is shifted by steadily inserting BaF_2 into the beam. At 65 s the phase has slipped by about 2π; Middle: Analytically extracted phase of the interference pattern. At time t_4 the lock is switched off; Bottom: Electric field profile of the center parts of the underlying pulses at three different times t_1, t_2 and t_3 with assumed CEP=0 as starting point.

5.4 Discussion, limitations and future prospects

The presented laser system shows unique performance in terms of generating a pulse train with constant CEP with a very low timing jitter next to a good long-term stability. The ability to tune the stabilized phase with a BaF_2 wedge pair within the output beam equips this system with all important degrees of freedom that are required for CEP sensitive experiments at nearly full oscillator power and repetition rate. However there are of course some aspects which could further improve the overall stability and performance.

As usual for CEP stabilization, the signal-to-noise ratio of the measured heterodyne beat note is one of the most important parameters to achieve a good locking performance with low CEO timing jitter. The signal levels obtained in this regard for the presented laser system feature a SNR of up to 30 dB, thereby being located at the lower limit where a reasonable locking performance can be obtained. Here a signal with more than 35 dB SNR would already make a difference for both, locking strength and stability and could improve the already very good stabilization results even more. Of course this signal could be increased directly by more available output power at the desired wavelength regions given by the laser oscillator itself, what is a sophisticated counter play between mirror reflectivity, laser dynamics and output-coupling mirror design. Here the achieved laser performance of 220 mW for octave-spanning operation is already an optimized result. Nevertheless, in this regard a special designed cavity mirror could be used within the laser resonator, only responsible for coupling-out the desired wavelengths required for f_{CEO} detection as presented in [Cre08]. Together with an enhanced diffraction efficiency of the AOFS this could lead to an increased f_{CEO} signal.

The slow thermal phase drift of this system, shown in Fig. 5.15, can be further minimized by integrating pump laser, femtosecond oscillator and f-to-$2f$ interferometer onto one water-cooled and temperature stabilized breadboard. For measurements performed at common integration times up to some seconds, thereby this drift can be neglected. Hence it does not really matter that an implementation of a slow feedback loop as done for amplified systems is not feasible for this system. The problem here is, that not sufficient power is available to generate both, the measurement signal necessary for driving the loop and the subsequent experiments.

In summary the laser system presented in this chapter is to the best of our knowledge the first octave-spanning Ti:sapphire laser oscillator stabilized with respect to carrier-envelope-offset frequency zero, delivering a pulse train with stable and identical field profiles for every pulse within the train [Rau09]. The measured timing jitter of the CEP fluctuations is smaller than 65 attoseconds allowing for the first time to investigate the spectral interference of oscillator pulses at 100 MHz repetition rate, proving an excellent CEP lock. With 220 mW usable average output power at a compressed pulse duration of 4.5 fs, this laser represents a light source with sub-two-cycle pulses, constant CEP and CEP-tuning ability that allows for integration times of several seconds together with an octave-spanning spectrum. All

these aspects make this laser system the ideal source for field sensitive experiments at high repetition rates, for broadband CEP-stable amplifier seeding and above all for delivering the few-cycle input pulses for the field synthesizer, presented in the next chapter.

Above all this laser system, an image shown in Fig. 5.18, is intended to be used as light source for two experiments, shortly introduced below.

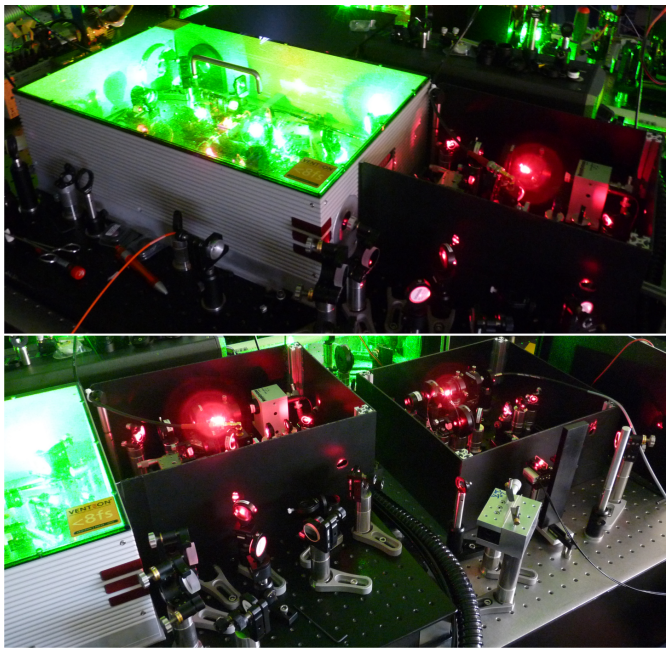

Figure 5.18: f_{CEO}-to-zero stabilized laser system; Top: Oscillator with pump laser and interferometer; Bottom: Extended f-to-$2f$ interferometer (left) and out-of-loop interferometer (right).

5.5 Applications

5.5.1 CEP-dependency of two-photon photoemission spectroscopy

The investigation of coherent optical processes on metal surfaces is a important field of research since it allows for an understanding of microscopic interactions and the physical phenomena related to this. The dynamics of such coherent processes, the time-scale ranging from some femtoseconds to hundreds of picoseconds [Güd08], can be probed by the interaction of an exited electron with the metal surface – its scattering-induced decay.

Recent achievements in femtosecond laser technologies opened up for probing even faster dynamics using two-photon photoemission (2PPE) [Rud77], a pump-probe type spectroscopic method which allows for the investigation of unoccupied electronic states

located between the Fermi level and the vacuum level of a metal or semiconductor surface. In comparison to optical spectroscopy this technique allows for a complete characterization of exited photoelectrons [Güd07].

The schematic principle of 2PPE is shown in Fig. 5.19. A first intense laser pulse (pump) excites an electron from a metal target to an unoccupied bound level below the vacuum energy. The dynamic of this electronic state is then probed by a second, but time-delayed few-cycle laser pulse, which ionizes the electron that can now be analyzed by special hemispheric detectors in terms of its kinetic energy as well as its emission angle.

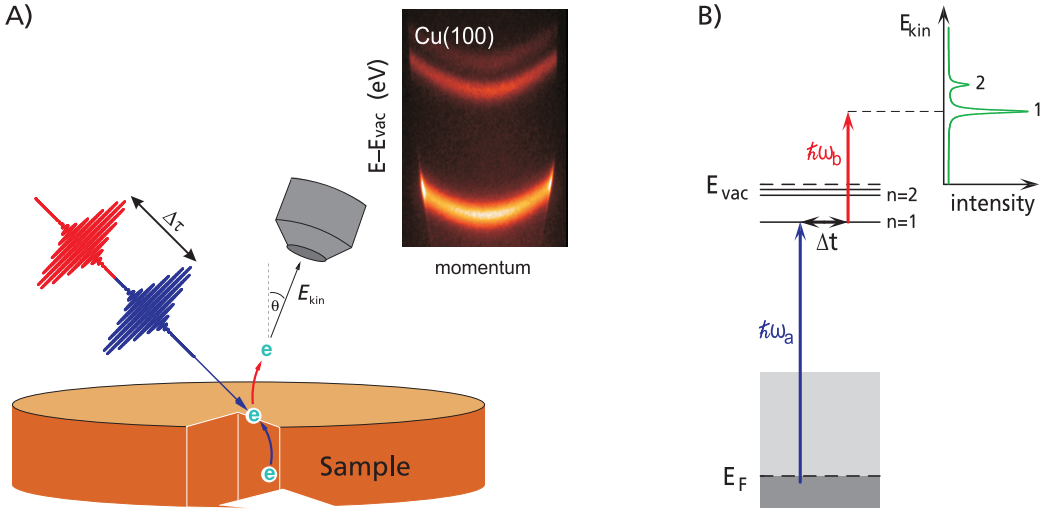

Figure 5.19: Principle of two-photon photoemission spectroscopy; A) Pump-probe type measurement scheme. The ionized photo-electrons are detected by a hemispherical detector in terms of kinetic energy and emission angle, a typical measurement image is shown in-between; B) Corresponding energy diagram. The probe pulse excites an electron to an unoccupied state below the ionization energy where it is caught in an image-potential state. The second, time delayed pulse probes this state and allows for an investigation of the dynamics.

One of the systems that can be analyzed with 2PPE are 'image-potential states' which are quantized electronic states that exist at metal surfaces with a band gap near the vacuum level. Charged particles in front of the surface of a conductive material will experience a Coulomb-like attractive image force, since the electric field strength is always orthogonal on the metal surface. The corresponding potential exhibits energy levels that can be described by a Rydberg series similar to electrons in the hydrogen atom, named image-potential states [Gie85]. Since an in-deep theory of two-photon photoemission is beyond the scope of this thesis, the interested reader is referred to the cited literature and especially the work done by the collaborating partner from the 'Fachbreich Physik und Zentrum für Materialwissenschaften' of the Philipps-Universität of Marburg, Prof. Ulrich Höfer and PD. Jens Güdde [Güd06, Güd07, Güd08].

2PPE with oscillator pulses

The Ti:sapphire laser system presented in this chapter will be used for investigations of the CEP sensitivity of image-potential states, their response to the ultrafast electric field respectively. Here the exited states will be probed with the CEP stabilized few-cycle laser pulses to measure the amount of generated photoelectrons depending on the electric field of the probing pulses. For this kind of investigations the complete pulse train with 100 MHz repetition frequency of the identical pulses can be used and no pulse picking has to be utilized to select the suitable pulses or detected photoelectrons. The phase of the applied few-cycle pulses will be tuned as depicted earlier using a movable BaF_2 wedge pair within the output beam of the laser.

Already a set of measurements have been performed to observe first photo-electrons using this laser source, but since these are the first experimental approaches using Ti:sapphire oscillator pulses to drive the whole 2PPE experiment – usually the intense probe pulses are prepared by an amplified laser system – some experimental aspects have still to be solved for a successful probing, mainly associated with the low pulse energy of the oscillator pulses. At present time the most demanding issue for a successful 2PPE with the phase-stabilized oscillator pulses is the ionization energy of the used metal species, which are e.g. for the commonly used probing-materials copper (Cu100) and silver (Ag111) in the order of 4 eV, 310 nm respectively. These ionization energies cannot be stemmed by the Ti:sapphire laser directly and thus one has to rely on multi-photon absorption processes, which is also quite demanding using the low-energy pulses from a Ti:sapphire oscillator. This laser source could only provide a photon energy of about 2 eV for driving a direct transition. To minimize or solve this problem one approach already under test is lowering the ionization energy of the present targets by e.g evaporating the metal targets with Xenon, resulting in a decreased ionization energy of about 0.5 eV. Another very promising approach is the use of Cesium as a target material, since it already features an ionization energy in the order of 2 eV. It is already in preparation for the experiments.

A different approach could be frequency-doubling the output of the Ti:sapphire laser and pumping the 2PPE experiments directly with frequencies within the target energy range. Unfortunately for few-cycle laser pulses and the involved large bandwidths a broadband frequency-doubling can only be realized with very thin crystals and thus small conversion efficiencies. Hence using the frequency-doubled output of the few-cycle laser oscillator would not be a big advance for this experiments.

Since the energy scaling of few-cycle laser sources with the ability for CEP-stabilization is still ongoing and meanwhile also few-cycle amplifier systems are readily available, a change to such a novel laser source might be an opportunity if the recent efforts concerning the oscillator pulses are not successful. Here one very interesting source could be a few-cycle OPCPA laser system [Sch10], meanwhile delivering sub-8-fs pulses with more than 2 μJ at

143 kHz repetition rate. The thereby used Ti:sapphire master oscillator is similar to the one presented in this chapter and can be CEP stabilized as well. This system could provide much more intense few-cycle pulses for the 2PPE experiments, although at a lower repetition frequency. A CEP conservation was recently demonstrated for the amplified pulses, the testing of its stability being performed at present time.

Another suitable light source for the intended 2PPE experiments could be the synchronously pumped Ti:sapphire laser oscillator, since it could deliver both, an intense green μJ-pulse for pumping the system and a synchronized phase-locked CEP-stabilized probe pulse that can be directly adapted to deliver a pulse train with constant CEP.

5.5.2 CEP-dependency of atomic bound state population

In a second approach to phase dependent physics, the laser system will be used as driving laser to investigate the CEP dependency of bound atomic state populations. Theoretical work has shown that the population probability is depending on the carrier-envelope-offset phase of the few-cycle exciting laser pulse [Nak06]. Recently for single-cycle RF-pulses this dependency was experimentally demonstrated for the ground state hyperfine levels in rubidium atoms [Li10]. A successful experimental verification by using optical few-cycle pulses approaching the single-cycle would allow for probing the atomic response on an attosecond time-scale using low-energy optical laser pulses.

Figure 5.20 (A) shows a two-level system in the semiclassical picture featuring the quantum mechanical atomic representation with the ground state $|0\rangle$ and the excited state $|1\rangle$. In this picture the system is optically pumped by the classical electric field of a few-cycle laser pulse $E(t)$. The quantum mechanical state $|\Psi\rangle$ of this system is a superposition of both states

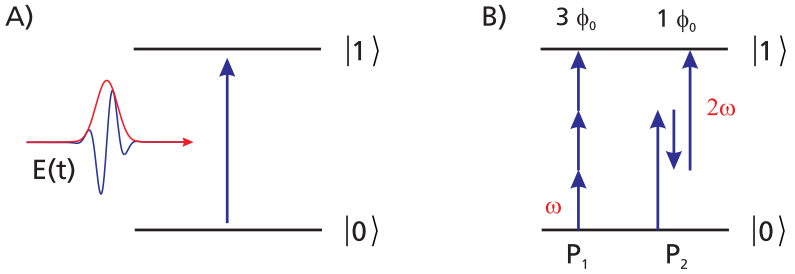

Figure 5.20: Energy level diagram of a two-level system; A) In the semiclassical picture the two-level quantum mechanical system is being pumped by a classical electric field of the driving laser pulse; B) The upper level can be populated by different multi-photon absorption paths, P_1 and P_2.

with the corresponding population probability amplitudes c_0 and c_1. The time depending population probability of the upper level $P_1(t)$, is the absolute square of the corresponding probability amplitude $c_1(t)$. This time dependency of the system can be modeled by the Schrödinger equation, where the population probability amplitudes $c_0(t)$ and $c_1(t)$ can be

described by a set of coupled differential equations:

$$\dot{c}_n(t) = \frac{-i}{\hbar} \sum_j \mu_{nj} E(t) e^{i\Delta\omega t} \cdot c_j(t) \qquad n,j \in \{0,1\} \tag{5.4}$$

with the transition dipole momentum μ_{ij} and the transition frequency $\Delta\omega$. For probing such a system with a few-cycle laser pulse, the time-evolution of the population amplitudes becomes more complex and $P_1(t)$ shows a behavior that is clearly depending on the phase of the incident few-cycle laser pulse.

A physical interpretation of this CEP dependency is based on quantum path interference [Rou07]. In this regime the population amplitudes can be analytically solved using the time dependent perturbation theory. Using this ansatz it can be shown that different paths that can be used to populate the upper level, exhibit different phase terms with respect to the CEP. Figure 5.20 (B) shows for example two different paths where the three-photon absorption features a phase-term including $3 \cdot \phi_0$ whereas the second path includes an $1 \cdot \phi_0$-dependency. These two paths interfere coherently and the resulting population probability depends on the carrier-envelope-offset phase of the driving input pulse. The CEP contribution of this path interference will be modulated with $2\phi_0 = 3\phi_0 - 1\phi_0$.

Thus by probing a compatible atomic system with the broadband CEP-stabilized laser system with constant phase and CEP-tuning ability as presented in this chapter, this CEP-dependency could be measured by detecting the fluorescence of the upper state using e.g. single photon counting. This can be used to investigate the atomic population and field response on an attosecond time scale, a first experimental setup in this regard is already under construction. Using this laser system the measurements can be performed with long integration times to enhance the number of detected photons. Here no de-population arising from different phase conditions that would by present for standardly stabilized laser systems and integrate will limit the measurements. At present time the challenging part is to find a suitable atomic system that can be excited by the spectral components the laser can provide with sufficient power to drive the multi-photon absorption processes.

6 Few-cycle field synthesizer

In this chapter a few-cycle field synthesizer is presented which is an unique combination of an octave-spanning CEP-stabilized Ti:sapphire laser oscillator with a prism-based double-LCD pulse shaper and a SPIDER pulse characterization apparatus. This system is capable to control and manipulate the electric field oscillation of the ultrashort input pulses on a sub-cycle time-scale to form tailored pulse profiles and sequences.

At the beginning of this chapter the principles of few-cycle pulse shaping and field-synthesis will be explained, followed by an introduction of the overall field synthesizer built-up in the scope of this thesis. In the next part of this chapter the experimental results of waveform- and field-synthesis will be presented showing the system's potential to form tailored pulse shapes and sequences in the time and frequency domain for coherent control and CEO-phase sensitive experiments, next to the ability to control the electric field of the input pulses below the cycle scale. Here field oscillations approaching the single-cycle with durations as short as 3.6 fs, which are to the best of our knowledge the shortest pulses ever generated from a laser oscillator [Rau08a], will be presented, followed by a final discussion on the field synthesizer and future prospects of this system.

6.1 Waveform and field synthesis principle

As known from Chapter 2.2 the electric field of a few-cycle laser pulse in the frequency domain can be described by

$$\tilde{E}(\omega) = A(\omega) \cdot e^{i\varphi(\omega)}, \tag{6.1}$$

what is directly connected via a Fourier-transformation with the time domain representation of the pulse, described by the pulse envelope and the carrier oscillation underneath. Due to this relation it is possible to manipulate the temporal representation of the pulse by controlling its spectral amplitude $A(\omega)$ and spectral phase $\varphi(\omega)$ in the frequency domain. From the earlier considerations concerning the carrier-envelope-offset phase (see Section 2.3) it is clear that for few-cycle laser pulses not only their temporal waveform is an important parameter, the exact position of the maximum of the carrier field oscillation underneath the envelope is important as well. Thus by tailoring the spectral characteristics of few-cycle laser pulses together with a stabilization and control of the CEP, all degrees of freedom of the electric field can be manipulated. Such a field synthesizer is a very powerful and versatile tool for numerous few-cycle experiments relying on the waveform or the field-properties of the few-cycle probe pulses.

6.2 Few-cycle field synthesizer

The schematic overview of the overall few-cycle field synthesizer is given in Fig. 6.1.

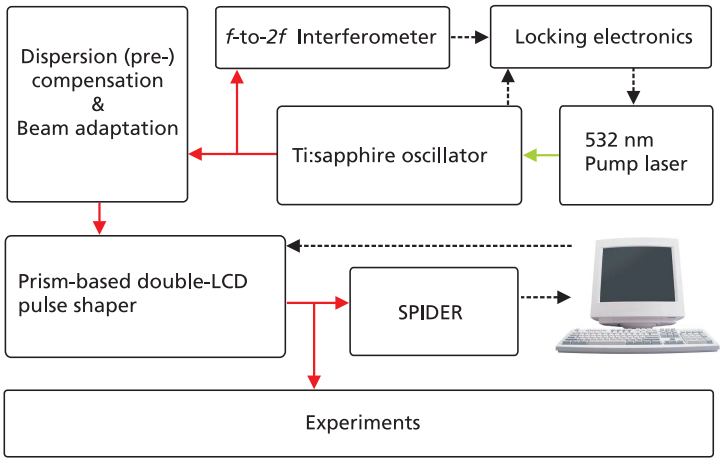

Figure 6.1: Overall scheme of a few-cycle field synthesizer consisting of an octave-spanning CEP stabilized Ti:sapphire oscillator, a double-LCD spatial light modulator, a SPIDER measurement system and a PC for data analysis and shaper control (electrical connections are indicated by dashed lines).

Seed oscillator of this system is the Ti:sapphire oscillator presented in Chapter 3, which serves as octave-spanning light source and can be stabilized with respect to its carrier-envelope-offset phase for electric field control. Within the field synthesizer the phase stabilized few-cycle pulses undergo a dispersion pre-compensation and beam adaption before they enter the prism-based pulse shaper in the next part of the setup. Here, the waveform of the input pulses can be controlled by independently manipulating the spectral phase and amplitude; this central part of the setup will be explained in more detail below. Finally, the shaped pulses can be characterized with a home-built SPIDER apparatus or launched towards the desired experiments. Both, shaper control and SPIDER measurement analysis is done computer-based and allow for a direct feedback to the spatial light modulator to apply the desired phase masks to the shaper.

6.2.1 Prism-based octave-spanning pulse shaper

Key element of the few-cycle field synthesizer is a prism-based pulse shaper, that allows for an independent manipulation of the spectral phase and amplitude, its setup shown in Fig. 6.2. Central element of this pulse shaper is a double-LCD[1] spatial light modulator positioned in the focal plane of a *4f*-geometry [Wei00], more details of this double-LCD will

1 LCD: liquid crystal display

be given in Section 6.3. Compared to different pulse shaper setups using e.g. gratings and lenses for the experimental realization, this shaper is capable of maintaining the octave-spanning input spectra and features a quite high efficiency. A comprehensive overview of different techniques used for femtosecond pulse shaping and the advantages and limitations of the technique used here can be found in [Bin06], since the presented pulse shaper is a further development with respect to amplitude shaping of a previously realized shaper for phase-only shaping [Bin05, Bin06].

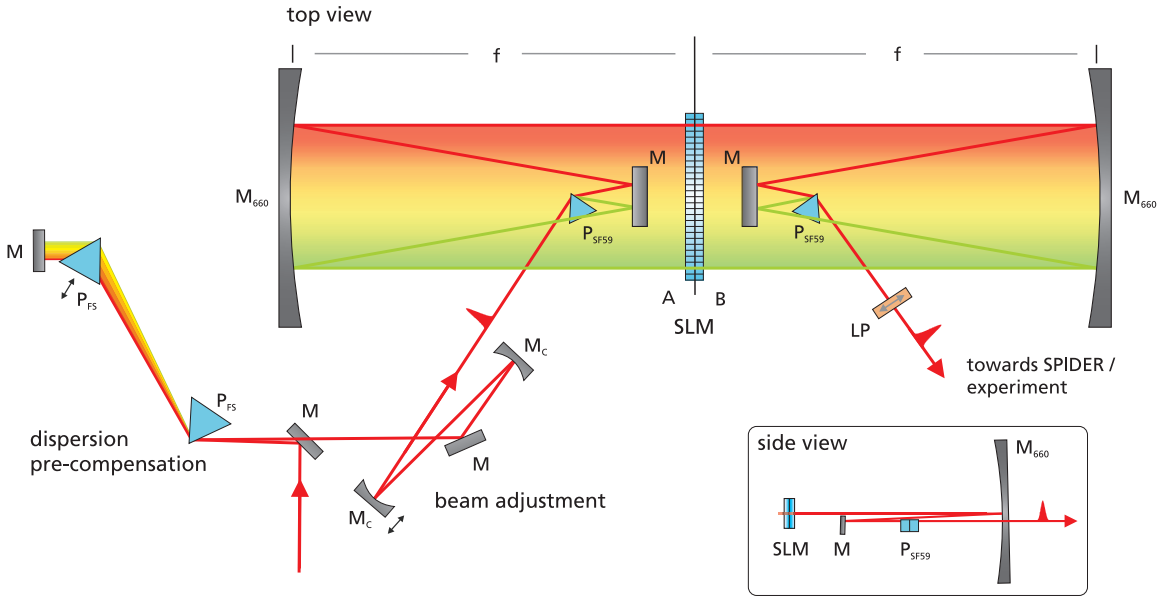

Figure 6.2: Optical setup of the prism-based pulse shaper; f: focal length, LP: linear polarizer, M: mirror, M_{660}: large focusing mirror (f = 660 mm), M_c: focusing mirror, P_{FS}: fused silica prism, $P_{SF_{59}}$: SF_{59} prism, SLM: spatial light modulator (A/B: display numbers).

As mentioned earlier, for an optimal performance of the pulse shaper the input pulse beam has to be adapted in terms of dispersion and geometry. For pre-compensation of the dispersive optics within the setup, especially the highly dispersive SF_{59} prisms introducing a second order dispersion of approximately 2350 fs^2 @ 800 nm for a material thickness of 8 mm[1], the input pulses travel through a fused-silica prism-sequence. This sequence is used in a double-pass configuration at an apex distance of about 1.25 m and generates a negative dispersion characteristic that can lower the second order dispersion within the setup into a range that can be covered by the shaper itself. In the next step the pre-compensated beam is adapted with respect to a 2 mm beam radius and collimated with an all-reflective telescope

1 Dispersion considerations and plots of the phase-only pulse shaper system using the same optical components can be found in [Bin06].

before entering the *4f* pulse shaper geometry, that is commonly used in this regard [Wei00]. By placing a collimating optic, a lens or focusing mirror, at a distance corresponding to the focal length f behind a dispersive element such as a grating or prism, the angular dispersed input beam first of all becomes collimated. Secondly, due to the focusing properties of the collimating optics, a line focus will be generated at the focal distance f behind this element at the Fourier-plane. This element essentially performs a Fourier-transformation that converts the angular dispersion arising from the prism to a spatial separation at the focal plane [Wei00]. Such a line-focus is shown in Fig. 6.3. With an initial beam radius of about 2 mm, a radius at the focal plane of 90 µm can be realized for this setup. By building the shaper symmetrical around this point, overall four times the focal length f is applied and the *4f*-geometry is completed.

Figure 6.3: Picture showing the spectrally dispersed and focused octave-spanning spectrum in the Fourier-plane at the pulse shaper display. The blue-white left part of the line focus arises from artifacts due to capturing the infrared part of the spectrum.

For the pulse shaper presented here, a SF_{59}-prism is used to spectrally disperse the input beam. This prism is located in the focal plane of a first focusing mirror ($f = 660$ mm) which converts the angular dispersion arising from this prism to a spatial separation at the focal plane, where the display of the spatial light modulator is located. This spectral separation now allows for independently manipulating the optical frequency components of the incident femtosecond laser pulse. As said before the pulse shaper setup is build-up symmetric with a second large focusing mirror and SF_{59}-prism together with an identical path geometry, guaranteeing the recombination of the frequency components into a single collimated output beam again. Since this pulse shaper is intended for the manipulation of few-cycle laser pulses, octave-spanning spectra respectively, the setup is built-up with prisms and focusing mirrors instead of gratings and lenses, as it can be done for longer pulses where dispersion and spectral acceptance bandwidth is not as crucial. Since the focusing mirrors have to be used in reflection with small angles, the setup has to be build up horizontally folded, using an additional flat folding mirror as shown in the inlay of Fig. 6.2. Still, after traveling through the overall shaper setup, the available spectral width remains octave-spanning but is slightly narrowed. Compared to the input spectrum (Fig. 3.5), the

spectral edges are steeper resulting from spectral clipping within the pre-compensation prism sequence and the shaper display. The nearly 20 bounces on silver coated mirrors lead together with the transmittance of the display to an optical throughput of the overall pulse shaper setup of about 50 %.

Pulse characterization of the field synthesizer is accomplished with a home-built SPIDER apparatus capable of characterizing few-cycle laser pulses with octave-spanning spectra, as necessary in this case. For this SPIDER system both, data acquisition and pulse reconstruction are performed in real-time allowing for a direct feedback of the present pulse characteristics in the frequency domain, such as SPIDER interferogram, original spectrum, group delay and group delay dispersion, next to the temporal pulse envelope and pulse duration. These informations are essential for a system set-up and a proper alignment e.g. of the dispersion pre-compensation, next to the analysis of the shaped pulses. Also the pulse shaper can be directly controlled by the SPIDER software, providing the basic routines to compute the phase masks to be applied to the shaper. For example, to shape a Fourier-limited pulse with flat spectral phase, the actual SPIDER-measured phase of the unshaped pulse is inverted, converted to a phase mask and applied to the LC displays. The shaping result can be analyzed immediately at the measurement software and in case of an unwanted shaping result it can be dismissed or iterated. Such a shaped pulse with flat spectral phase is exemplarily given in Fig. 6.7(B).

The pulse shaper and field synthesizer as presented above is in general not limited to seed pulse energies in the low nanojoule regime, which is typical for broadband Ti:sapphire oscillators. With respect to the used optics, damage thresholds and nonlinearities respectively, the setup can be used for pulse energies up to some microjoules of any broadband light source in the present wavelength regime. From the experimental point of view e.g. high-energy CEO-phase stabilized broadband seed pulses from an OPCPA system [Fuj06, Ada07, Sch10] would be applicable for a high-energy field synthesizer. This combination would open up for numerous experiments where higher pulse energies are indispensable.

6.3 Spatial light modulator SLM-S640d

Central element of the octave-spanning pulse shaper is a commercial double-LCD spatial light modulator (SLM, Jenoptik SLM-S640d), capable of independently manipulating the spectral phase and amplitude of femtosecond laser pulses. The SLM's specifications are given in Tab. 6.1. This device features two separately controllable and mechanically precisely combined liquid crystal displays with 640 stripe-sized pixels, each featuring a width of 97 µm, shown in Fig. 6.4.

Table 6.1: Double-LCD pulse shaper specifications [Jen06]

Parameter	Value
Wavelength range	430 – 1600 nm
Active area	63.7 mm x 10 mm
Number of stripes (pixels)	2 x 640
Stripe size	96.5 µm x 10 mm
Gap	3.05 µ
Driving voltage (dynamic)	0–8 V (12 bit)
Driving frequency	6 kHz

Each liquid crystal display comprises two electrode plates and a nematic liquid crystal in between. The transparent stripe electrodes (ITO, indium-tin-oxide) themselves are attached to glass substrates. The liquid crystal layer thickness is set to 10 µm and maintained with a spacer. A voltage can be applied between the ITO stripe electrodes with 12 bit resolution to induce an electric field for altering the orientation direction of the liquid crystals in between. Here an alignment layer causes an initial homogenous orientation of the elongated LC molecules in a defined direction [Jen06], which tend to have a parallel orientation and forming an optical anisotropic material. Without an applied electric field, the orientation of the molecules is parallel to the glass plates along the x-axis. For linearly polarized

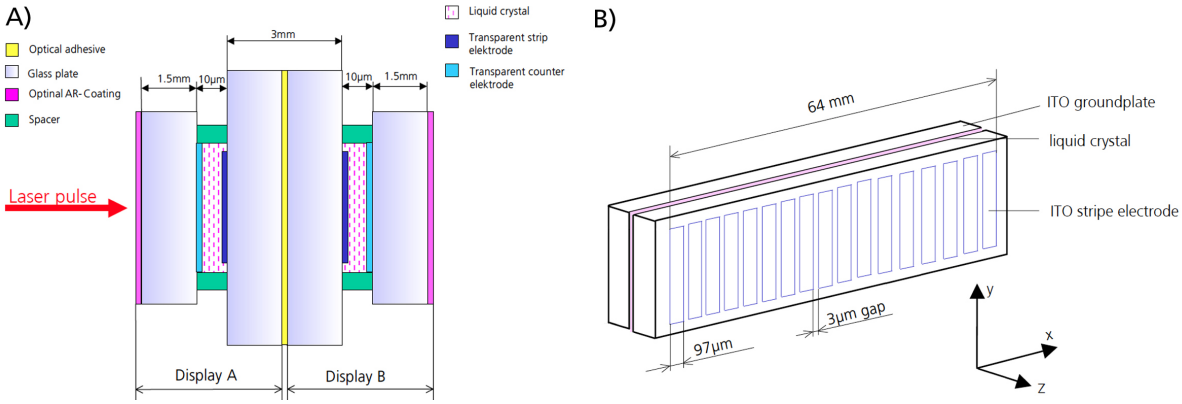

Figure 6.4: Liquid crystal display used for broadband manipulation of few-cycle laser pulses; A) Arrangement of the two independently controllable liquid crystal displays (shown sideways); B) Layout of the ITO stripe electrode of a single LC-cell. The liquid crystal is disposed between the ITO ground plate made out of a glass substrate and carrying the optical transparent ITO electrodes [Jen06].

input light traveling along the z-axis the LC molecules act as an uniaxial birefringent crystal, decomposing input light into two polarizations, one experiencing the extraordinary refractive index n_e (parallel to the x-axis) and the other one the ordinary refractive index n_o (parallel to the y-axis). This optical anisotropy $\Delta n = n_e - n_o$ can be changed by a

voltage-controlled deflection of the LC molecules in the xz-plane, away from their initial position where Δn is maximal. By this deflection the effective extraordinary refractive index becomes lowered. Since the molecule orientation is changed in the xz-plane, the ordinary polarized beam is not affected and a voltage-controllable phase retardation $\Delta\Phi(U)$ can be introduced between the two orthogonal polarization states:

$$\Delta\Phi(U) = \frac{2\pi d}{\lambda} \cdot \left(n_\Theta(U) - n_o\right), \tag{6.2}$$

with the LC layer thickness d, the wavelength λ and the effective voltage controlled projection of n_e, $n_\Theta(U)$.

6.3.1 Independent control of spectral phase and amplitude

For an independent control of amplitude and phase, this concept can be extended by placing a second LCD back-to-back to the first display, their optical axis oriented perpendicular with respect to each other and orientated 45° with respect to the x-axis, shown in Fig. 6.5.

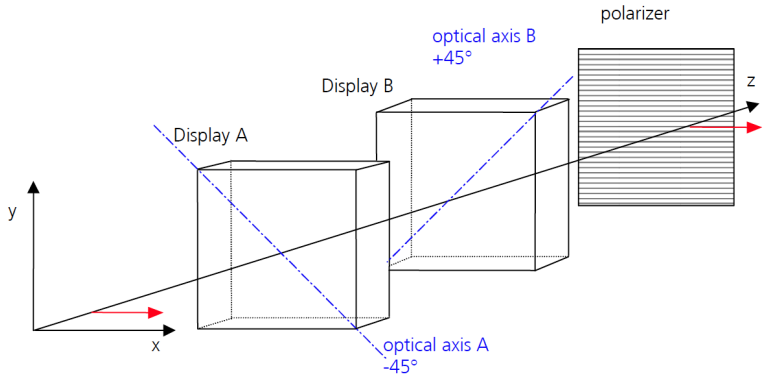

Figure 6.5: Coupling of two LC cells for independent modulation of amplitude and phase of a linear polarized incident light wave [Jen06].

This situation can be mathematically described by a Jones formalism which calculates the output E-field vector according to the input wave traveling through one pixel of the shaper displays and a linear polarizer. Using this formalism, the output field behind a linear x-polarizer writes for a linearly x-polarized input wave traveling along the z-axis to[1]:

$$\vec{E}(t,z) = \begin{bmatrix} 1 \\ 0 \end{bmatrix} \cdot \cos\left(\frac{\Delta\Phi_1 - \Delta\Phi_2}{2}\right) \cdot e^{i\left(\frac{\Delta\Phi_1+\Delta\Phi_2}{2}\right)} \cdot E_0 e^{i(\omega t - kz)}. \tag{6.3}$$

Here the first term, denoted in squared brackets, describes the linear polarizer. $\Delta\Phi_1$ and

1 The exact Jones formalism and considerations can be found in [Jen06].

$\Delta\Phi_2$ appearing in the second and third term are the controllable display phases (phase retardations). According to Eq. (6.3) the phase retardation of the first and the second display act on the amplitude (A) and phase (Φ) of the electric field passing one pixel of the double-LCD as the following:

$$A = E_0 \cdot A_D = E_0 \cdot \cos\left(\frac{\Delta\Phi_1 - \Delta\Phi_2}{2}\right); \quad \Phi = \Phi_0 + \Delta\Phi = \Phi_0 + \frac{\Delta\Phi_1 + \Delta\Phi_2}{2}, \tag{6.4}$$

with E_0 the input amplitude and Φ_0 the input phase respectively. A_D denotes the display amplitude transfer function that can reach values between zero and one. $\Delta\Phi$ gives the additional phase introduced by the display. In order to realize single phase shaping, for the display phases results $\Delta\Phi_1 = \Delta\Phi_2$, as it is for a single amplitude shaping $\Delta\Phi_1 = -\Delta\Phi_2$. For a given amplitude transfer function and phase, the display phases can be calculated by:

$$\Delta\Phi_1 = \Delta\Phi + \arccos(A_D) \qquad \Delta\Phi_2 = \Delta\Phi - \arccos(A_D). \tag{6.5}$$

6.3.2 LCD calibration and shaper control

When using an LCD pulse shaper for few-cycle pulse manipulation, special care has to be taken in terms of a correct calibration of the overall system, since the spectral components of the input pulses are spectrally separated for manipulation and spread over the whole display. First off all a pixel-to-frequency mapping has to be performed, exactly defining which shaper pixel acts on which frequency component. This pixel-to-frequency mapping is done with a special phase pattern applied to the shaper display, setting each 50^{th} pixel to π whereas the other remain at zero. This results in distinct dips within the optical spectrum, that is simultaneously recorded with high resolution behind the shaper[1]. Approximately eight pairs of pixel numbers with corresponding wavelengths of the observed dips are sufficient to calculate a calibration curve using a second order polynomial fit. This calibration curve allows for an exact mapping of frequencies and shaper pixels. Secondly, like for any other diffractive optical element, the LC molecules exhibit a wavelength depended refractive index and thus the desired phase change for a specific pixel has to account for that dependency as well. In this regard the optical anisotropy in Eq. (6.2) has to be added by a wavelength dependency as well:

$$\Delta\Phi(U,\lambda) = \frac{2\pi d}{\lambda} \cdot \Delta n(U,\lambda). \tag{6.6}$$

1 More information about this procedure next to the underlying mechanism can be found in [Bin06].

For these two dependencies of the LC molecules it can be shown that they act in good approximation independently from each other and can be considered separately [Jen06, Bin06]. The wavelength dependency $\Delta n(\lambda)$ can be simply computed for any wavelength by a given fit function related to a reference measurement. This is especially important when working with octave-spanning spectra spanning from 600 nm up to 1200 nm. To account for the voltage dependency, a special calibration measurement can be applied for one specific wavelength, the routine given in [Jen06]. For example, a calibration curve measured with 633 nm light from a HeNe laser is shown in Fig. 6.6.

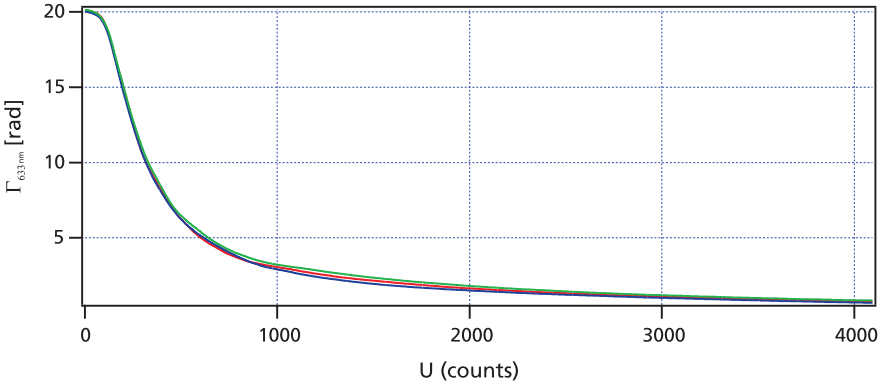

Figure 6.6: Voltage dependency $\Gamma(U,633\,\text{nm})$ of the phase difference measured for a wavelength of 633 nm. The plot shows the calibration data measured for the present system within the laboratory (red, blue) next to the manufacturers data (green).

Finally these two aspects can be combined to the following relation:

$$\Delta\Phi(U,\lambda) = \Gamma_{633\,\text{nm}}(U) \cdot \frac{633\,\text{nm}}{\lambda} \cdot \frac{\Delta n(\lambda)}{\Delta n(633\,\text{nm})} \tag{6.7}$$

Equation (6.7) yield the voltage counts necessary to generate a specific phase difference at a certain wavelength.

After the shaper is calibrated with respect to the above mentioned aspects, the phase masks necessary for the desired phase and amplitude shaping can be applied to the shaper according to the equations given in Eq. (6.5). The last point to be mentioned here is the right choice of a suitable working range of 2π within the plot given in Fig. 6.6. In this regard the important aspect is the wavelength dependency of the optical anisotropy again. Please note here that the calibration plot is given for 633 nm. A phase value of 9.4 rad (3π) @ 633 nm increases to 10.2 rad for 600 nm but decreases to 4.4 rad for 1200 nm. In the scope of this thesis a working range of $0.5 - 2.5\pi$ was found to be ideally suited for the desired shaping needs, since an offset from zero is also required to exclude a negative phase value resulting from Eq. (6.5) (2).

For the experimental realization, a self-written C++ program allows for a data preparation for the shaper. The desired phase and amplitude plots are input to the software and processed to phase masks, voltages pattern respectively, that can be applied to the shaper.

6.4 Pulse-shaping and field-synthesis results

6.4.1 Pulse shaping

In the following paragraphs the results of phase and amplitude shaping are presented. Here the shaping is performed without stabilizing the seed oscillator with respect to its carrier-envelope-offset phase. This establishes a waveform synthesizer that allows for the generation of tailored spectral and temporal pulse shapes next to complex pulse sequences. Please note, that the presented waveforms can be generated identically with CEP stabilized input pulses if this would be required for the specific application. The results obtained with a CEP stabilized laser system in terms of the few-cycle field synthesizer are presented further below. First experiments using the waveform synthesizer were performed by phase-only shaping. Nearly Fourier-limited pulses with a flat spectral phase are generated by applying the inverted SPIDER-measured phase to the shaper. Such a Fourier-limited pulse is shown in Fig. 6.7. The flattened spectral phase together with the octave-spanning spectrum lead to a very clean temporal pulse profile with a duration as short as 4.2 fs, shown Fig. 6.7 (B). The presented spectrum, measured behind the shaper, shows the system's ability to support such broadband spectra. Similar results can be achieved for CEP stabilized input pulses as given in Fig. 3.7, which could be compressed to their Fourier-limited pulse duration with an average output power of about 45 mW using phase-only shaping as well.

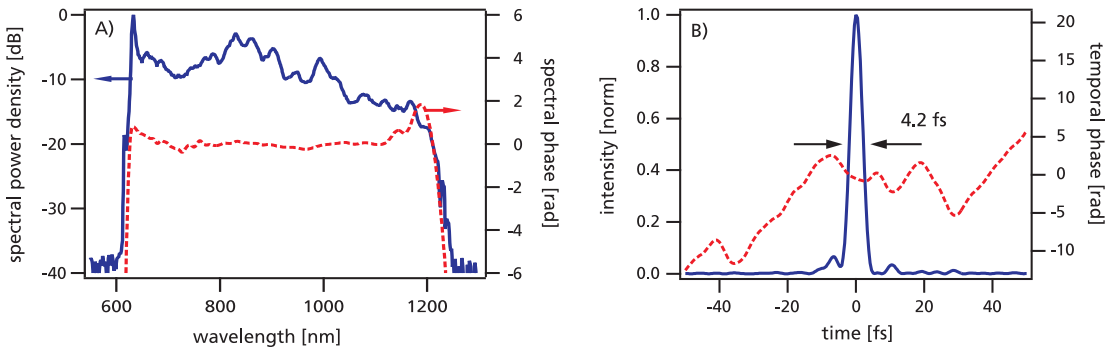

Figure 6.7: Phase-only pulse shaping; A) Available spectrum for pulse shaping experiments together with flattened spectral phase; B) Corresponding pulse in the time domain featuring a duration as short as 4.2 fs (FWHM), characterized with SPIDER.

In this configuration the system is a very efficient tool for flexible dispersion compensation and can balance e.g. the dispersion of up to 30 mm bulk fused silica. Thus this system can

be used e.g. to compensate for the dispersion of input windows to vacuum chambers or a flexible pulse compression with respect to other optical components within the beam path towards the experiment. In comparison, a pulse compression setup realized with dispersion compensating mirrors is usually only appropriate for one specific setup and very inflexible. Even for minimal changes the mirror sequence has to be adapted or wedges have to be moved.

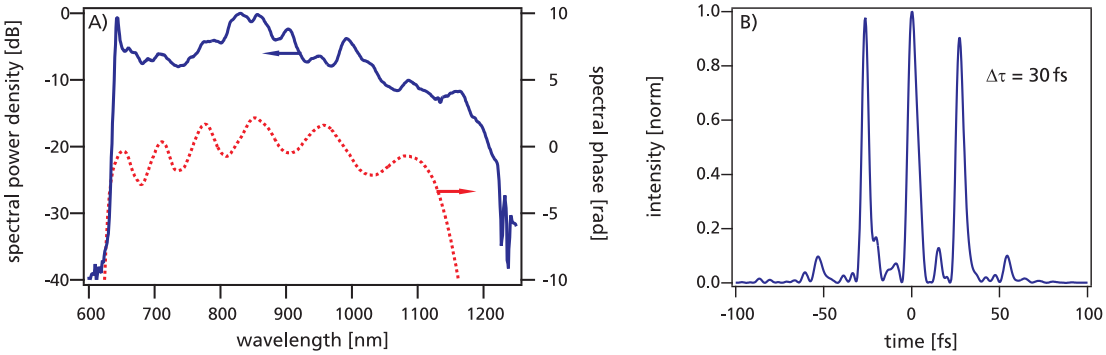

Figure 6.8: Pulse sequence generated by phase-only shaping and introducing a sinusoidal spectral phase to the pulse; A) Spectrum and reconstructed spectral phase; B) Resulting pulse sequence measured with SPIDER.

By phase-only shaping also various pulse sequences can be generated comfortably. Figure 6.8 shows a pulse sequence that is generated by shaping a flat spectral phase followed by the introduction of a sinusoidal modulation onto it. In the time domain this results in a few-cycle pulse sequence where the pulse separation in time is depending on the spectral phase modulation in the frequency domain. Here the presented experimental results are in very good agreement with simulated considerations. In the ideal case, for such pulse sequences the ultrashort input pulse duration is preserved. From the experimental point of view sometimes it can be more desirable to suppress the central part of the sequence to obtain only two pulses with controllable delay that are applicable e.g. to the coherent control experiment. This was realized by applying a more rectangular phase to the shaper, as presented in Fig. 6.9. Using such a spectral phase shape a clean double-pulse structure in the time domain could be generated.

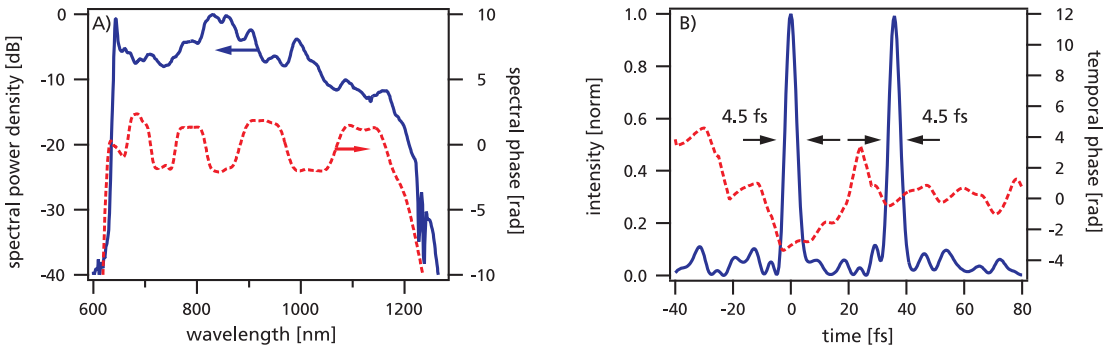

Figure 6.9: Pulse sequence generated by phase-only shaping; A) Underlying pulse spectrum and modulated spectral phase; B) Resulting pulse sequence in the time domain with a duration for the single pulses as short as 4.5 fs (FWHM).

As presented by Binhammer et al. also a two-colored double pulse sequence can be generated by dividing the spectrum and applying a different group delay for each part of the spectrum [Bin05].

In combination with amplitude shaping pulses with almost any desired spectral or temporal shape can be generated out of the octave-spanning input spectrum. Figure 6.10 exemplary shows a shaped pulse with flat spectral phase and rectangular spectrum, resulting in a Sinc-shaped pulse in the time domain. The perfect correlation between experimentally measurement (solid line) and calculated (crossed line) pulse profile shows the potential of this system to shape clean pulses with controllable spectral characteristics from 600 nm up to 1200 nm out of one single broadband input spectrum. Next to rectangular spectral shapes, also triangular and Gaussian-like spectra could be realized with this system.

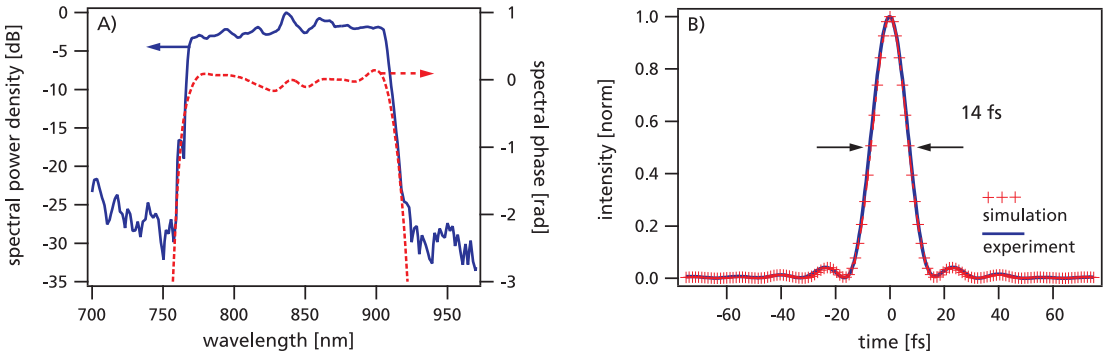

Figure 6.10: Sinc-shaped pulse generated by a combination of phase and amplitude shaping; A) Rectangular spectrum with flat spectral phase; B) Measured and calculated Sinc-shaped pulse in the time domain.

The power of waveform synthesis, combining spectral phase- and amplitude-shaping respectively, to generate ultrashort laser pulses is shown in Fig. 6.11. Here a pulse as short

as 3.6 fs is generated by multiplying the octave-spanning input spectrum with a Gaussian notch filter function centered at 845 nm, enhancing the spectral wings compared to the center parts of the spectrum. Such an M-shaped spectrum supports shorter pulse durations compared to flat spectra with the same spectral bandwidth. For the presented data the Fourier-limited pulse duration for the unshaped input spectrum (dotted blue line) is as short as 4.0 fs, whereas the shaped M-type spectrum (solid blue line) supports Fourier-limited pulses as short as 3.4 fs. For this waveform synthesis the spectral phase is again shaped to be flat to realize a nearly Fourier-limited pulse. This shaped and SPIDER-characterized pulse with a duration as short as 3.6 fs is to the best of our knowledge the shortest pulse ever generated directly from a laser oscillator [Rau08a], featuring an electric field oscillation of the carrier frequency of only 1.3 optical cycles resulting in a considerable CEP contrast enhancement as presented in the following section. Although the presented results are

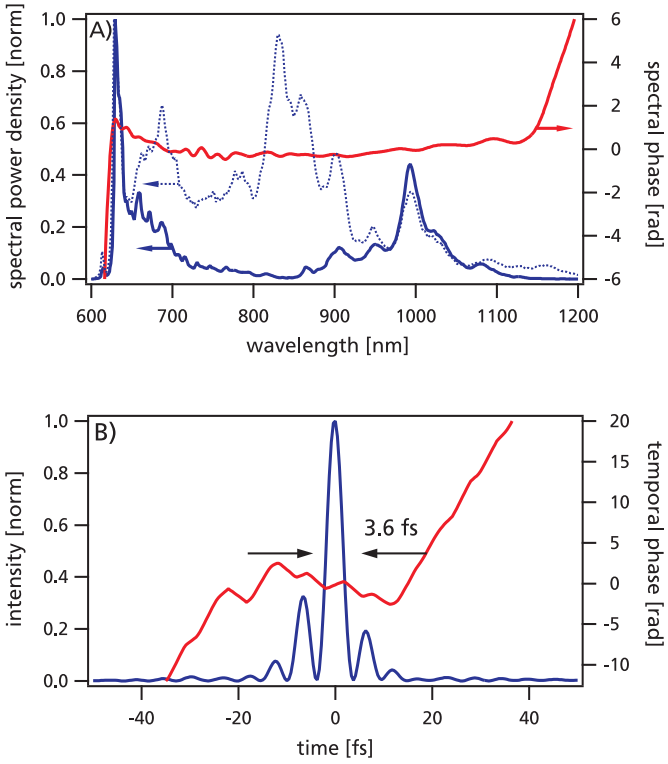

Figure 6.11: Ultrashort pulse generated by phase and amplitude shaping; A) M-shaped shaped spectrum (solid line) and input spectrum (dotted line) with flattened spectral phase; B) SPIDER-characterized pulse in the time domain, measured to be as short as 3.6 fs (FWHM), the shortest pulse ever generated directly from a Ti:sapphire oscillator.

very unique and give rise to control the electric field of such ultrashort pulses below the cycle-scale as presented in the following section, one has to put up with some unwanted side effects of this technique as well. The biggest issue here is losing considerable pulse

energy, since this technique is a subtractive technique and shaping can only be achieved by blocking or attenuating the spectral amplitudes to weight them relatively to each other. Also for the pulse presented in Fig. 6.11 the applied amplitude mask intrinsically lowers the available output pulse energy, since nearly 66 % of the power in the center part of the spectrum is sacrificed due to the M-shaped spectrum. Another side effect of this spectral shape is that it introduces pre-pulses in the time domain, as it can be seen in the lower part of Fig. 6.11.

6.4.2 Field synthesis

For the considerations and results presented in the following paragraphs the main focus is on the ultrashort pulse duration, since the temporal pulse envelope e.g. with a duration as short as 3.6 fs also defines the boundaries for the electric field oscillations underneath. Thus to control the electric field below the cycle scale and form field oscillations approaching the single cycle limit, a pulse duration as short as possible together with CEP stabilized input pulse are an indispensable prerequisite.

The electric field of the nearly single-cycle pulse from Fig. 6.11 is shown in Fig. 6.12. Here the electric field oscillation is plotted below the square root of the pulse intensity envelope. The two inlays show the center part of the pulse for assumed zero and $\pi/2$ carrier-evelope-offset phase[1]. This pulse exhibits a maximum field contrast (maximum electric field amplitude difference between zero and $\pi/2$ CEO-phase) of about 4 %, a contrast between positive and negative oscillation direction of 15 % and a duration as short as 1.3 optical cycles which is 2.7 fs for a carrier oscillation of 375 THz (800 nm).

Figure 6.13 gives a comparison of the central part of the electric field convolution concerning the maximum field contrast. Here a 7 fs-pulse (A) is shown next to a 4.4 fs-pulse (B) from Section 3.11 and the 3.6 fs-pulse (C) presented earlier. It can be seen that for this minimal change in the pulse duration the CEP contrast changes from below 1 % to 3 % and finally to 4 %, since the boundaries given by the waveform become more and more steep for shorter pulse durations. For the presented pulses the contrast between positive and negative direction changes from only 2 % for the 7 fs pulse to 11 % for the 4.4 fs pulse, whereas the 3.6 fs pulse here features enormous contrast of 15 %. This overall contrast enhancement for the ultrashort pulse durations paves the way for further experiments investigating carrier-envelope-offset phase. These field profiles are now ideally suited for probing various systems in terms of CEP sensitivity and electric field response.

The above presented results are performed with pulses stabilized using the standard CEP locking scheme, generating a pulse train with reproduced electric field for every 4^{th} pulse in row. A much preferable seed source for the field synthesizer would be the laser system presented in Chapter 5, generating a pulse train with constant CEP and carrier-envelope timing jitter as low as 65 as, since sophisticated pulse picking to select each 4^{th} identical

1 As usual for such considerations the absolute phase can not be distinguished from these experiments, but can be relatively tuned as presented in Section 5.3.2 and therefore assumed to be e.g. zero.

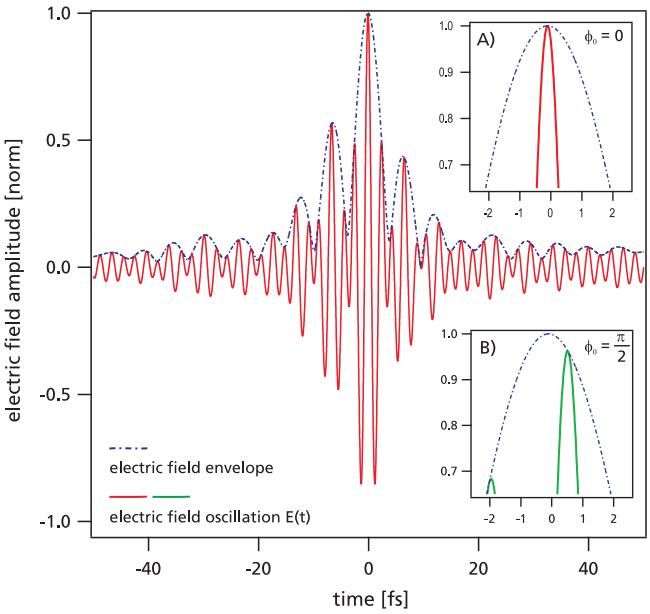

Figure 6.12: Electric field evolution of a shaped 3.6 fs short laser pulse; Inlay A) Zoomed-in field maximum with assumed zero CEO-phase; B) Zoomed-in field maximum with assumed CEO-phase of $\pi/2$.

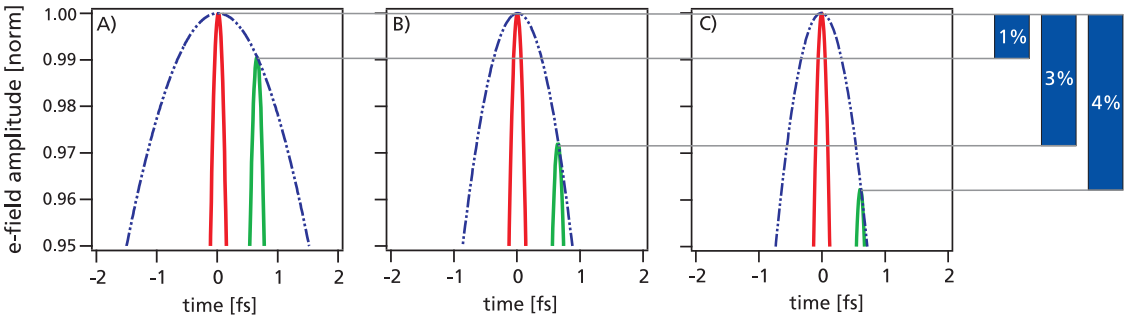

Figure 6.13: Comparison of the maximal electric field contrast for three few-cycle laser pulses with a duration of 7 fs (A), 4.4 fs (B) and 3.6 fs (C).

pulse could be avoided[1]. This timing jitter can be directly transferred to the seed oscillator of this field synthesizer. Since the SNR for the f_{CEO} beat note is even better for this system and thus the locking-performance, the CEP timing jitter can be assumed to be even in the order of 50 attoseconds.

1 The laser system with constant CEP was realized in the second part of this thesis and primarily intended for different experiments, whereas the field synthesis experiments have been performed more at the beginning. Nevertheless the new system should be 100 % compatible to the field synthesizer and will be used in this regard for further experiments.

6.5 Discussion

The above presented results show a very powerful and flexible field synthesizer system opening up to form tailored pulse shapes and sequences next to the shortest pulses ever generated directly from an oscillator with a duration as short as 1.3 optical cycles. On the other hand, together with the ability to control the CEP of the seed pulses with less than 65 as timing jitter, the electric field of the synthesized waveforms can be controlled below the cycle scale. Next to this, nearly any desired spectral phase and amplitude curve can be realized within the limits of the system, which are for example the frequency resolution given by the SLM-display and the shaper setup, the dynamic range for amplitude shaping, the maximal phase shift that can be applied between the frequency components and a SPIDER-measurable shaping result.

The potential of this unique system can be further enhanced, since the pulse shaper setup is directly compatible to different broadband light sources. In this respect another promising light source would be a broadband CEP stabilized OPCPA system with μJ pulse energies, as it is already under investigation in the research group [Sch10]. Such a system with nearly octave-spanning output spectra, more than 2 μJ of pulse energy at a repetition rate of 143 kHz together with the ability of CEP control would highly increase the systems usability for experiments requiring an increased pulse energy. The drawback arising form the lossy subtractive pulse shaping technique could be counteracted with such a powerful seed source, since it delivers sufficient output power that to a certain extend the power-loss by the shaping process can be tolerated. The associated pulse energies are compatible to the field synthesizer as well, since the damage thresholds e.g. of the LC-displays are higher than the thereby involved energies. Of course care has to be taken not to generate white-light within the used prisms of the dispersion pre-compensation and the *4f*-setup.

Nevertheless the field synthesizer exhibits potential for further improvements as well. For example the SLM can be upgraded to be used in a double-pass configuration. In this regard a silver mirror can be directly attached behind the shaper plane, reflecting the light back to the display. This allows for an increased maximal phase change of the displays since they are passed twice. This double-pass configuration would allow as well for a more compact setup, since it is folded in the middle. Also the computer control of the shaper shows potential for further improvements, especially with respect to a more automated operation. At present time the desired phase masks applied to the shaper are generated manually and loaded into the software. Here a software add-on allowing for the basic shapes and e.g. an genetic algorithm automatically optimizing the pulses with respect to the desired experiment, could further improve the usability and the experimental impact of this system.

Although this field-synthesizer is a very complex system consisting out of several parts, the stable setup and numerous beam references allow for an easy handling and reproducible operation, even after long periods without use.

7 Conclusion and outlook

The goal of this work was the generation and control of few-cycle field oscillations approaching the single-cycle limit.

In this thesis an octave-spanning Ti:sapphire oscillator was realized to deliver broadband few-cycle femtosecond pulses. At present time this laser system produces to the best of our knowledge the shortest pulses ever generated directly from a femtosecond oscillator, featuring a Fourier-limited pulse duration as short as 3.7 fs and a SPIDER-characterized pulse duration as short as 4.3 fs [Rau08b]. The octave-spanning output spectrum spans more than one optical octave and exhibits substantial spectral power even above 1200 nm. This system can be directly stabilized with respect to its carrier-envelope-offset phase without additional spectral broadening.

The octave-spanning Ti:sapphire oscillator was used to seed a few-cycle field synthesizer, which is an unique combination of that laser with a prism-based double-LCD pulse shaper setup that is capable of an independent manipulation of the spectral amplitude and phase of few-cycle input pulses. A SPIDER measurement apparatus for spectral characterization of the generated field profiles completes the field synthesizer as diagnostic unit. This overall system allows for the control and manipulation of all parameters necessary to influence the electric field of few-cycle laser pulses to generate tailored field oscillations with durations approaching the cycle-scale. Using this tool it was possible to generate field profiles with a duration as short as 3.6 fs [Rau08a] and an enhanced electric field contrast of about 15 % for the CEP stable pulses. The overall modular setup of this synthesizer can easily accept any broadband laser source for seeding, besides Ti:sapphire oscillators also broadband amplified systems like OPCPA or NOPA.

Different approaches have been made in this thesis to further enhance broadband Ti:sapphire oscillators. A synchronously-pumped Ti:sapphire oscillator, pumped by a frequency-doubled Yb:KLuW thin-disk oscillator, was realized [Bin10], delivering an octave-spanning output spectrum next to an ability for self-starting, not present for cw-pumped Kerr-lens mode-locked Ti:sapphire oscillators. Also a self-synchronization of the femtosecond laser and the thin-disk pump was observed, adding another desirable feature to this system, since this combined laser source could deliver both, an intense green or infrared pump pulse together with a synchronized broadband CEP-stabilized few-cycle pulse.

The carrier-envelope-offset phase stabilization of octave-spanning Ti:sapphire oscillators was extended in this work as well to generate a few-cycle pulse train with constant CEP. Such a pulse train features an identical electric field profile for each pulse within the train

and simplifies the experimental application for field sensitive experiments relying on long integration times. Here sophisticated pulse picking can be omitted and the full available oscillator power used at full repetition rate for the experiments. For the realized laser system thereby a self-referenced spectral interference of 10^{11} oscillator pulses could be demonstrated in an out-of-loop interferometer [Rau09]. This special few-cycle oscillator was realized in terms of a scientific cooperation with the Philips University of Marburg to investigate the CEP dependency of two-photon photoemission on metal surfaces.

The potential to generate few-cycle laser pulses directly from Ti:sapphire oscillators can be assumed to be fully exploited by the results of this thesis. In order to generate even broader output spectra from an oscillator, novel concepts have to be found to assist the Ti:sapphire crystal, for example by combining the gain spectra of different laser crystals within one resonator. In this regard a very promising approach could be the combination of a Ti:sapphire crystal with a Cr:forsterite crystal, the combined gain spectra theoretically allowing to enhance the output spectrum further into the infrared wavelength region even beyond the telecom window around 1500 nm. Such an enormous spectral output characteristic would allow for the generation of single-cycle femtosecond laser pulses and would comprise an usable bandwidth from 600 nm up to 1500 nm. This would be directly beneficial e.g. for the experiments related to probing the CEP dependency of atomic state populations with optical pulses.
Also the intra-cavity combination of Ti:sapphire with a nonlinear crystal for frequency conversion to different spectral regions might be a feasible route for further spectral broadening.

The broadband amplification of few-cycle pulses delivered by Ti:sapphire oscillators can be already provided by OPCPA systems, whereas pulse energies of some μJ at hundreds of kilohertz repetition frequency and sub-10- fs pulse durations have already been demonstrated [Sch10]. The CEP preservation and stability of such amplified broadband few-cycle sources has already been shown. The concept of the few-cycle field synthesizer presented in this thesis can be easily transferred to these powerful few-cycle pulses as well and thus has most relevance to further enhance the experimental impact of this tool, since many applications in ultrafast science e.g. probing nonlinear light matter interactions, require an increased pulse energy beyond the typical femtosecond oscillator. Such applications would directly benefit from a few-cycle field synthesizer delivering μJ pulse energies with controllable electric field properties of the underlying electric field on the cycle-scale.

Bibliography

[Ada07] S. Adachi, H. Ishii, T. Kanai, N. Ishii, A. Kosuge, S. Watanabe, *1.5 mJ, 6.4 fs parametric chirped-pulse amplification system at 1 kHz*, Opt. Lett. **32**, 2487–2489 (2007).

[Ada08] S. Adachi, N. Ishii, T. Kanai, A. Kosuge, J. Itatani, Y. Kobayashi, D. Yoshitomi, K. Torizuka, S. Watanabe, *5-fs, multi-mJ, CEP-locked parametric chirped-pulse amplifier pumped by a 450-nm source at 1 kHz*, Opt. Exp. **16**, 14341–14352 (2008).

[And00] M. Anderson, L. de Araujo, E. Kosik, I. Walmsley, *The effects of noise on ultrashort-opticalpulse measurement using SPIDER*, Appl. Phys. B **70**, 85–93 (2000).

[Apo00] A. Apolonski, A. Poppe, G. Tempea, C. Spielmann, T. Udem, R. Holzwarth, T. W. Hänsch, F. Krausz, *Controlling the Phase Evolution of Few-Cycle Light Pulses*, Phys. Rev. Lett. **85**, 740–743 (2000).

[Apo04] A. Apolonski, P. Dombi, G. G. Paulus, M. Kakehata, R. Holzwarth, T. Udem, C. Lemell, K. Torizuka, J. Burgdörfer, T. Hänsch, F. Krausz, *Observation of Light-Phase-Sensitive Photoemission from a Metal*, Phys. Rev. Lett. **9**, 073902 (2004).

[Bae10] C. R. Baer, C. Kränkel, C. J. Saraceno, O. H. Heckl, M. Golling, T. Südmeyer, U. Keller, R. Peters, K. Petermann, G. Huber, *Efficient mode-locked Yb:Lu_2O_3 thin disk laser with an average power of 103 W*, Advanced Solid-State Photonics Conference (ASSP) **AMD2** (2010).

[Bal02] A. Baltuška, T. Fuji, T. Kobayashi, *Controlling the Carrier-Envelope Phase of Ultrashort Light Pulses with Optical Parametric Amplifiers*, Phys. Rev. Lett. **88**, 133901 (2002).

[Bal03] A. Baltuška, T. Udem, M. Uiberacker, M. Hentschel, E. Goulielmakis, C. Gohle, R. Holzwarth, V. S. Yakovlev, A. Scrinzi, T. W. Hänsch, F. Krausz, *Attosecond control of electronic processes by intense light fields*, Nature **421**, 611–615 (2003).

[Bar07] A. Bartels, R. Gebs, M. S. Kirchner, S. A. Diddams, *Spectrally resolved optical frequency comb from a self-referenced 5 GHz femtosecond laser*, Opt. Lett. **32**, 2553–2555 (2007).

[Bet04] M. Betz, F. Sotier, F. Tauser, S. Trumm, A. Laubereau, A. Leitenstorfer, *All-optical phase locking of two femtosecond Ti : sapphire lasers: a passive coupling mechanism beyond the slowly varying amplitude approximation*, Opt. Lett. **29**, 629–631 (2004).

[Bin05] T. Binhammer, E. Rittweger, R. Ell, F. X. Kärtner, U. Morgner, *Prism-based Pulse Shaper for Octave Spanning Spectra*, IEEE Journ. of Quantum Electron. **41**, 1552–1557 (2005).

[Bin06] T. Binhammer, *Erzeugung und Anwendung geformter Laserpulse mit oktavbreitem Spektrum*, Dissertation, Universität Heidelberg (2006).

[Bin10] T. Binhammer, S. Rausch, M. Jackstadt, G. Palmer, U. Morgner, *Phase-stable Ti:Sapphire Oscillator Quasi-Synchronously Pumped by a Thin-Disk Laser*, Appl. Phys. B **100** (2010).

[Che99] Y. Chen, F. Kärtner, U. Morgner, S. Sho, H. Haus, E. Ippen, J. Fujimoto, *Dispersion-managed mode locking*, J. Opt. Soc. Am. B **16**, 1999–2004 (1999).

[Cre08] H. M. Crespo, J. R. Birge, E. L. Falcão-Filho, M. Y. Sander, A. Benedick, F. X. Kärtner, *Nonintrusive phase stabilization of sub-two-cycle pulses from a prismless octave-spanning Ti:sapphire laser*, Opt. Lett. **33**, 833–835 (2008).

[Did05] S. A. Diddams, J. Ye, L. Hollberg, *Femtosecond Lasers for Optical Clocks and Low Noise Frequency Synthesis*, in *Femtosecond Optical Frequency Comb: Princile, Operation, and Applications* (J. Ye and S. Cundiff, 2005).

[Die06] J.-C. Diels, W. Rudolph, *Ultrashort Laser Pulse Phenomena* (Academic Press, 2006).

[Dud02] N. Dudovich, D. Oron, Y. Silberberg, *Single-pulse coherently controlled nonlinear Raman spectroscopy and microscopy*, Nature **418**, 512–514 (2002).

[Ega98] W. F. Egan, *Phase-Lock Basics* (John Wiley & Sons, INC., 1998).

[Ell03] R. Ell, *Sub-two cycle Ti:sapphire laser and phase sensitive nonlinear optics*, Dissertation, Universität Karlsruhe (2003).

[Ell05] R. Ell, G. Angelow, W. Seitz, M. Lederer, H. Huber, D. Kopf, J. Birge, F. X. Kärtner, *Quasi-synchronous pumping of mode-locked few-cycle Titanium Sapphire lasers*, Opt. Exp. **13**, 9292–9298 (2005).

[For06] T. M. Fortier, Y. L. Coq, J. E. Stalnaker, D. Ortega, S. A. Diddams, C. W. Oates, L. Hollberg, *Kilohertz-Resolution Spectroscopy of Cold Atoms with an Optical Frequency Combs*, Phys. Rev. Lett. **97**, 163905 (2006).

[Fri08] J. Friebe, A. Pape, M. Riedmann, T. E. Mehlstäubler, N. Rehbein, C. Lisdat, E. M. Rasel, W. Ertmer, H. Schnatz, B. Lipphardt, G.Grosche, *Absolute frequency*

measurement of the magnesium intercombination transition 1S0–>3P1, Phys. Rev. A **78**, 33830 (2008).

[Fuj04] T. Fuji, A. Apolonski, F. Krausz, *Self-stabilization of carrier-envelope offset phase by use of difference-frequency generation*, Opt. Lett. **29**, 632–634 (2004).

[Fuj06] T. Fuji, N. Ishii, C. Y. Teisset, X. Gu, T. Metzger, A. Baltuška, N. Forget, D. Kaplan, A. Galvanauskas, F. Krausz, *Parametric amplification of few-cycle carrier-envelope phase-stable pulses at 2.1 μm*, Opt. Lett. **31**, 1103–1105 (2006).

[Gal01] L. Gallmann, *Generation and Characterization of Few-Femtosecond Optical Pulses*, Dissertation, ETH Zürich (2001).

[Gar05] F. M. Gardner, *Phaselock Techniques* (John Wiley & Sons, INC., 2005).

[Gie85] K. Giesen, F. Hage, F. Himpsel, H. Riess, W. Steinmann, *Two-Photon Photoemission via Image-Potential States*, Phys. Rev. Lett. **55**, 300–303 (1985).

[Goh06] C. Gohle, *A Coherent Frequency Comb in the Extreme Ultraviolet*, Dissertation, Ludwig-Maximilians-Universität München (2006).

[Gre09a] C. Grebing, S. Koke, B. Manschwetus, G. Steinmeyer, *Performance comparison of interferometer topologies for carrier-envelope phase detection*, Appl. Phys. B **95**, 9581–84 (2009).

[Gre09b] C. Grebing, S. Koke, G. Steinmeyer, *Self-referencing of optical frequency combs*, Conference on Lasers and Electro-Optics (CLEO) **CTuK5** (2009).

[Güd06] J. Güdde, M. Rohleder, U. Höfer, *Time-resolved two-color interferometric photoemission of image-potential states on Cu(100)*, Appl. Phys. A **85**, 345–350 (2006).

[Güd07] J. Güdde, M. Rohleder, T. Meier, S. W. Koch, U. Höfer, *Time-Resolved Investigation of Coherently Controlled Electric Currents at a Metal Surface*, Science **318**, 1287–1291 (2007).

[Güd08] J. Güdde, U. Höfer, *Kohärenz an Oberflächen*, Physik Journal **11**, 33–39 (2008).

[Hel03] F. W. Helbing, G. Steinmeyer, U. Keller, *Carrier-envelope offset phase-locking with attosecond timing jitter*, IEEE J. Sel. Top. Quantum Electron. **9**, 1030–1040 (2003).

[Iac98] C. Iaconis, I. A. Walmsley, *Spectral phase interferometry for direct electric-field reconstruction of ultrashort optical pulses*, Opt. Lett. **23**, 792–794 (1998).

[Iac99] C. Iaconis, I. Walmsley, *Self-referencing Spectral interferometry for Measuring Ultrashort Optical Pulses*, IEEE Journ. of Quantum Electron **35**, 501–509 (1999).

[Jen06] Jenoptik, *SLM-640d Technical Documentation* (2006).

[Jon00] D. J. Jones, S. A. Diddams, J. K. Ranka, A. Stentz, R. S. Windeler, J. L. Hall, S. T. Cundiff, *Carrier-Envelope Phase Control of Femtosecond Mode-Locked Lasers and Direct Optical Frequency Synthesis*, Science **288**, 635–639 (2000).

[Jon05] D. J. Jones, *Carrier-Envelope Phase Stabilization of Single and Multiple Femtosecond Lasers*, in *Few-Cycle Laser Pulse Generation and Its Application* (F. X. Kärtner, 2005).

[Kär97] F. Kärtner, N. Matuschek, T. Schibli, U. Keller, H. Haus, C. Heine, R. Morf, V. Scheuer, M. Tilsch, T. Tschudi, *Design and fabrication of double-chirped mirrors*, Opt. Lett. **22**, 831–833 (1997).

[Kär01] F. X. Kärtner, U. Morgner, R. Ell, T. Schibli, J. G. Fujimoto, E. P. Ippen, V. Scheuer, G. Angelow, T. Tschudi, *Ultrabroadband double-chirped mirror pairs for generation of octave spectra*, J. Opt. Soc. Am. **B 18**, 882–885 (2001).

[Kär05] F. X. Kärtner, E. P. Ippen, S. T. Cundiff, *Femtosecond Laser Development*, in *Femtosceond Optical Frequency Comb: Principle, Operation, and Applications* (J. Ye and S. T. Cundiff, 2005).

[Kre06] M. Kreß, T. Löffler, M. D. Thomson, R. Dörner, H. Gimpel, K. Zrost, T. Ergler, R. Moshammer, U. Morgner, J. Ullrich, H. G. Roskos, *Determination of the carrier-envelope phase of few-cycle laser pulses with terahertz-emission spectroscopy*, Nature Physics **2**, 327–331 (2006).

[Lan02] C. Langton, *Intuitive Guide to Principles of Communications - Unlocking the Phase Lock Loop - Part 1*, www.complextoreal.de (2002).

[Lee05] Y. S. Lee, J. H. Sung, C. H. Nam, T. J. Yu, K.-H. Hong, *Novel method for carrier-envelope-phase stabilization of femtosecond laser pulses*, Opt. Exp. **13**, 2969–2976 (2005).

[Lee08] J. Lee, Y. S. Lee, J. Park, T. J. Yu, C. H. Nam, *Long-term carrier-envelope-phase stabilization of a femtosecond laser by the direct locking method*, Opt. Exp. **16**, 12624–12631 (2008).

[Li10] H. Li, V. A. Sautenkov, Y. V. Rostovtsev, M. M. Kash, P. M. Anisimov, G. R. Welch, M. O. Scully, *Carrier-Envelope Phase Effect on Atomic Excitation by Few-Cycle rf Pulses*, Phys. Rev. Lett. **104**, 103001 (2010).

[Lin86] D. Linde, *Characterization of the Noise in Continously Operating Mode-Locked Lasers*, Appl. Phys. B **39**, 201–217 (1986).

[Man06] C. Manzoni, C. Vozzi, E. Benedetti, G. Sansone, S. Stagira, O. Svelto, S. De Silvestri, M. Nisoli, G. Cerullo, *Generation of high-energy self-phase-stabilized pulses by difference-frequency generation followed by optical parametric amplification*, Opt. Lett. **31**, 963–965 (2006).

[Mar04] A. Marian, M. C. Stowe, J. R. Lawall, D. Felinto, J. Ye, *United Time-Frequency Spectroscopy for Dynamics and Global Structure*, Science **306**, 2063–2068 (2004).

[Mar08] S. V. Marchese, C. R. E. Baer, A. G. Engqvist, S. Hashimoto, D. J. H. C. Maas, M. Golling, T. Südmeyer, U. Keller, *Femtosecond thin disk laser oscillator with pulse energy beyond the 10-microjoule level*, Opt. Exp. **16**, 6397–6407 (2008).

[Mor99] U. Morgner, F. X. Kärtner, S. H. Cho, Y. Chen, H. A. Haus, J. G. Fujimoto, E. P. Ippen, V. Scheuer, G. Angelow, T. Tschudi, *Sub-two-cycle pulses from a Kerr-lens mode-locked Ti:sapphire laser*, Opt. Lett. **24**, 411–413 (1999).

[Mor00] U. Morgner, W. Drexler, F. X. Kärtner, X. D. Li, C. Pitris, E. P. Ippen, J. G. Fujimoto, *Spectroscopic optical coherence tomography*, Opt. Lett. **25**, 111–113 (2000).

[Mor06] U. Morgner, *Optik und Photonik* (Leibniz Universität Hannover, 2006).

[Mor07] U. Morgner, *Nichtlineare Optik* (Leibniz Universität Hannover, 2007).

[Müc04] O. D. Mücke, T. Tritschler, M. Wegener, U. Morgner, F. X. Kärtner, G. Khitrova, H. M. Gibbs, *Carrier-wave Rabi flopping: role of the carrier-envelope phase*, Opt. Lett. **29**, 2160–2162 (2004).

[Müc05] O. D. Mücke, R. Ell, A. Winter, J.-W. Kim, J. R. Birge, L. Matos, F. X. Kärtner, *Self-Referenced 200 MHz Octave-Spanning Ti:Sapphire Laser with 50 Attosecond Carrier-Envelope Phase Jitter*, Opt. Exp. **13**, 5163–5169 (2005).

[Nak06] T. Nakajima, S. Watanabe, *Effects of the Carrier-Envelope Phase in the Multiphoton Ionization Regime*, Phys. Rev. Lett. **96**, 213001 (2006).

[Pal08] G. Palmer, M. Schultze, M. Siegel, M. Emons, U. Bünting, U. Morgner, *Passively mode-locked Yb:KLu(WO_4)$_2$ thin-disk oscillator operated in the positive and negative dispersion regime*, Opt. Lett. **33**, 1608–1610 (2008).

[Pas04a] R. Paschotta, *Noise of mode-locked lasers (Part I): numerical model*, Appl. Phys. B **79**, 153–162 (2004).

[Pas04b] R. Paschotta, *Noise of mode-locked lasers (Part II): timing jitter and other fluctuations*, Appl. Phys. B **79**, 163–173 (2004).

[Pas06] R. Paschotta, A. Schlatter, S. C. Zeller, H. R. Telle, U. Keller, *Optical phase noise and carrier-envelope offset noise of mode-locked lasers*, Appl. Phys. B **82**, 265–273 (2006).

[Pop98] A. Poppe, L. Xu, F. Krausz, C. Spielmann, *Noise Characterization of Sub-10-fs Ti:Sapphire Oscillators*, IEEE J. Sel. Top. Quantum Electron. **4**, 179–184 (1998).

[Pop01] A. Poppe, R. Holzwarth, A. Apolonski, G. Tempea, C. Spielmann, T. W. Hänsch, F. Krausz, *Few-cycle optical waveform synthesis*, Appl. Phys. **B 72**, 373–376 (2001).

[Pos08] S. Postma, A. van Rhijn, J. P. Korterik, P. Gross, J. L. Herek, H. L. Offerhaus, *Application of spectral phase shaping to high resolution CARS spectroscopy*, Opt. Exp. **16**, 7985–7996 (2008).

[Pro09] O. Prochnow, *Rauscheigenschaften von passiv modengekoppelten Ytterbium-Faserlasern*, Dissertation, Leibniz Universität Hannover (2009).

[Rau08a] S. Rausch, T. Binhammer, A. Harth, F. X. Kärtner, U. Morgner, *Few-cycle femtosecond field synthesizer*, Opt. Exp. **16**, 17410–17419 (2008).

[Rau08b] S. Rausch, T. Binhammer, A. Harth, J. Kim, R. Ell, F. X. Kärtner, U. Morgner, *Controlled waveforms on the single-cycle scale from a femtosecond oscillator*, Opt. Exp. **16**, 9739–9745 (2008).

[Rau09] S. Rausch, T. Binhammer, A. Harth, E. Schulz, M. Siegel, U. Morgner, *Few-cycle oscillator pulse train with constant carrier-envelope- phase and 65 as jitter*, Opt. Exp. **17**, 20282–20290 (2009).

[Roo05] P. A. Roos, X. Li, J. A. Pipis, T. M. Fortier, S. T. Cundiff, R. D. R. Bhat, J. E. Sipe, *Characterization of carrier-envelope phase-sensitive photocurrent injection in a semiconductor*, J. Opt. Soc. Am. **22**, 362–368 (2005).

[Rou07] V. Roudnew, B. D. Esry, *General Theory of Carrier-Envelope Phase Effects*, Phys. Rev. Lett. **99**, 220406 (2007).

[Rub06] E. Rubiola, *Phase Noise*, Lecture Note (2006).

[Rud77] H. Rudolf, W. Steinmann, *Two photon photoelectron effect in the surface plasma resonance of aluminium*, Phys. Lett **61A**, 471 (1977).

[Rul05] C. Rullière, *Femtosecond Laser Pulses* (Springer, 2005).

[San06] G. Sansone, E. Benedetti, F. Calegari, C. Vozzi, L. Avaldi, R. Flammini, L. Poletto, P. Villoresi, C. Altucci, R. Velotta, S. Stagira, S. De Silvestri, M. Nisoli, *Isolated Single-Cycle Attosecond Pulses*, Science **314**, 443–446 (2006).

[Sch94] V. Scheuer, M. Tilsch, T. Tschudi, *Reduction of absorption losses in ion beam sputter deposition of optical coatings for the visible and near infrared*, SPIE Conf. Proc. **2253**, 445–454 (1994).

[Sch03] T. R. Schibli, O. Kuzucu, J.-W. Kim, E. P. Ippen, J. Fujimoto, F. Kärtner, V. Scheuer, G. Angelow, *Toward Single-Cycle Laser Systems*, IEEE J. Sel. Top. Quantum Electron. **9**, 990–1000 (2003).

[Sch10] M. Schultze, T. Binhammer, A. Steinmann, G. Palmer, M. Emons, U. Morgner, *Few-cycle OPCPA system at 143 kHz with more than 1 μJ of pulse energy*, Opt. Exp. **18**, 2836–2841 (2010).

[Sei02] W. Seitz, T. R. Schibli, U. Morgner, F. X. Kärtner, C. H. Lange, W. Richter, B. Braun, *Passive synchronization of two independent laser oscillators with a Fabry-Perot modulator*, Opt. Lett. **27**, 454–456 (2002).

[Sie09] M. Siegel, *Pulse dynamics in mode-locked high energy laser oscillators*, Dissertation, Leibniz Universität Hannover (2009).

[Son92] J. Son, J. V. Rudd, J. F. Whitaker, *Noise characterization of a self-mode-locked Ti:sapphire laser*, Opt. Lett. **17**, 733–735 (1992).

[Sor05] E. Sorokin, *Solid-State Materials for Few-Cycle Pulse Generation and Amplification*, in *Few-Cycle Laser Pulse Generation and Its Application* (F. X. Kärtner, 2005).

[Sto06] M. C. Stowe, F. C. Cruz, A. Marian, J. Ye, *High Resolution Atomic Coherent Control via Spectral Phase Manipulation of an Optical Frequency Comb*, Phys. Rev. Lett. **97**, 163905 (2006).

[Sut99] D. H. Sutter, G. Steinmeyer, L. Gallmann, N. Matuschek, F. Morier-Genoud, U. Keller, V. Scheuer, M. Tilsch, T. Tschudi, *Semiconductor saturable-absorber mirror-assisted Kerr-lens mode-locked Ti:sapphire laser producing pulses in the two-cycle regime*, Opt. Lett. **24**, 631–633 (1999).

[Sve98] O. Svelto, *Principles of Lasers* (Plenum Press, 1998).

[Tak82] M. Takeda, H. Ina, S. Kobayashi, *Fourier-transform method of fringe-pattern analysis for computer-based topography and interferometry*, J. Opt. Soc. Am. **72**, 156 (1982).

[Tel99] H. R. Telle, G. Steinmeyer, A. E. Dunlop, J. Stenger, D. H. Sutter, U. Keller, *Carrier-envelope offset phase control: A novel concept for absolute optical frequency measurement and ultrashort pulse generation*, Appl. Phys. B **69**, 327–332 (1999).

[Tre10] R. Trebino, *Ultrashort Laser Pulses I* (2010).

[Ude99] T. Udem, J. Reichert, R. Holzwarth, T. Hänsch, *Absolute optical frequency measurement of the cesium D_1 line with a mode-locked laser*, Phys. Rev. Lett. **82**, 3568–3571 (1999).

[Ude02a] T. Udem, *Die Messung der Frequenz von Licht mit modengekoppelten Lasern* (2002).

[Ude02b] T. Udem, R. Holzwarth, T. Hänsch, *Optical frequency metrology*, Nature **416**, 233–237 (2002).

[Vac06] B. Vacano, M. Motzkus, *Time-resolved two color single-beam CARS employing supercontinuum and femtosecond pulse shaping*, Opt. Commun. **264**, 488–493 (2006).

[Vog06] G. Vogt, P. Nürnberger, R. Selle, F. Dimler, T. Brixner, G. Gerber, *Analysis of femtosecond quantum control mechanisms with colored double pulses*, Phys. Rev. A **74**, 33413 (2006).

[Wal75] F. L. Walls, A. DeMarchi, *RF Spectrum of a Signal After Frequency Multiplication; Measurement and Comparison with a Simple Calculation*, IEEE Trans. Instrum. Meas. **24**, 210–217 (1975).

[Wei00] A. Weiner, *Femtosecond pulse shaping using spatial light modulators*, Rev. Sci. Instrum. **71** (2000).

[Wei01] Z. Wei, Y. Kaboyashi, K. Torizuka, *Passive synchronization between femtosecond Ti : sapphire and Cr:forsterite lasers*, Appl. Phys. B **74**, 171–176 (2001).

[Wit04] S. Witte, R. Zinkstok, W. Hogervorst, K. S. Eikema, *Control and precise measurement of carrier-envelope phase dynamics*, Appl. Phys. B **78**, 5–12 (2004).

[Ye05] J. Ye, S. T. Cundiff, *Femtosecond Optical Frequency Comb: Principle, Operation, and Application* (Springer, 2005).

A Few-cycle pulse characterization - SPIDER

Spectral Phase Interferometry for Direct Electric-Field Reconstruction (SPIDER) [Iac98] is a powerful and mathematical unique technique to characterize femtosecond laser pulses via a spectral phase reconstruction. SPIDER uses the spectral interference of two delayed replica of the pulse to be characterized to obtain the desired spectral phase information. These replica are identical with the exception that their frequencies are shifted - 'spectrally sheared' - with respect to each other. The spectral phase information can be extracted from an interference pattern generated by these two pulses, exemplarily shown in Fig. A.1 (A), at which the phase information is recorded within the fringe spacing[1] and can be reconstructed by a set of linear functions and transformations.

The required spectral shear between the two delayed pulse replica is generated via a third copy of the input pulse. This pulse is temporally stretched up to a factor of approximately 10^3 while propagating through a solid glass block. During a sum frequency generation of the two replica with the chirped pulse copy in a nonlinear crystal, shown in Fig. A.1 (B), each of the replica will be up-converted with a different frequency component of the stretched pulse copy, resulting in a frequency-difference of both, the spectral shear Ω. Ω thereby is dependent on the delay τ between the two replica and the stretching-amount of the third pulse copy.

The spectral phase information of the input pulse can be extracted from the interferogram of the two up-converted pulse replica by a robust phase retrieval procedure introduced by Takeda et al. [Tak82] using Fourier-transformations, filtering and concatenation (integration). This linear non-iterative algorithm extracts the phase with a very small reconstruction error associated with it and even in a noisy environment SPIDER delivers an excellent performance [And00]. This algorithm first of all comprises a Fourier-transformation of the interferogram. The desired phase information is included in the two resulting AC sidebands. Since these are complex conjugates with respect to each other only one, by convention the positive sideband, is needed to reconstruct the spectral phase of the input pulse. Thus the negative AC sideband and the DC component can be removed in the second step of the routine by filtering. By inverse Fourier-transforming the filtered AC sideband and extracting the argument, the phase term $\varphi(\omega+\Omega)-\varphi(\omega)+\omega\tau$ can be isolated. An intermediate step in the retrieval routine is to remove the linear phase contribution $\omega\tau$, which arises from the time delay between the two replica and is present in the extracted argument next to the desired phase difference. This removal can be done by an additional calibration

1 For two identical replica without spectral shear the interferogram will exhibit a constant fringe spacing $\omega\tau$ over the whole spectral range.

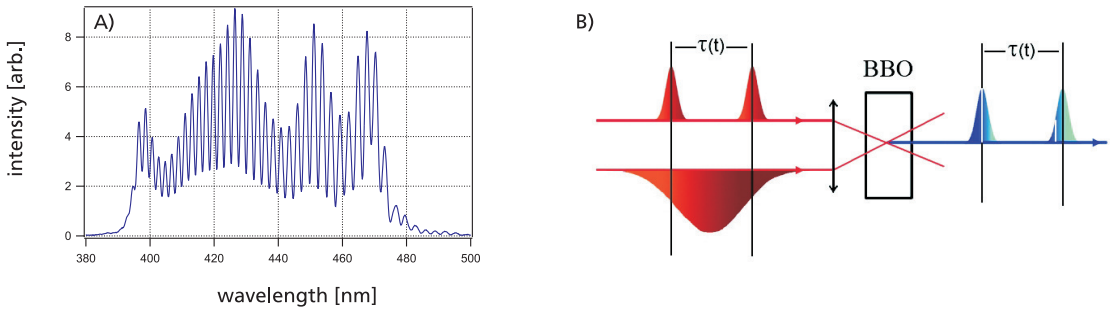

Figure A.1: Principal of SPIDER; A) Interferogram of the two delayed pulse replica, the fringe spacing including the spectral phase information; B) The two delayed pulse replica are mixed each with a different slice of the stretched pulse copy within a nonlinear crystal. Two up-converted and spectrally sheared pulses result.

measurement whereat the two pulse replica interfere without being spectrally sheared. A interference pattern with constant fringe spacing $\omega\tau$ will result, whose argument can be subtracted from the extracted argument of the SPIDER interferogram and only the desired phase difference $\theta(\omega)$ will remain.

$$\theta(\omega) \equiv \varphi(\omega+\Omega) - \varphi(\omega) \qquad \varphi(\omega) \approx \frac{1}{\Omega}\int \theta(\omega) d\omega. \tag{A.1}$$

In the last step of the routine the desired spectral phase of the input pulse is reconstructed by the phase difference given in Eq. (A.1). This can be done following two different approaches, either by concatenation or integration. For concatenation one initial start frequency ω_0 is being chosen and the the spectral phase $\varphi(\omega)$ set to zero. From this starting point $\varphi(\omega)$ can be concatenated for frequencies separated by multiples of Ω [Iac99]. On the other hand, if the spectral shear is small relative to the structure of the spectral phase, the phase differences may be approximated the first derivative of the spectral phase. In this case, the spectral phase can be obtained by integration [Gal01], given in the right hand side of Eq. (A.1). One advantage of this integration method is that all measured data is being used. By applying the concatenation in comparison, only a subset of the available data is taken into account, because the data step size is usually much smaller than the spectral shear Ω.

The last necessary step, which has to be applied to reconstruct the total electric field of the laser pulse is the combination of the pulse power spectrum and the reconstructed spectral phase. The Fourier-transformation of this combination yields the desired temporal representation of the pulse.

B Phase-locked loops

A phase-locked loop (PLL) is a widely used and powerful electronic circuit to synchronize the phase and thus frequency of a voltage controlled oscillator (VCO) to a reference frequency. In the scope of this thesis phase-locked loops are used to stabilize Ti:sapphire laser oscillators – the VCOs – either with respect to their repetition frequency, tunable by a voltage controlled resonator length change or their carrier-envelope-offset phase, assessable by a voltage controlled pump power.

A PLL in general is capable of tracking the input frequency and pulling the VCO frequency according to this reference. In the ideal case the frequency spectrum of the VCO is additionally cleaned-up with respect to the input spectrum [Ega98] and thus stable and noise-less reference signals are highly regarded for this type of operation. The other way round a PLL can also be used to clean up a noisy input frequency by tracking this signal by a VCO with better noise characteristics and use this signal for further processing. Such PLLs are used for e.g. signal demodulation.

A schematic of a classical PLL is given in Fig. B.1. It consists out of three main elements, a phase detector (PD) which compares the phase of a periodic input waveform to the phase of the VCO signal and generates an error signal proportional to the phase difference of both. The loop filter (LF) filters and possesses the phase detector output to generate the VCO control signal. The design of this loop filter, in most cases a complex regulator unit, is mainly responsible for the PLL characteristics and locking behavior. The VCO, the third crucial element than changes its frequency according to the control voltage and feed back to the phase detector. The frequency change is of that kind that the resulting phase error becomes smaller, since this techniques uses a negative feedback.

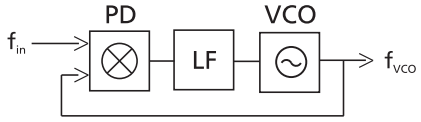

Figure B.1: Schematic diagram of a phase-locked loop consisting of the phase detector (PD) a loop filter (LF) and a voltage controlled oscillator (VCO), the latter representing the laser oscillator to be controlled.

For a locked loop the control voltage sets the average frequency of the VCO exactly equal to the average frequency of the input signal [Gar05].

B.1 Phase detector

As already mentioned, the phase detector within a PLL generates an error signal that is proportional to the phase difference between the input signal waveform and the VCO signal waveform. To get an understanding of the fundamental idea, a frequency multiplier holds for a simple version of a phase detector. For two input waveforms with nearly similar frequencies the output of such a phase detector will be a series of several multiplication terms, half of them related to the low-frequency difference of both signals and the others located at twice the input frequencies. For PLL concerns only the difference-frequency terms are important since they contain a phase difference dependency as given in Eq. B.1. The 'ripples' at twice the input frequency can be simply filtered from the output signal.

The phase term contained within the output of a multiplier phase detector for two input signals with equal frequency but different phases $\phi_1(t)$ and $\phi_2(t)$ writes to:

$$s_{out}(t) = \frac{K_D A_1 A_2}{2} \cdot sin\left[\phi_1(t) - \phi_2(t)\right] + ... \tag{B.1}$$

With K_D the gain of the multiplier and A_1 and A_2 being the input signal amplitudes. This DC signal changes depending of the phase difference between the two input signal waveforms and can be use to drive a PLL[1] by changing one of the frequencies that a constant DC value results. From Eq. (B.1) it becomes clear that the output DC signal of the multiplier is also depending on the input signal amplitudes, a negative characteristic of a multiplier PD, since changes within these amplitudes will influence the lock of a PLL.

In modern state-of-the-art phase detector ICs the operation principle is different and more complex. This class of PDs, called sequential, is often referred to as digital PDs and the PLLs as digital PLLs. These phase detectors generate their output signal solely depending on the timing between the transition of the input signal waveform and the transition of the VCO waveform [Gar05], other characteristics do not contribute to the PD output, delivering a stable operation of the PLL. Such devices are build-up from digital logic circuits like flip-flops or gates. The error signal generation of such a sequential PD is illustrated in Fig. B.2 (A) exemplarily for an RS flip-flop. The resulting output signal θ_d cannot be used as applicable driving voltage for the VCO. Here a useful output is the DC average voltage V_d on the output terminal of the flip-flop[Gar05], given in Fig. B.2 (B):

$$V_d = \frac{V_H \theta_d}{2\pi} = K_d \cdot \theta_d \tag{B.2}$$

For this type of phase detectors the linear range is centered at $\theta_d = 180°$ and the phase detector gain is $K_d = V_H/2\pi$, its units in [V/rad]. K_d is a very important parameter for phase-

1 The full analysis of a multiplier PD containing all multiplication terms can be found in [Gar05] and with illustrating waveforms in [Lan02]

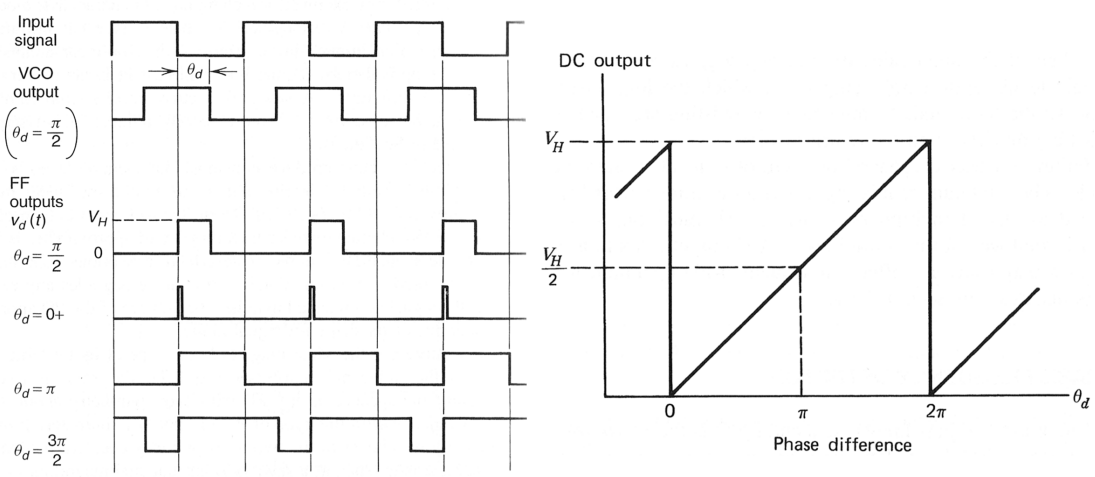

Figure B.2: Sequential phase detector; A) Waveforms in an RS flip-flop phase detector taken from [Gar05]. The output θ_d is shown for four phase differences. Negative transitions of the input signal waveform sets the flip-flop into true state, whereat negative transitions at the second input resets the device to false state again; B) Output curve of a flip-flop phase detector what is the DC average output of the output terminal of the flip-flop.

locked loops and also their application within the scope of this thesis, see Section 3.2.2. This is because K_d is independent from the working frequency. Thus for a repetition frequency stabilization the overall 'phase resolution' can be increased by choosing a higher harmonic of the native frequency for locking. Because the phase of the high harmonic frequency can be resolved equally, the resulting resolution for the native frequency is increased about the harmonic order, compared to locking directly at the fundamental frequency. The stabilization in this thesis for example is performed at 1.3 GHz instead of locking at the fundamental repetition frequency of 81.25 MHz. Thereby the resolution is increased by a factor of 16.

B.2 Loop filter – PI(D) regulator

The loop filter (LF) determines the performance of the PLL. First of all the loop filter generates an usable output signal from the phase detector such as filtering for higher frequency ripples or converting the discrete signals from a sequential phase detector into an applicable DC voltage. On the other hand the loop filter is responsible for the PLL characteristics in terms of bandwidth, settling time, gain, tracking performance and noise. These characteristics are determined by the chosen filter / regulator design that can be simple linear or a complex higher-order filter arrangement. A comprehensive discussion on different types of PLLs and filter orders including their theoretical treatment is beyond the scope of this thesis ands can be found in [Ega98, Gar05].

C Acknowledgements (German)

An dieser Stelle möchte ich mich ganz herzlich bei allen bedanken, die mich in den letzten vier Jahren begleitet, und somit direkt oder indirekt zum Gelingen dieser Arbeit beigetragen haben. Mein besonderer Dank gilt:

Meinem Doktorvater *Uwe Morgner*, für meine Aufnahme in seine damals noch sehr überschaubare Arbeitsgruppe und die Möglichkeit bei ihm im Bereich der ultrakurzen Laserpulse promovieren zu dürfen. Für sein Vertrauen und seine Unterstützung. Für den stets motivierenden und zuversichtlichen Zuspruch und das ausgezeichnete Arbeitsklima in seiner Gruppe.

Meinem Kollegen, Geschäftspartner und Freund *Thomas*, für die unzähligen Diskussionen, Anregungen und Gespräche, nicht nur auf fachlicher Ebene. Für die exzellente Zusammenarbeit im Labor, die gemeinsame Zeit im Büro und auf Reisen.

Meinen Mitstreitern, Kollegen bzw. Freunden – ganz besonders *Emilia*, für den Ausgleich und den "ruhenden Pol" in unserem Büro, und *Moritz* für seine Unterstützung in allen Lebenslagen, aber auch *Guido, Tino, Marcel, Anne, Olli, Daniel, Heiko, Claudia, Mathias, Matthias, Nils, Tobi* und *Milo*, den ehemaligen Kollegen *Andy, Martin* und *Michael*, meinem Diplomanden Michael und dem Rest der Arbeitsgruppe! Vielen Dank für die schöne gemeinsame Zeit und die fantastische Zusammenarbeit!

Den Mitarbeitern am Institut für Quantenoptik, stellvertretend *Frau Hünitzsch*, *Frau Pfennig* und *Frau Faber*, für die Hilfsbereitschaft und Organisation, die gute Stimmung und das stets offene Ohr für die Probleme eines Doktoranden.
Der *Werkstatt*, für die ausgezeichnete fein-mechanische Unterstützung meiner Arbeit. Für Rat und Tat und auch die Annahme des ein oder anderen Paketes.
Stephan Pfalz und dem gesamten *QUEST-Team* für den wissenschaftlichen Rahmen und die finanzielle Unterstützung meiner Forschung und Arbeitsstelle.

Prof. Dr. Piet O. Schmidt für die Übernahme des Korrefereats meiner Dissertation und *Prof. Dr. Michael Oestreich* für den Prüfungsbeisitz.

Am Schluss möchte ich ganz besonders meiner Freundin Wiebke und meinen Eltern danken! Vielen Dank für Eure Geduld, den liebevollen Zuspruch und Ausgleich, besonders in Zeiten in denen nicht alles auf Anhieb funktionieren wollte! Danke aber auch für die finanzielle und emotionale Unterstützung während meines gesamten Studiums!

D Curriculum Vitae

Personal Data

Name:	Stefan Rausch
Date of birth:	07.05.1980
Place of birth:	Neuwied, Germany
Nationality:	German
Martial status:	unmarried

Education

1986 - 1990:	St. Martin Grundschule, Remagen
1990 - 1999:	Rhein-Gymnasium Sinzig, Sinzig
Juni 1999:	Abitur

Alternative Civilian Service

1999 - 2000:	'Tagesförderstätte für Schwerstbehinderte', Caritas Werkstätten Sinzig

University Education

2000 - 2004:	Studies in Laser Technology at the University of Applied Science Koblenz / RheinAhrCampus Remagen
2003 - 2004:	Visiting scientist & diploma thesis at the Massachusetts Institute of Technology (MIT), Cambridge, USA - Research group of Prof. Franz X. Kärtner Diploma thesis: *'Prototype of a Spectral Interferometer (SPIDER) for Time- and Frequency Domain Few-Cycle Laser Pulse Characterization'*
September 2004:	Final degree: Diplom-Ingenieur (FH) - 'mit Auszeichnung'
2004-2006:	Master of Science (Applied Physics) at the University of Applied Science Koblenz / RheinAhrCampus Remagen Master thesis: *'Development of an Interferometric Autocorrelator for Few-Cycle Laser Pulse Characterization'*
April 2006:	Final degree: Master of Science (FH) - 'mit Auszeichnung'

Ph.D. Studies

since Mai 2006:	Ph.D. student at the Institute of Quantum Optics at the Leibniz Universität Hannover, research group of Prof. Uwe Morgner
2007:	Theoretical exam in Quantum Mechanics at the Leibniz Universität Hannover

Related Work Experience

2000 - 2006:	Student research assistant: RheinAhrCampus Remagen
2004 - Oct. 2008:	Part time job: Nanolayers Optical Coatings GmbH, Rheinbreitbach: *Production of Ti:sapphire laser oscillators*
Oct. 2008 - present:	Associate & founding member: VENTEON Laser Technologies GmbH, Garbsen: *Product manager few-cycle laser oscillators and pulse characterization tools*

Memberships

VDI - Verein Deutscher Ingenieure
DPG - Deutsche Physikalische Gesellschaft
EPS - European Physical Society
OSA - Optical Society of America

E Publications

Journal Publications

1. S. Rausch, T. Binhammer, A. Harth, J. Kim, R. Ell, F. X. Kärtner, and U. Morgner
Controlled waveforms on the single-cycle scale from a femtosecond oscillator,
Optics Express **16**, 9739–9745 (2008)

2. S. Rausch, T. Binhammer, A. Harth, F. X. Kärtner, and U. Morgner
Few-cycle femtosecond field synthesizer,
Optics Express **16**, 17410–17419 (2008)

3. M. Siegel, N. Pfullmann, G. Palmer, S. Rausch, T. Binhammer, M. Kovacev, and U. Morgner
Microjoule pulse energy from a chirped-pulse Ti:Sapphire oscillator with cavity-dumping,
Optics Letters **34**, 740–741 (2009)

4. E. Schulz, T. Binhammer, D. S. Steingrube, S. Rausch, M. Kovacev, and U. Morgner
Intense few-cycle laser pulses from self-compression in a self-guiding filament,
Applied Physics B **95**, 269–272 (2009)

5. S. Rausch, T. Binhammer, A. Harth, E. Schulz, M. Siegel, and U. Morgner
Few-cycle oscillator pulse train with constant carrier-envelope-phase and 65 as jitter,
Optics Express **17**, 20282–20292 (2009)

6. S. Rausch, T. Binhammer, A. Harth, F. X. Kärtner, and U. Morgner
CEO-Phase Stabilized Few-Cycle Field Synthesizer, in: ULTRAFAST PHENOMENA XVI: SPRINGER SERIES IN CHEMICAL PHYSICS **92**, 837–839 (2009), Springer-Verlag Berlin

7. T. Binhammer, S. Rausch, M. Jackstadt, G. Palmer, and U. Morgner
Phase-stable Ti:Sapphire Oscillator Quasi-Synchronously Pumped by a Thin-Disk Laser,
Applied Physics B **100**, (2010)

Contributions to International Conferences

1. S. Rausch, T. Binhammer, V. Scheuer, F. X. Kärtner, and U. Morgner
   Oral Presentation: *Octave-spanning Optical Waveform Synthesizer for Coherent Control Experiments*,
   Conference on Lasers and Electro-Optics (CLEO), **CthHH7**, May 2007, Baltimore, USA

2. S. Rausch, T. Binhammer, A. Harth, N. Meiser, F. X. Kärtner, and U. Morgner
   Oral Presentation: *Few-Cycle Femtosecond Waveform Synthesizer*,
   Conference on Lasers and Electro-Optics (CLEO), **CFA6**, May 2008, San Jose, USA

3. S. Rausch, T. Binhammer, A. Harth, F. X. Kärtner, and U. Morgner
   Oral Presentation: *Few-Cycle Femtosecond Field Synthesizer*,
   Conference on Ultrafast Phenomena (UP), **WED2A.2**, June 2008, Stresa, Italy

4. M. Siegel, N. Pfullmann, G. Palmer, S. Rausch, T. Binhammer, and U. Morgner
   Oral Prentation: *Microjoule Pulse Energy from a Chirped-Pulse Ti:Sapphire Oscillator with Cavity-Dumping*,
   Advanced Solid-State Photonics (ASSP), **WE3**, January 2009, Denver, USA

5. S. Rausch, T. Binhammer, A. Harth, F. X. Kärtner, and U. Morgner
   Oral Presentation: *Few-Cycle Femtosecond Field Synthesizer*,
   Advanced Solid-State Photonics (ASSP), **WA5**, January 2009, Denver, USA

6. M. Siegel, N. Pfullmann, G. Palmer, S. Rausch, T. Binhammer, and U. Morgner
   Oral Presentation: *Microjoule pulse energy from a chirped-pulse Ti:sapphire oscillator with cavity-dumping*,
   European Conference on Lasers and Electro-Optics (CLEO/Europe), **CA7.5 WED**, June 2009, München, Germany

7. S. Rausch, T. Binhammer, A. Harth, M. Siegel, and U. Morgner
   Poster Presentation: *Ti:sapphire Frequency Comb with Octave-Spanning Spectrum for Spectroscopy and Few-Cycle Pulse Shaping*,
   European Conference on Lasers and Electro-Optics (CLEO/Europe), **EG.P.2 WED**, June 2009, München, Germany

8. S. Rausch, T. Binhammer, A. Harth, and U. Morgner
   Oral Presentation: *Oscillator Pulse Train with Constant Carrier-Envelope-Offset Phase and 65 Attosecond CE Jitter*,
   Advanced Solid-State Photonics (ASSP), **AWC2**, February 2010, San Diego, USA

9. S. Rausch, T. Binhammer, G. Palmer, M. Jackstadt, and U. Morgner
   Oral Presentation: *Self-Starting Octave-Spanning Ti:sapphire Laser Pumped by an*

Yb:KLu(WO_4)$_2$ Thin-Disk Oscillator,
Conference on Lasers and Electro-Optics (CLEO), **CTuK1**, Mai 2010, San Jose, USA

10. S. Rausch, T. Binhammer, A. Harth, and U. Morgner
Oral Presentation: *Octave-Spanning Ti:sapphire Laser Locked to Carrier-Envelope-Offset Frequency Zero*,
Conference on Lasers and Electro-Optics (CLEO), **CWJ2**, May 2010, San Jose, USA

11. S. Rausch, T. Binhammer, A. Harth, and U. Morgner
accepted Oral Presentation: *Self-Referenced Oscillator Pulse Train with Constant Carrier-Envelope-Offset Phase*,
Conference on Ultrafast Phenomena (UP), **MB5**, July 2010, Snowmass Village, USA

Contributions to National Conferences

1. D. Schäfer, T. Nisius, S. Rausch, M. Wieland, R. Früke, U. Vogt, und Thomas Wilhein
Oral Presentation: *Tabletop X-Ray Microscope*,
DPG Frühjahrstagung, March 2006, Frankfurt, Germany

2. Stefan Rausch, Thomas Binhammer, Emilia Schulz, Claudia Hoffmann und Uwe Morgner
Oral Presentation: *Oktavbreiter optischer Wellenform-Synthesizer*,
DPG-Früjahrstagung, March 2007, Düsseldorf, Germany

3. S. Rausch, T. Binhammer, A. Harth, N. Meiser, und U. Morgner
Oral Presentation: *Femtosekunden Wellenform-Synthesizer*,
DPG Frühjahrstagung, March 2008, Darmstadt, Germany

4. E. Schulz, T. Binhammer, S. Rausch, M. Kovacev, und U. Morgner
Oral Presentation: *Verkürzung hochenergetischer Laserpulse durch Selbstkompression in einem Filament*,
DPG Frühjahrstagung, March 2008, Darmstadt, Germany

5. G. Palmer, M. Schultze, A. Steinmann, A. L. Lindemann, M. Siegel und U. Morgner
Poster Presentation: *Femtosekunden Yb:KLuW Scheibenoszillator im solitären und positiven Dispersionsregime*,
DPG Frühjahrstagung, March 2009, Hamburg, Germany

6. S. Rausch, T. Binhammer, A. Harth, und U. Morgner
Oral Presentation: *Titan:Saphir-Oszillator mit konstanter Träger-Einhüllenden-Phase*,
DPG Frühjahrstagung, March 2010, Hannover, Germany

7. M. Jackstadt, S. Rausch, T. Binhammer, G. Palmer, und U. Morgner
   Oral Presentation: *Quasisynchron gepumpter Titan:Saphir Oszillator mit oktavbreitem Spektrum*,
   DPG Frühjahrstagung, March 2010, Hannover, Germany

8. F. Elster, A. Harth, S. Rausch, T. Binhammer, M. Hoffmann, und U. Morgner
   Poster Presentation: *Effects of the carrier-envelope phase of few-cycle laser pulses on atomic bound states*,
   DPG Frühjahrstagung, March 2010, Hannover, Germany